

THESE EN CO-TUTELLE

FRANCE – THAILANDE

PRÉSENTÉE À

L'UNIVERSITE BORDEAUX 1
ECOLE DOCTORALE DES SCIENCES CHIMIQUES

ET

KASETSART UNIVERSITY
GRADUATE SCHOOL KASETSART UNIVERSITY

PAR CHOMPUNUCH WARAKULWIT

POUR OBTENIR LE GRADE DE

DOCTEUR

SPECIALITE: CHIMIE-PHYSIQUE

FONCTIONNALISATIONS DE NANOTUBES DE CARBONE:
ETUDE EXPÉRIMENTALE ET THÉORIQUE

THESE DIRIGEE PAR PROF. J.LIMTRAKUL ET PROF. A.KUHN

SOUTENUE LE: 29.11.2007

APRÈS AVIS DE:

PROF. MICHAEL PROBST, UNIVERSITÄT INNSBRUCK
ASST. PROF. BUNJERD JONGSOMJIT, CHULALONGKORN UNIVERSITY BANGKOK

RAPPORTEUR
RAPPORTEUR

DEVANT LA COMMISSION D'EXAMEN FORMÉE DE:

ASSOC. PROF. SUPA HANNONGBUA, KASETSART UNIVERSITY BANGKOK
PROF. JUMRAS LIMTRAKUL, KASETSART UNIVERSITY BANGKOK
PROF. ALEXANDER KUHN, UNIVERSITE BORDEAUX 1
PROF. PHILIPPE A. BOPP, UNIVERSITE BORDEAUX 1
PROF. MICHAEL PROBST, UNIVERSITÄT INNSBRUCK
ASST. PROF. BUNJERD JONGSOMJIT, CHULALONGKORN UNIVERSITY BANGKOK

PRÉSIDENT
EXAMINATEUR
EXAMINATEUR
EXAMINATEUR
EXAMINATEUR
EXAMINATEUR

Chompunuch Warakulwit 2007: Functionalizations of Carbon Nanotubes: An Experimental and Theoretical Study, Doctor of Philosophy (Chemistry), Major Field: Physical Chemistry, Department of Chemistry. Thesis advisor: Professor Jumras Limtrakul, Ph.D., and Professor Alexander Kuhn, Ph.D. 158 pages.

In this thesis work, state-of-the-art experimental techniques have been employed to synthesize and functionalize carbon nanotubes (CNTs). Owing to the difficulties in controlling the diameter, length and alignment during the synthetic procedure, as synthesized CNTs are usually random oriented and mainly have defects such as tube bending and twisting. This results in a serious impediment to many applications of CNTs. To address this problem, the use of a template for controlling the diameter, length and alignment of the tubes during synthesis was studied. Using our experimental set-up as well as an optimized synthetic system and conditions, complete, straight and metal-catalyst free carbon nanotubes with uniform diameter can be formed as copies of the channel in the template used.

Apart from homogeneity in the structure and straightness, other unfavorable properties, e.g. purity, dispersion and solubilization in the solvent, also prohibit CNTs from being used as major appliances for material applications. In order to overcome such unfavorable properties, the combination of polyoxometalate and the sonication technique was developed and studied. Under our optimized experimental conditions, CNTs with high purity, dispersibility and water-solubility can be obtained by using this combined technique. A similar procedure can be used to shorten CNTs in the preparation of tubes with a monodisperse length distribution. Thus, this technique is considered as an important step forward that will lead to many applications using CNTs.

Subsequently, the structural diversity of the tubes was considered since it had been expected that it would open up the way for the development of many applications in the field of analytical chemistry. The 'gold metal decoration' on CNTs is our prospect for this issue. The deposition on carbon nanotubes was developed and extensively studied by two complementary methods, the electroless and the bipolar electrochemical deposition techniques. In the case of the chemical modification (electroless deposition), metal is generated by dismutation and the carbon

nanostructures act as the nucleation site. As a result, CNTs become covered by a metal layer. As for bipolar electrochemical deposition, a potential gradient along the object is created and then leads to the electrodeposition of metal without the object being in direct contact with an electrode. This provides a metal deposit with dissymmetric characteristic. In this study, capillary electrophoresis was adapted to deposit gold locally on one end of carbon nanotubes through bipolar chemistry. Therefore, this technique is very promising, not only to deposit metal onto carbon nanostructures, but it might also be adapted to deposit other materials (metal oxides, conducting polymer, etc.) for making conducting, or at least semiconducting materials.

In addition to these experimental studies, the Diels-Alder cycloadditions of single wall carbon nanotubes (SWNTs) with different types of dienes was investigated theoretically within the framework of our-Own-N-layered-Integrated molecular Orbital and molecular Mechanics (ONIOM) approach utilizing a two-layered ONIOM scheme (B3LYP/6-31G*:AM1). Structure and activity relationships for a series of different dienes, interacting with armchair (5,5) SWNTs were established, i.e. the reactivity of the Diels-Alder reaction has been correlated to the distance between the methylene carbons in the butadiene moiety of these dienes. The reactivity increases as the $R_{1,4}$ becomes shorter. This information clarifies that the diene most appropriate for the reaction can be selected. The calculations also revealed that the SWNT has a low viability for the Diels-Alder reaction, even when a reactive diene is used. To enhance the capability of the Diels-Alder reaction of SWNTs at the sidewall, a metal cation was introduced into the SWNTs. The observed decrease in activation energy of the Diels-Alder is due mainly to the electron deficiency nature of the double bond of Na@SWNT and to the stabilization of the LUMO and HOMO of the dienophile.

ACKNOWLEDGEMENTS

First and foremost, my deep thank is addressed to my supervisor in Thailand (Kasetsart University), Professor Jumras Limtrakul for giving me a very good chance to participate in his professional work group. I am extremely grateful for his suggestions, supports, kind helps and all he has done for me during my Ph.D thesis.

I also would like to express a big thank to Professor Alexander Kuhn, my co-supervisor in France (Université Bordeaux I), who introduced me into the theoretical and experimental aspects of electrochemistry. I gained much valuable experience while working on the project under his supervision. I was touched by the warmth of welcome. Thanks for being patient to train me and having always encouraged me in pursuing the objectives of my research work. I am very pleased by his kindness during my stay in France.

I would also like to express my gratitude to the members of my thesis jury, Professor Philippe Anthony Bopp, Professor Michael Probst, Professor Supa Hannongbua, and Professor Bunjerd Jongsomjit, who gave me the possibility to complete this thesis, their useful comments and suggestions. I am especially grateful to Professor Bopp who worked hard many days during his vacation to correct parts of my thesis writing. Professor Piboon Pantu is also appreciatively acknowledged for his precious discussion and suggestion for carbon nanotubes synthesis.

I gratefully acknowledge financial support from the Commission on Higher education Staff Development Project for the jointed Ph.D. program in Physical Chemistry at Kasetsart University, Thailand for being able to spend one year of my research at Université Bordeaux I, France. The Laboratory for Computational and Applied Chemistry (LCAC), Kasetsart University, Thailand as well as the groupe “Nanosystèmes Analytiques” of the “Institut des Sciences Moléculaires”, Université Bordeaux I, France are gratefully acknowledged for the research facilities.

Special sincere thanks to Dr. Marie-Hélène Delville for her great contribution to the analytical part of my experimental work in France, Thi Van Anh Nguyen for her contribution to the capillary electrophoresis part, and Leela Ruckthong for her contribution to the carbon nanotubes synthesis part. Professor Matta Chareonpanich, staff member at the Department of Chemical Engineering, Kasetsart University and Boonruen Sunpetch are also acknowledged here for their kind help and discussions on requisite instrument set up used for my previous experience of carbon nanotubes synthesis.

Grateful thanks are also due to the following people for their help: Dr. Valérie Ravaine, Véronique Lapeyre, Patrick Garrigue, Aline Simon-Lalande, Isabelle Boukourt and many helpful friends at LCAC and ex-LACReM, especially to Dr. Somkiat Nokbin, Dr. Pipat Khongpracha, Dr. Jakkapan Sirijaraensre, Dr. Tanin Nanok, Nongnuch Artrith, Frédérique Deiss and Marie-Laurence Dumartin. Thank you for the warm welcome in Professor Alexander Kuhn's and Dr. Jean Christophe Soetens families.

Finally, I have to thank my parents, my grandmother and my brothers for supporting my success. For whatever I am and will become, I owe it to my family and their endless love. I also would like to thank Mathieu Deglas for his encouragement on all difficult days that I encountered during my work.

Chompunuch Warakulwit

September, 2007

TABLE OF CONTENTS

	Page
TABLE OF CONTENTS	i
LIST OF TABLES	iv
LIST OF FIGURES	v
CHAPTER I. GENERAL INTRODUCTION	1
CHAPTER II. PREPARATION OF CARBON NANOTUBES BY USING THE CHEMICAL VAPOR DEPOSITION METHOD IN POROUS ANODIC ALUMINUM OXIDE TEMPLATES	3
1. Introduction	3
2. Method	6
3. Results and discussions	11
3.1. Experimental setup and optimization of synthetic system and conditions	11
3.2. Characteristic of templates used in this study	14
3.2a. Unheated template	14
3.2b. High temperature heated membrane	18
3.3. Carbon nanotubes synthesized by using the commercial AAO membrane filters with average pore diameter about 200 nm and 20 nm as templates	22
4. Conclusions	28
CHAPTER III. DIELS-ALDER CYCLOADDITION OF SINGLE- WALLED CARBON NANOTUBES WITH ELECTRON RICH DIENES : A THEORETICAL STUDY	30
1. Introduction	30
2. Theoretical approaches	35
3. Some backgrounds of the ONIOM approach	37
4. Functionalization of SWCNTs studied by ONIOM	40
5. Computational Procedures	47
6. Results and Discussions	50

TABLE OF CONTENTS (cont'd)

	Page
6.1. The Diels-Alder reaction of the sidewall armchair (5,5) SWCNT (C ₁₃₀ H ₂₀) with different types of dienes	50
6.2. The Diels-Alder reaction of Na@SWCNT with 2,3-dimethylene-1,4-dioxane	54
7. Conclusions	56
CHAPTER IV. CONTROLLED PURIFICATION, SHORTENING AND DISPERSION OF CARBON NANOTUBES	57
1. Introduction	57
2. Experimental section	61
3. Result and discussion	62
3.1. The optimized condition: the POM solution	62
3.2. The purification, dispersion and water-solubilization of carbon nanotubes	66
4. Conclusion	74
CHAPTER V. METAL DECORATION OF CARBON NANOTUBES	75
1. Introduction	75
2. Electroless chemical deposition of gold nanoparticles on carbon nanotubes	78
2.1. Introduction	78
2.2. Experimental section	79
2.3. Results and Discussions	81
3. Electrochemical deposition of gold nanoparticles on carbon structures by bipolar electrochemistry	83
3.1. Introduction	83
3.2. Electrochemical deposition of gold nanoparticles on carbon fiber by bipolar electrochemistry	86
3.2.1. Experimental materials and method	86
3.2.2. Results and discussions	88

TABLE OF CONTENTS (cont'd)

	Page
3.3. Electrochemical deposition of gold nanoparticles on carbon nanotubes by bipolar electrochemistry	92
3.3.1. Experimental section	92
3.3.2. Results and discussions	95
3.4. Bipolar electrochemical deposition of gold nanoparticles on carbon nanotubes by capillary electrophoresis	99
3.4.1. Introduction	99
3.4.2. Experimental section	101
3.4.3. Results and discussions	103
3.5. Conclusions	111
CHAPTER VI. CONCLUDING REMARKS	112
LITERATURE CITED	114
APPENDIX	146
Appendix A	147
Appendix B	152
Appendix C	155
CURRICULUM VITAE	157

LIST OF TABLES

Table		Page
1	The distances between the methylene carbons in the butadiene moiety ($R_{1,4}$) of various dienes obtained from the B3LYP/6-31G* level of theory, the computed activation energies (E_a), reaction energies (E_r) and the percentages of bond lengthening and shortening for the Diels-Alder reaction of three dienes considered in this study onto the 1,2-pair site side wall of (5,5) SWCNT ($C_{130}H_{20}$) obtained from an ONIOM(B3LYP/6-31G*:AM1) calculation.	52
2	Details of the experimental method of electroless gold deposition on CNTs by using the prepared <i>CNT/ECF60</i> solution as a starting reagent.	80
3	Details of the experimental method of the bipolar electrochemical gold deposition on CNTs by using the prepared <i>CNT/HAuCl₄</i> solution as a starting reagent.	94

LIST OF FIGURES

Figure		Page
1	Photograph of an anodic aluminum oxide film with a pore diameter of about 200 nm, as used in this study.	6
2	Schematic illustration showing the experimental set up of the system in the furnace.	7
3	The set-up of the vertical CVD reactor for CNT synthesis used in this study.	8
4	The solvents obtained after several cycles of washing.	10
5	The liquid trap parts between the tube and the gas outlet line.	11
6	The real temperature inside the work tube (<i>Measured temperature</i>) at the middle of work tube compared with the temperature which was read out from temperature controller (<i>Setpoint Temperature</i>), in both cases, without N ₂ flow and with 20 ml/min N ₂ flow.	12
7	The <i>Measured temperature</i> inside the work tube at varying dwell time (min) with 20 ml/min N ₂ flow (<i>Setpoint temperature</i> = 1050°C).	13
8	The real temperature inside the work tube at varying position, <i>Measured Temperature</i> , in the work tube. The set temperature, <i>Setpoint Temperature</i> , is 1175°C. The flow rate of nitrogen gas was 20 ml/min.	14
9	E-SEM photographs of a commercial aluminum anodic oxide film (ANODISC25, WHATMAN) with 200 nm channel diameter showing a) surface b-d) cross section views.	15
10	E-SEM images of heated anodic alumina with nominal 200 nm pore diameter showing the surface (a-b) and cross-section (c-e) view.	19
11	The CNTs/AAO composites obtained from our CVD synthesis.	22
12	Surface view (a-b) and cross-section view (c) SEM images of a specimen taken after synthesis showing a thick carbon overgrowth layer on top of the surface and the opened end nature of synthesized tubes.	23

LIST OF FIGURES (cont'd)

Figure		Page
13	Very light black powders obtained after removing template by immersing in HF solution, centrifugation, particle isolation and rinsing with DI water, drying in oven at 200°C for 1 h.	24
14	Raman spectrum of CNT sample obtained from the CVD synthesis showing multi-walled structure characteristic.	25
15	TEM images of CNTs synthesized by the CVD technique showing a) arrays of parallel and straight channels of the synthesized tubes, b) parallel, straight and complete tubes with uniform outer diameter of about 200 nm, c) open ended nature of the synthesized tubes, and d) a synthesized branched tube.	26
16	a) Low-magnification and High-magnification TEM image of a typical CNT obtained from CVD synthesis using 20 nm pore diameter template (a commercially available membrane filter of 25 mm o.d. wide, 60 μm thick, average diameter of about 20 nm, ANODISC25, WHATMAN). The growth temperature was 900°C. The reaction time was 3 h. The total gas flow rate was 20 ml/min. The gas mixture composition was 10% acetylene and 90% nitrogen.	27
17	Graphene tubules are made by rolling a graphene sheet into a cylinder. The tubules are uniquely determined by their lattice vectors, \overline{C}_h . The chiral angle is denoted by θ , while a_1 , and a_2 , denote the unit vectors of graphite, see text for more details	31
18	Molecular models of SWCNTs exhibiting different chiralities: (a) armchair configuration ($n = m$ ($\theta = 30^\circ$)), (b) zigzag arrangement ($n \neq 0$ and $m = 0$ ($\theta = 0^\circ$)), and (c) chiral conformation (all other SWCNTs)	32

LIST OF FIGURES (cont'd)

Figure		Page
19	Scheme of the electronic properties of all structures of SWCNTs as a function of their indices (n, m) . The circled dots (●) and dots (●), denote metallic and semiconducting behavior, respectively (Saito <i>et al.</i> , 1992).	33
20	Diagram of (a) pyramidalization angles (θ_P) of trigonal and tetrahedral carbon atoms, and (b) the π -orbital misalignment angles between adjacent pairs, the pair perpendicular to the nanotube axis and the pair nearly along the nanotube axis, of conjugated carbon atoms in SWCNTs.	34
21	Schematic concept of the ONIOM method: (a) the two-layers ONIOM approach (ONIOM2) (b) the three-layers ONIOM approach (ONIOM3) (Dapprich <i>et al.</i> , 1999; Feliu Maseras, 1995).	38
22	Schematic representations of the ONIOM extrapolation schemes for a molecular system portioned into two (left) and three (right) layers. See text for description (Dapprich <i>et al.</i> , 1999; Feliu Maseras, 1995).	39
23	The ONIOM2 model of a CNT that has been extensively used for studying functionalization of SWCNTs ('Real' is $C_{130}H_{20}$ cluster (typically treated with B3LYP/6-31G* level of theory) and 'Model' is C_{16} cluster (typically treated at the AM1 level of theory, see the highlighted atoms in the figure) (Lu <i>et al.</i> , 2002a; Lu <i>et al.</i> , 2002b; Lu <i>et al.</i> , 2003a; Lu <i>et al.</i> , 2003b; Lu <i>et al.</i> , 2003c; Lu <i>et al.</i> , 2002c).	40
24	The simplest Diels-Alder Reaction is the reaction of 1,3-butadiene and ethylene to yield cyclohexene.	42
25	Diagram of the π molecular orbitals of 1,3-butadiene and ethylene and the electron configuration.	43

LIST OF FIGURES (cont'd)

Figure		Page
26	The π molecular orbitals of 1,3-butadiene and ethylene that correspond with the FMOs in the normal and inverse electron-demand Diels-Alder cycloadditions.	44
27	Diagram showing FMOs level and their electron configuration of diene and dienophile. Blue arrow shows changing in the FMOs in the a) normal and b) inverse electron-demand Diels-Alder cycloadditions when the reaction is facilitated by some substituents group. D denotes a donor substituent, A denotes an acceptor substituent.	45
28	The Diels-Alder reactivity with 2,3-dioxy-substituted cis-fixed butadienes with C_{60} relates as a function of the distance between the carbons in the butadiene moiety ($R_{1,4}$) of the diene (Torres-Garcia and Mattay, 1996).	46
29	a) The ONIOM model of (5,5) SWCNT ($C_{130}H_{20}$ cluster) and three different types of dienes : b) <i>diene (1)</i> ; c) <i>diene (2)</i> ; and d) <i>diene (3)</i> . Atoms belonging to the quantum cluster (B3LYP/6-31G*) region are drawn as balls and sticks; the rest is treated at the AM1 level of theory.	48
30	Selected parameters (bond length in Å) obtained at the ONIOM (B3LYP/6-31G*:AM1) level of theory for the transition states of the Diels-Alder reaction of 5,5-armchair SWCNT fragment ($C_{130}H_{20}$) with three dienes: a) <i>diene (1)</i> ; b) <i>diene (2)</i> ; and c) <i>diene (3)</i> .	50
31	Selected parameters (bond length in Å) obtained at the ONIOM (B3LYP/6-31G*:AM1) level of theory for the products of the Diels-Alder reaction of 5,5-armchair SWCNT fragment ($C_{130}H_{20}$) with three dienes: a) <i>diene (1)</i> ; b) <i>diene (2)</i> ; and c) <i>diene (3)</i> .	51

LIST OF FIGURES (cont'd)

Figure		Page
32	Selected parameters (bond lengths in Å) obtained at the ONIOM(B3LYP/6-31G*:AM1) level of theory for a) the transition state and b) the product of the Diels-Alder reaction of the embedded metal cation SWCNT (<i>Na@SWCNT</i>) with the 2,3-dimethylene-1,4-dioxane, <i>diene (I)</i> .	54
33	The Frontier Molecular Orbital (FMO) energies (E_{HOMO} and E_{LUMO} , in eV) of SWCNT and <i>Na@SWCNT</i> , obtained from ONIOM(B3LYP/6-31G*:AM1) calculations and of 2,3-dimethylene-1,4-dioxane, <i>diene (I)</i> , obtained from the B3LYP/6-31G* level of theory.	55
34	TEM micrographs of POM solubilized-CNTs after the treatment, 3 h sonication in an aqueous POM solution (10 mM $\text{H}_3\text{PMo}_{12}\text{O}_{40}$ / <i>ultrapure water</i>) showing a POM-film formed on the tube surface (see black arrow) during the treatment.	64
35	TEM micrographs of gold modified-POM solubilized CNTs obtained by an electrochemical reaction (30kV, 2 min) of the POM-solubilized CNTs in 1 mM HAuCl_4 . These images show that the gold decoration prefers to take place on the POM-film on the tube surface (see black arrow) instead on bare tubes.	65
36	Photographs showing (a) untreated CNTs aggregated in water, (b) the black-green suspension of CNTs (treated CNTs still suspended in the used POM solution), and (c) the stable quite homogeneous grey aqueous CNTs suspension (treated CNTs suspended in water). The treatment was performed by 1 hour of sonication in the POM solution.	67

LIST OF FIGURES (cont'd)

Figure		Page
37	(a) TEM image of raw CNTs (black arrow points a position of impurities contained in the sample) and (b) SEM image of purified and dispersed CNTs (treated with 1h sonication in 10 mM $\text{H}_3\text{PMo}_{12}\text{O}_{40}/0.1\text{M H}_2\text{SO}_4$) (white arrow indicates a shortened tube).	69
38	TEM images of the obtained carbon nanotubes and corresponding energy dispersive X-ray spectroscopy (EDXS) spectra showing Mo and Fe compositions of the selected zones of POM treated CNTs.	71
39	The size distribution in terms of volume fraction of raw CNTs (dashed line) and shortened CNTs (solid line) (obtained after 4 h sonication in POM solution) suspended in water.	72
40	TEM images of shortened CNTs (treated with 4h sonication in 10 mM $\text{H}_3\text{PMo}_{12}\text{O}_{40}/0.1\text{M H}_2\text{SO}_4$).	73
41	HRTEM image showing a typical cut of the shortened CNTs (treated by 4h sonication in 10 mM $\text{H}_3\text{PMo}_{12}\text{O}_{40}/0.1\text{M H}_2\text{SO}_4$). Black arrows indicate the nanotube wall with an aligned multilayer of graphene sheets. The white arrow indicates the cut section showing circular arranged graphene sheets.	74
42	Schematic illustration of experimental procedure for preparation of a suspension of shortened CNTs in the ECF60 solution (<i>CNT/ECF60</i>).	79
43	Low-magnification (a-c) and high-magnification (d) HRSEM images of CNT/gold composites synthesized by electroless chemical deposition (the reagent was 6M HCl).	82
44	Orange color appearance of the treated solution demonstrates the gold nanoparticle formation 30s after adding the CNT/ECF60 solution to 6MHCl.	82

LIST OF FIGURES (cont'd)

Figure		Page
45	Scheme of the electrochemical reaction occurring on a tubular object in AuCl_4^- solution (See details in text).	85
46	a) Schematic illustration of the experimental set up of VIALS/CAPILLARY. A carbon fiber was introduced in the glass capillary from a 10 mM HAuCl_4 suspension. Two segmented gold coated slides separated by a distance of 10 cm were used as electrodes. The electrodes were connected to a high voltage DC power supply and voltmeter (V). The reaction occurring on the fiber in the capillary was observed under the microscope. b) The experimental setup of VIALS/CAPILLARY under the microscope.	87
47	Optical micrographs at the same magnification of a carbon fiber (length about 1.3 mm) with gold deposited by bipolar electrochemistry (70V, 10 mM HAuCl_4) as a function of time.	89
48	Optical micrograph of a carbon fiber (length about 1.2 mm) with gold deposited by bipolar electrochemistry (300V, 30 S, 10 mM HAuCl_4).	90
49	a) Low- and b) high-magnification HRSEM picture of a carbon fiber with gold deposited by bipolar electrochemistry (40V, deposition time 30s, 10 mM HAuCl_4).	91
50	Schematic illustration of our first experimental setup for bipolar electrochemical gold deposition of CNTs. The electrochemical reaction was performed in a disposable cuvette by using the $\text{CNT}/\text{HAuCl}_4$ suspension as a starting suspension. Two segmented gold-coated glass slides were used as electrodes. These electrodes were fixed on the wall of the cuvette by resin. Applied voltage from a DC power supply was used to drive the electrochemical reaction.	93

LIST OF FIGURES (cont'd)

Figure		Page
51	HRSEM image of the carbon nanotubes, which were completely covered by gold deposits during bipolar electrodeposition (300V, 5 min and 10 mM HAuCl ₄).	96
52	HRSEM image of the carbon nanotubes with gold deposits obtained by bipolar electrochemistry (100V, 1 min and 10 mM HAuCl ₄).	97
53	HRSEM images of carbon nanotubes modified with gold deposited by bipolar electrochemistry (100V, 30 s and 1 mM HAuCl ₄).	98
54	Schematic illustration of a capillary electrophoresis apparatus. An open-end capillary (purple) is placed between two buffer reservoirs. A high voltage is applied across this capillary. This voltage causes the migration of analytes (red, yellow, and blue shapes) from the anode side (+) to the cathode (-) (through detector). Electrophoresis speeds up the migration of cations and retards the migration of anions through the capillary (Linhardt and Toida, 2002).	100
55	Electropherogram of <i>ultrapure water</i> passing through the capillary as a function of time (at 30 kV). Insignificant variations in the UV absorbance (254 nm) with time show that the capillary is clean (there is no other species except water passing in front of the detection window).	103
56	Electropherogram of the CNT/WATER suspension showing the large variation in the UV absorbance at 254 nm between 2-4 min after the capillary was conditioned at 30 kV. This variation indicates that the CNTs start to leave the capillary at about 2 min after the capillary conditioning and all CNTs have left 4 min after the capillary conditioning.	104
57	High-magnification TEM image of shortened, POM-modified CNTs taken after the CE experiment (30 kV, 2 min). Some of the tubes are modified with gold concentrating only on the tip.	105

LIST OF FIGURES (cont'd)

Figure		Page
58	High-magnification TEM image of shortened, POM-modified CNTs taken after the CE experiment (30kV, 2 min). The CNTs here are modified by gold locally on the tip.	107
59	High-magnification TEM image of CNTs (obtained by the CE experiment (30 kV, 2 min) and the supposed alignment of the tube A and B (see details for tube C in the text) in the field. These alignments are deduced from the obtained gold structures. The locations that give maximum potential difference (parallel to the field) of the tubes are supposed to be almost at the tips of tube A and closest to the electrodes for tube B. For tube C, this potential is supposed to be not high enough to drive an electrochemical reaction because gold deposition on tube C was not found.	108
60	High-magnification TEM image of an irregular curved CNT (obtained after the CE experiment (30 kV, 2 min)), its supposed alignment in the field and its supposed effective length.	109
61	High-magnification TEM image of irregular curved CNTs (obtained after the CE experiment (30 kV, 2 min)), illustrating the different size of the deposited gold particles as a function of the nanotube length.	110

CHAPTER I. GENERAL INTRODUCTION

History of carbon nanostructures begins in 1985, when the first member of a new family of carbon allotropes, Buckminsterfullerene: C₆₀ was discovered by Kroto *et al.* Since that time, the number of discovered carbon nanostructure has rapidly increased including the family of fullerenes (Dorset and Fryer, 2001; Kroto *et al.*, 1985; Kuzuo *et al.*, 1994), carbon nanotubes (Iijima, 1991), carbon nanocones (Ge and Sattler, 1994), carbon nanohorns (Iijima *et al.*, 1999), nanoscale carbon toroidal structure (Itoh *et al.*, 1993), helicoidal tubes (Amelinckx *et al.*, 1994), periodic carbon structure Schwarzites (Mackey and Terrones, 1991), Haeketites (Terrones *et al.*, 2000) etc. Among these, carbon nanotubes (CNTs) have attracted most attention both from a theoretical and an experimental point of view. This is due to their exceptional physical and chemical properties that open up many perspectives for future applications in the fields of energy storage, molecular electronics, nanomechanic devices, and composite materials (Ajayan, 1999; Zhou *et al.*, 2002).

The synthesis of carbon nanotubes can be accomplished with a wide variety of methods. Some of the common techniques are chemical vapor deposition (Amelinckx *et al.*, 1994), arc discharge (Hinds *et al.*, 2004), and laser ablation synthesis (Guo *et al.*, 1995). However, out of the various synthetic procedures reported for large scale production, only the catalytic chemical vapor deposition method is efficient enough to produce CNTs as practical materials. This is because the CCVD method is simple, cheap, easy to implement and yields high amount of the tubes (Iijima and Ichihashi, 1993; Journet *et al.*, 1997; Kong *et al.*, 1998). However, while each technique has its own advantages, the common disadvantages of CVD techniques are that the as-grown tubes are “spaghetti-like” (randomly oriented with many defects such as tube bending and twisting) and have the large distribution in tube diameters and length (Wong *et al.*, 2004). This results in a serious impediment of CNTs applications to new functional material and devices.

To address such problems, like the heterogeneity in diameter and non-straightness of CNTs, a template-synthesis technique based on self-ordered hexagonal nanopore alumina templates was applied to synthesize highly ordered carbon

nanotube in this study. The resultant carbon nanotubes are expected to be uniform in diameter and length as they are copies of the template channel and have open ends.

Apart from the advances in production processes which have improved the high structural perfection of the obtained CNTs, the strong intertube forces keeps CNT together in bundles, making their manipulation, characterization and analytical investigation very difficult. Surface functionalization offers the great advantage of producing soluble and easy-to-handle CNT. Therefore, the functionalizations of carbon nanotubes were further studied in this work by two complementary approaches, an experimental study and a theoretical study.

With respect to the experimental investigation, a simple method for functionalization of CNTs, using polyoxometalates in combination with ultrasonication technique, was developed and studied here. The outcome are open and uniformly shortened CNTs with high purity that are well-dispersed in aqueous solutions. This is an important starting condition for some future CNT-based technologies. In addition, the highly controlled and site specific modification of the tubes with gold nanoparticles was developed and studied here. The obtained dissymmetric hybrid gold/CNT nanoobjects may open up many applications in technologically relevant disciplines, such as electronics, catalysis, material science and sensing.

In addition to the experimental study, which is sometimes difficult to carry out at the molecular level, a study of functionalization of carbon nanotube was performed using a complementary theoretical approach. In this study, a pericyclic reaction, Diels-Alder reaction, which has been very successfully employed in the functionalization of fullerenes, was considered. By using a computationally efficient hybrid method for the study of chemical reactions involving large molecular system, which was introduced by Morokuma et al., our own N-layered integrated molecular orbital and molecular mechanics (ONIOM) approach, the structure-reactivity relationship for the reaction of a single-walled carbon nanotube (SWCNT) can be investigated here.

CHAPTER II. PREPARATION OF CARBON NANOTUBES BY USING THE CHEMICAL VAPOR DEPOSITION METHOD IN POROUS ANODIC ALUMINUM OXIDE TEMPLATES

1. Introduction

Carbon nanotubes with different structure and morphology can be produced by various strategies and methods, which can be grouped into the following categories: arc discharge (Iijima, 1991; 1993; Iijima and Ichihashi, 1993; Bethune *et al.*, 1993; Ebbesen and Ajayan, 1992), chemical vapor deposition (CVD) (Oberlin *et al.*, 1976), plasma techniques (Ren *et al.*, 1998), laser ablation (Guo *et al.*, 1995; Thess *et al.*, 1996), and several more (Alekseev *et al.*, 2006; Vander Wal *et al.*, 2000 ; Laplaze *et al.*, 1998). The most frequently used methods to produce carbon nanotubes are the arc discharge method and chemical vapor deposition (CVD) of hydrocarbons (Derycke *et al.*, 2002; Huczko, 2002; Jeong *et al.*, 2002; 2004; Lee *et al.*, 2001; Sander and Tan, 2003; Pradhan *et al.*, 1998). Compared with the arc discharge, the CVD method is simpler, cheaper, and easier to implement. Therefore this method has been widely used to produce a large amount of CNTs (Iijima and Ichihashi, 1993; Journet *et al.*, 1997; Cassell *et al.*, 1999).

In general, carbon nanotube growth by CVD method requires catalyst nanoparticles (usually Fe, Co, or Ni), a carbon feedstock (e.g. hydrocarbon or CO), and heat. The growth processes of CNTs by CVD generally involve adsorption and decomposition of hydrocarbon gases or carbon containing compounds on metal surfaces, dissolution and diffusion of the released carbon atoms in catalyst, and precipitation of the graphite-like layers (Dai, *et al.*, 1996a).

Aligned carbon nanotube (CNT) arrays put forward the development of several applications such as field emission and chemical and biological sensing (Parthangal *et al.*, 2007). Various techniques of CVD method have been developed for growing well-aligned CNTs based on variant alignment mechanisms such as

'overcrowding growth', 'template hindrance growth' and 'electric field induced growth'.

A method termed 'template synthesis' entails the preparation of a variety of micro- and nano-materials of a desired morphology. This method provides a route for enhancing nanostructure order. Various porous templates are employed and the nanostructures are synthesized within the pores. If the templates that are used have cylindrical pores of uniform diameter, monodisperse nanocylinders are obtained within the voids of the template material. Depending on the operating parameters, these nanocylinders may be solid (a nanorod) or hollow (a nanotubules). The nanostructures can remain inside the pores of the templates or they can be freed and collected as an ensemble of free nanoparticles. Alternatively, they can protrude from the surface like the bristles of brush. Thus, with the template approach, one is able to prepare monodisperse nanorods and nanotubules with desired geometry. The methods has been used to prepare both nanotubules and nanofibrils composed of conductive polymer, metals, semiconductors, carbons, and other solid matters (Huczko, 2000).

The essentially major strategies to carry out template synthesis of nanostructures can be classified into five categories: Electrochemical and electroless deposition, chemical polymerization, sol-gel deposition, and chemical polymerization, sol-gel deposition, and chemical vapour deposition (CVD) (Martin, 1996, Lakshmi *et al.*, 1997). The technique that has successfully been developed for the template synthesis of carbon nanotubules is the CVD technique (Hulteen and Martin, 1997; Che *et al.*, 1998a; Terrones *et al.*, 1997). The starting reactants, i.e. ethylene and pyrene (Che *et al.*, 1998b; Fan *et al.*, 1999), acetylene (Song *et al.*, 1995; Li *et al.*, 1996), tripropylamine (Sun *et al.*, 1999), methane (Kong *et al.*, 1998), propylene (Kyotani *et al.*, 1996), or 2-amino-4,6-dicholoro-s-triazine (Terrones *et al.*, 1997), were thermally activated and decomposed to solid carbon within porous templates while traversing the length of the pores. Thermal decomposition of the gas occurs throughout the pores, resulting in the deposition of carbon films along the length of the pore walls and formation of carbon nanotubules within the pores. The thickness is dependent on total reaction time and precursor pressure. The method offers control

over length (up to 100 μm) and fairly uniform diameters in nanometer range, as well as efficient-producing carbon tubules (Huczko, 2000).

Most of studies in the template synthesis have been entailed the use of two types of nanoporous materials, 'track-etch' polymeric membranes and porous alumina or silica membranes. However, there are variety of other, both natural and synthetic, materials that could be utilized as templates. Formerly synthesized nanostructures e.g. can also be used as templates.

The synthesis of CNTs using an anodic aluminum oxide (AAO) template has drawn considerable attention due to its capability of producing a highly ordered array of CNTs with controllable dimensions (Li *et al.*, 1999; Suh *et al.*, 1999). The various pore sizes and distribution patterns, which can be easily obtained by varying the oxidation voltage and acid electrolyte, is the main advantage of AAO templates (Brumlik and Martin, 1991; Brumlik *et al.*, 1994; Che *et al.*, 1998a; Che *et al.*, 1998b; Dwyer *et al.*, 2002; Kajiura *et al.*, 2002; Liang and Martin, 1990; Marinakos *et al.*, 1998; Parthasarathy *et al.*, 1995). Hydrocarbon can be deposited on the pore surface of an AAO template with and without metal catalysts (Hornyak *et al.*, 1999; Kyotani *et al.*, 1996, Li *et al.*, 1998; Li *et al.*, 1999, Che *et al.*, 1998b). Because the subsistence of catalyst particles constitutes a serious impediment when as-prepared nanotubes are to be used as technological materials (Babaa *et al.*, 2004), then we considered only the formation of carbon nanotubes inside the pores of AAO without catalyst.

In this research, we adopt the CNTs formation over the commercially available AAO template, which have precise control of template dimensions such pore diameter, length and density by CVD method. The synthesized carbon nanotubes construction was analyzed by Raman spectroscopy and Transmission Electron Microscopy (TEM). The effect of the template pore size on the diameter and feature of the synthesized carbon tubes was studied.

2. Method

In this study, the synthesis of carbon nanotubes was performed typically as follows: Commercially available membrane filters of 25 mm o.d. width and 60 μm thickness (ANODISC 25, WHATMAN), the porosity of which consists of an array of parallel and straight channels with diameters of about 200 nm, perpendicular to the film surface, were used as templates. A photograph of such a film is shown in Figure 1. The polymer edge of the films was removed with scissors in order to minimize problems from due to contamination of the synthetic system.

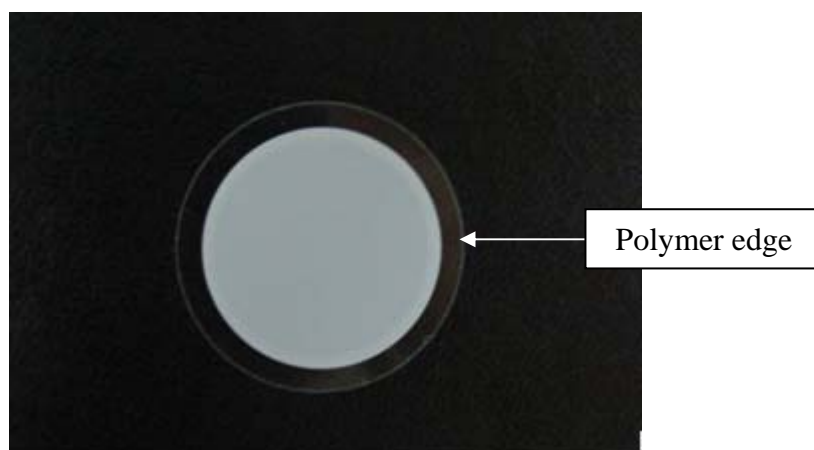


Figure 1 Photograph of an anodic aluminum oxide film with a pore diameter of about 200 nm, as used in this study.

The remainder of the filter was placed on quartz wool (ALTECH) in a vertical impervious aluminum porcelain work tube (23 mm i.d., 45.8 cm long) at the middle position, 22.9 cm from the upper end of work tube (see Figure 2). The work tube can be operated at a maximum temperature of 1,300°C. The work tube was placed in a vertical wire-wound tube furnace (LENTON LTF12/38/250). The experimental set up of the furnace is shown schematically in Figure 3.

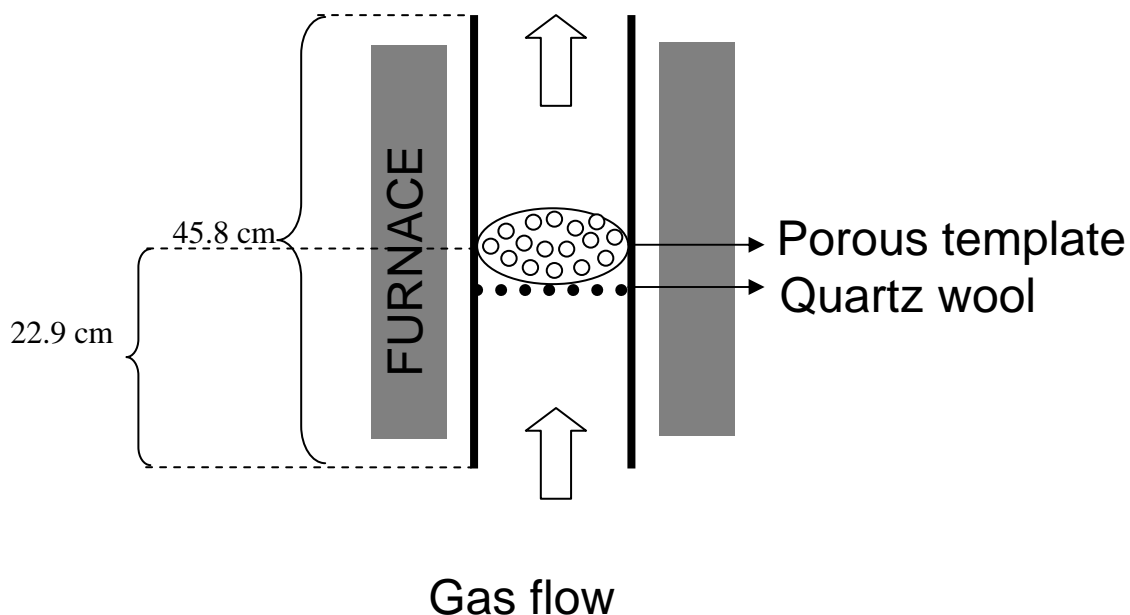


Figure 2 Schematic illustration showing the experimental set up of the system in the furnace.

Nitrogen gas was introduced into the CVD reactor with a flow rate of 18 ml/min. The reactor temperature was gradually increased to 900°C (1050°C on the temperature controller setting) with a constant heating rate of 10°C/min, under the nitrogen flow. After the desired temperature was reached, the synthetic system was kept under the nitrogen flow for 15 min before the reactant gas was introduced in order to avoid uncontrolled temperature variations in the beginning of synthesis. Acetylene (99.9% purity) was then passed through the work tube. The gas mixture concentration was 10% C₂H₂ and 90% N₂ with a total flow rate of 20 ml/min. After 3 h, the acetylene flow was stopped. The work tube was allowed to cool down to room temperature under the nitrogen flow.

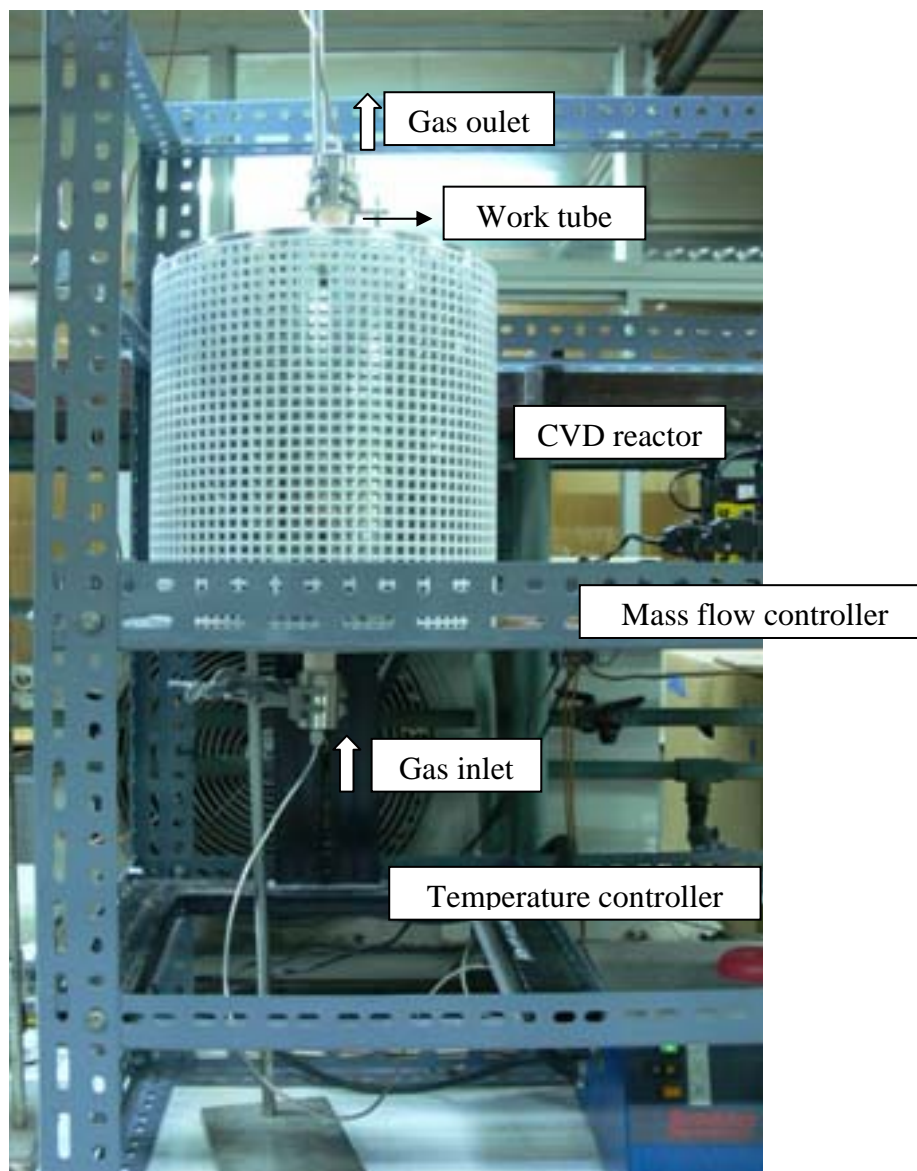


Figure 3 The set-up of the vertical CVD reactor for CNT synthesis used in this study.

The sample was taken out of the reactor and crushed to very small pieces to facilitate the dissolution of the AAO template in HF solution. Next, the sample was immersed in an excess amount of 46% HF solution (about 10 ml) overnight in a chemical-resistant centrifuge tube. The AAO template was totally dissolved in this step. As a result, carbon was obtained as an insoluble fraction, which can be separated from the HF solution by centrifugation (10000 rpm, 1 h). The formed precipitate was separated from the supernatant. The precipitate was washed twice by DI water. The

final precipitate was dried in an oven at 100°C. The vibrational characteristics of the CNTs were recorded by Raman spectroscopy (performed on RENISHAW 2000 Raman microscope with excitation by an Ar laser with excitation wavelength of 514 nm) in the wavenumber range of 600-2000 cm^{-1} . The features of the sample were also studied by transmission electron microscopy (TEM). For these studies, the CNTs sample was dispersed in absolute ethanol for 30 min in an ultrasonic bath and then deposited on a TEM grid.

The effect of the pore size in AAO films on the diameter and other features of the synthesized tubes was further studied by comparing synthesized nanotubes obtained with a 20 nm pore diameter-template with those synthesized from a 200 nm pore diameter-template. The synthesis of CNTs in the 20 nm pore diameter-template was similar to that with the 200 nm template. The diameters and other features of the tubes synthesized from both templates were studied by TEM (JEM 1220, with an accelerated voltage of 100 kV).

After the synthesis, by-products like oil and grease may appear in the gas outlet line connected to the work tube because of the lower temperature there. Before the next synthesis a cleaning of the system is required. The washing of the work tube can be done with solvents with the different polarities, for example, acetone and toluene. In this study, before starting every new synthesis, the gas outlet line was cleaned several times by introducing alternatively acetone and toluene. The solvents after washing are shown in Figure 4; it shows that they contain oil and carbon particle. The washing was continued until clear solvents were obtained. Usually, at least 10 cycles off washing were required.

In order to avoid time consuming washing procedure, a liquid trap was introduced after the gas outlet from the work tube. Because of back streaming from the early part of the gas outlet line may cause undesired product in the work tube, e.g. amorphous carbon particle or hydrocarbon oil and grease, then the introduction of the liquid trap prevents such undesired-products formation. A liquid trap introduced here

was set up by simple equipment, a simple volumetric flask containing water, as shown in Figure 5.

Moreover, before restarting the synthesis, the work tube was also cleaned by heating the furnace to 1000°C with an air flow. This diminishes the amount of undesired amorphous carbon deposited at the work tube wall during the synthesis. The tightness of system was also checked by using surfactant solution.



a) 1st-10th washing by acetone solvent



a) 1st-6th washing by toluene solvent

Figure 4 The solvents obtained after several cycles of washing.

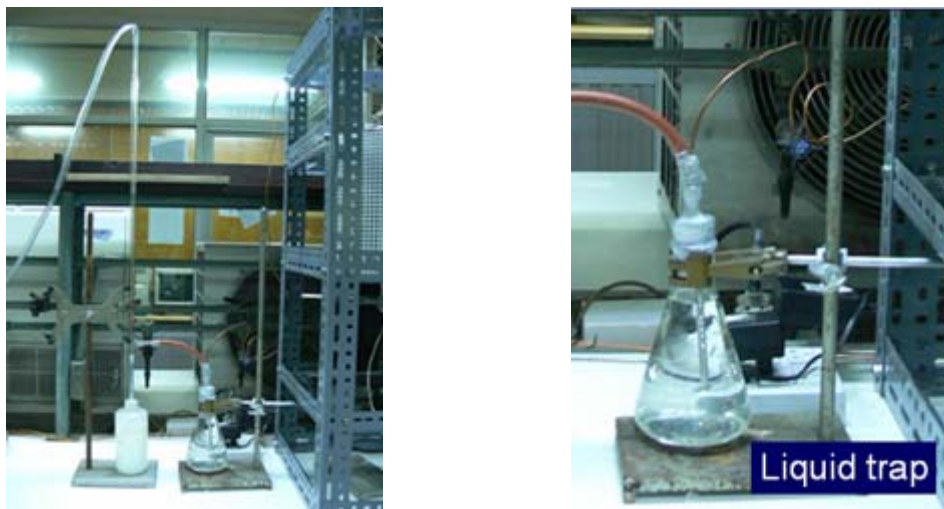


Figure 5 The liquid trap parts between the tube and the gas outlet line.

3. Results and Discussions

3.1. Experimental setup and optimization of synthetic system and conditions

Because an accurate temperature is needed for the synthesis, a calibration is required in the beginning of synthesis. In order to avoid perturbations by uncontrolled temperature variations, we performed a set of experiment to study the actual temperature inside work tube (called as '*Measured Temperature*'), which may be different from of the temperature indicated on the temperature controller, '*Setpoint Temperature*', at varying position in the work tube, and the stability of the temperature inside the work tube.

The *Measured Temperatures* were measured inside the work tube with a thermocouple (TYPE K) for the both cases, with and without N₂ flow. Figure 6 shows that during the temperature ramp, the *Setpoint Temperature* were different from the *Measured Temperature* for the both cases. The difference increases as the temperature is increased. The flow rate of N₂ gas (of 20 ml/min) did not significantly affect the temperature inside the work tube. At a *Setpoint Temperature* range of 800-1000°C, the actual temperature was observed to be about 150°C lower than the set-point value.

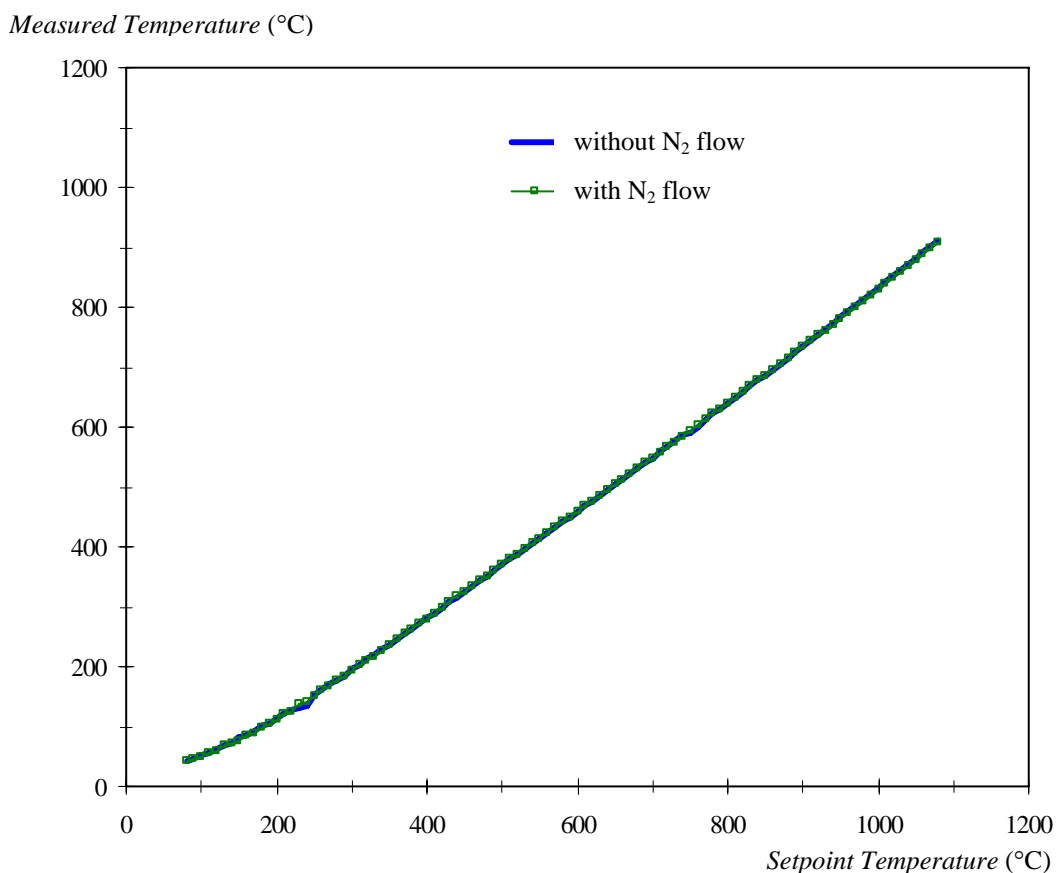


Figure 6 The real temperature inside the work tube (*Measured temperature*) at the middle of work tube compared with the temperature which was read out from temperature controller (*Setpoint Temperature*), in both cases, without N₂ flow and with 20 ml/min N₂ flow.

The stability of the *Measured Temperature* inside the work tube was tested after when a temperature was set. The *Setpoint Temperature* was at 1050°C. After this desired temperature was reached, the actual temperature inside the work tube was recorded at every one minute for 30 min. The results are shown in Figure 7.

Figure 7 shows that the real temperature inside work tube was not stable immediately after the desired temperature was reached. The stable temperature was obtained after the *Setpoint temperature* has been reached at least 5 minute. Then, in our synthesis, we set the temperature of 1050°C (*Setpoint temperature* = 1050°C) and

the dwell time of 15 minutes was provided before started the reactant gas mixture. The desired temperature of 900°C can be reached by this temperature setting.

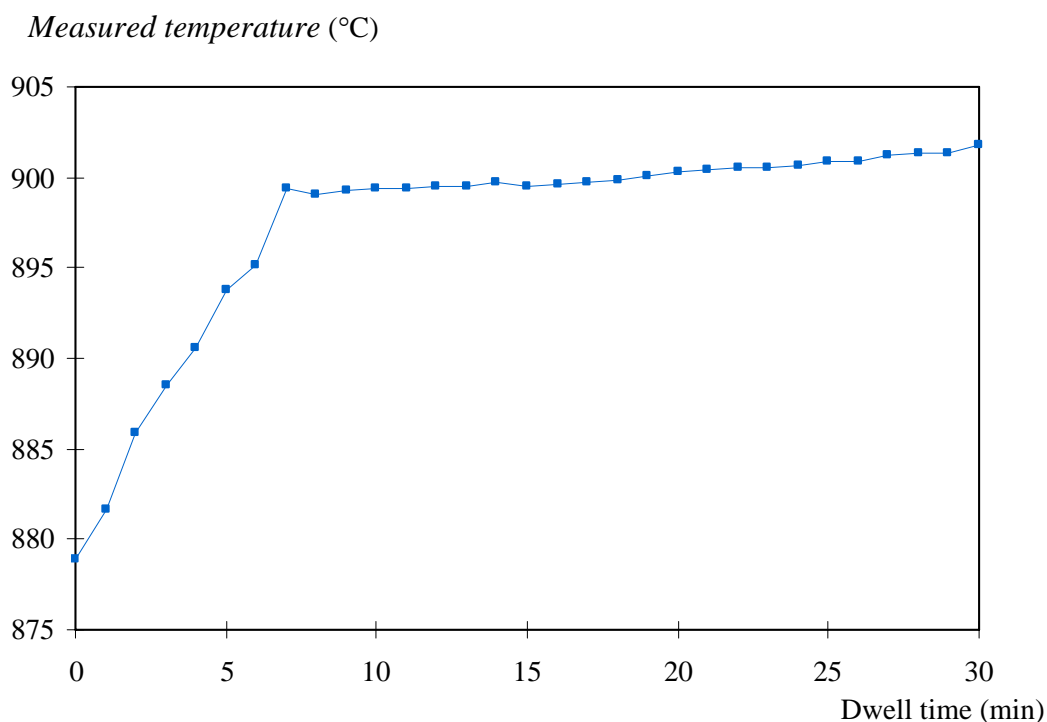


Figure 7 The *Measured temperature* inside the work tube at varying dwell time (min) with 20 ml/min N₂ flow (*Setpoint temperature* = 1050°C).

The *Measured Temperatures* at varying positions in the work tube were measured inside the work tube. This experiment was performed under 20 ml N₂ flow. The temperature was set by the temperature controller (EUROTHERM2416) at 1175°C (heating rate was 10°C/min). The obtained results are shown in Figure 8.

Figure 8 demonstrates that a little difference of position in the work tube results significantly on the temperature. In order to avoid the variation temperature, we control our synthesis by introducing the template at the middle of work tube (22.9 cm from the upper end) carefully.

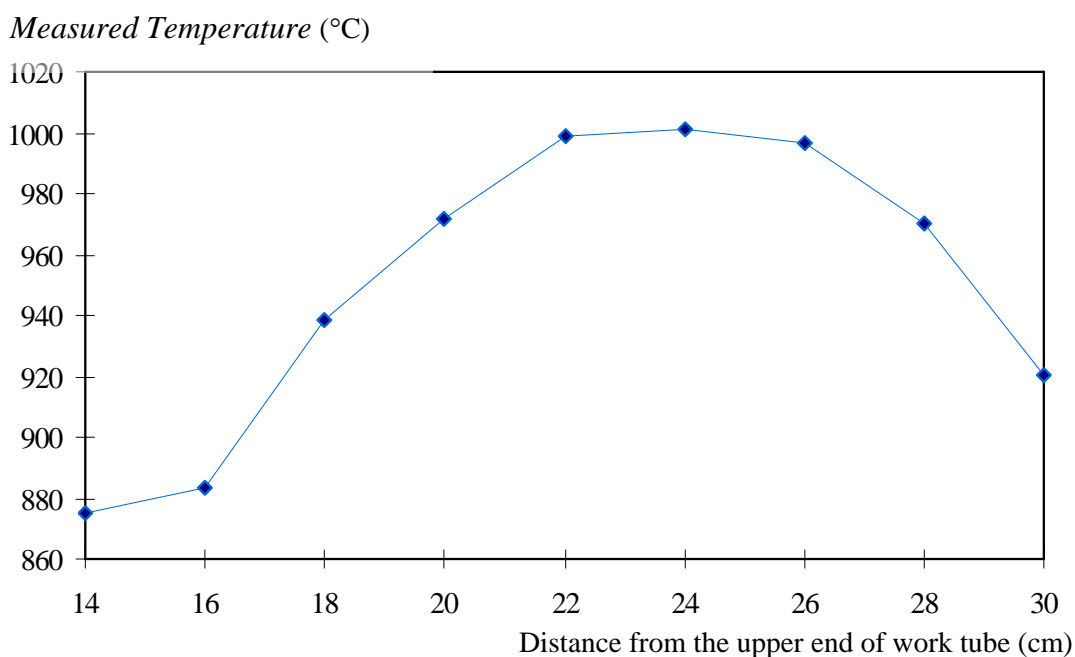


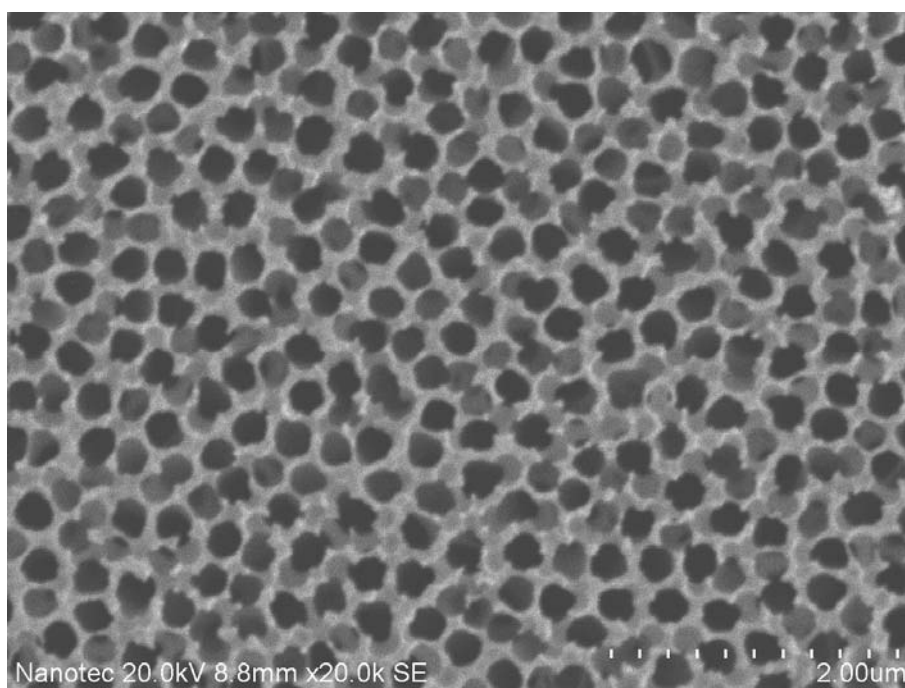
Figure 8 The real temperature inside the work tube at varying position, *Measured Temperature*, in the work tube. The set temperature, *Setpoint Temperature*, is 1175°C. The flow rate of nitrogen gas was 20 ml/min.

3.2. Characteristic of templates used in this study

3.2a. Unheated template

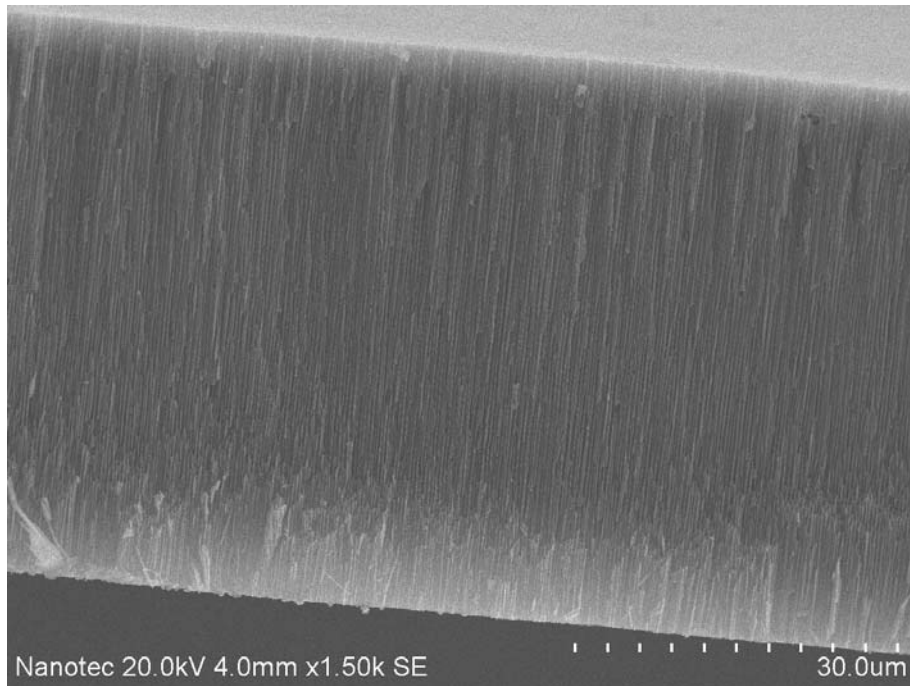
Because the diameter, length, and alignment of the nanotubes grow within the alumina pores should reflect from the original template then the feature of the template used in this study was first examined by using Environment Scanning Electron Microscope (E-SEM Hitachi S3400 with an accelerated voltage of 20 kV). In this work, we use commercially available membrane filter of 25 mm diameter and 60 μm thick (ANODISC25, WHATMAN), whose porosity consisted of an array of parallel and straight channels with average pore diameter of about 200 nm and 20 nm. However, because of the sensitivity limitation of the instrument, only the template whose average pore diameter of 200 nm was characterized here. Figure 9 shows the surface (Figure 9a) and cross section view (Figure 9b-d) E-SEM images of the template. The surface view image shows many uniform openings with average

diameter of about 200 nm of the template. The low magnification cross-section view (Figure 9b) indicates an array of parallel and straight channels perpendicular to the film surface. Thickness of the membrane was about 60 μm . The high-magnification cross-section view image focused on the surface (Figure 9c) indicates the opened-end character of the channels where the image that focused on the middle of the template shows the parallel, straight and hollow structure of the channels. The defect in the structure can also be noticed from the figure, Therefore we suppose that the tubes grown within the channels should be parallel, straight with uniform diameter of about 200 nm and length of 60 μm as the replicates of the channels. However, the imperfect tubes, branched tubes and tubes with diameter variation, can also be formed during the synthesis.

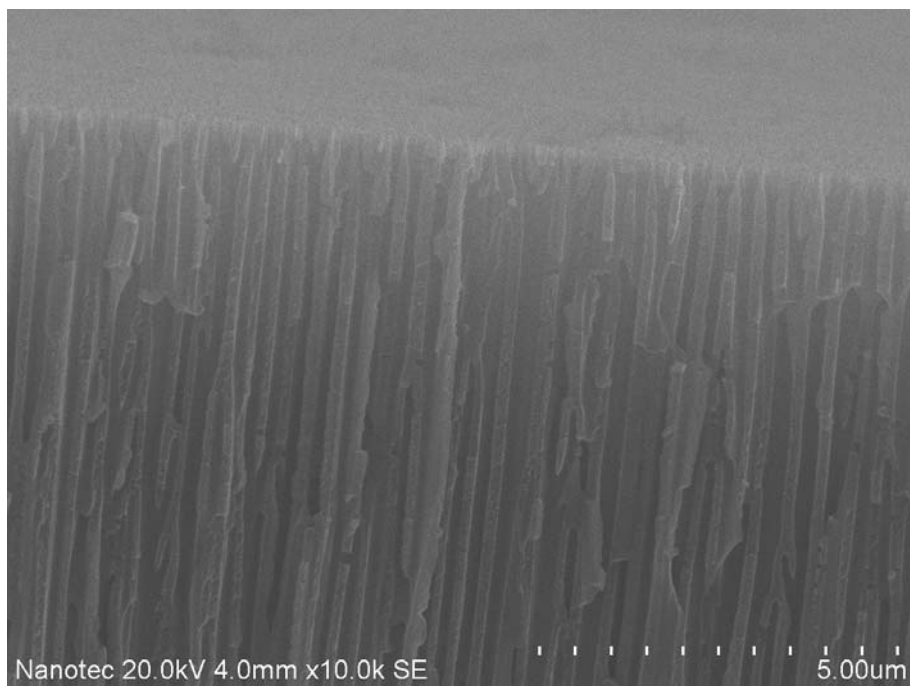


(a)

Figure 9 E-SEM photographs of a commercial aluminum anodic oxide film (ANODISC25, WHATMAN) with 200 nm channel diameter showing a) surface b-d) cross section views.

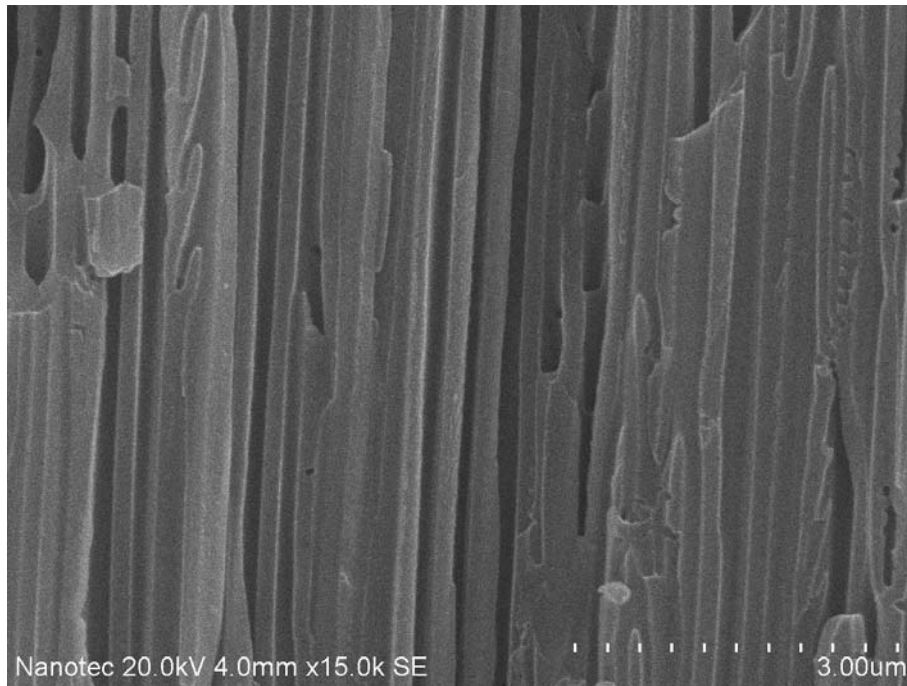


(b)

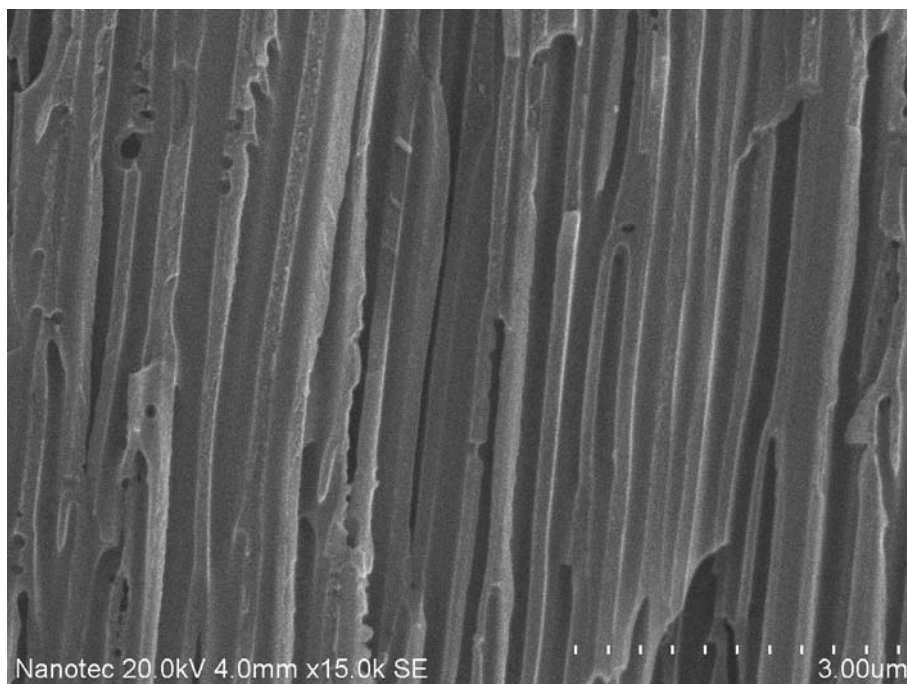


(c)

Figure 9 (continued)



(d)



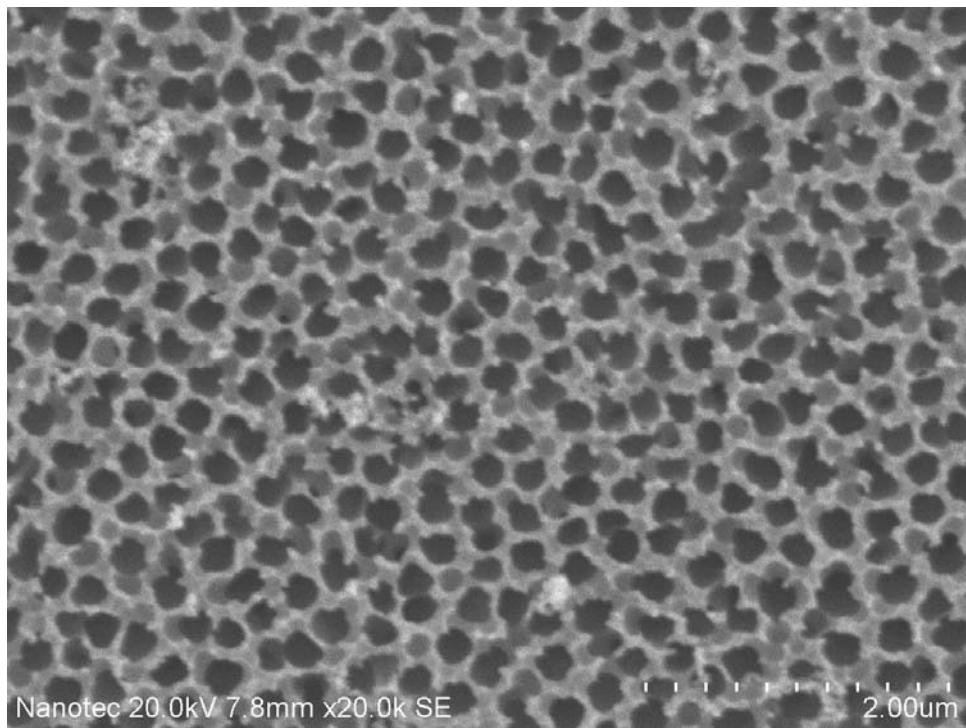
(f)

Figure 9 (continued)

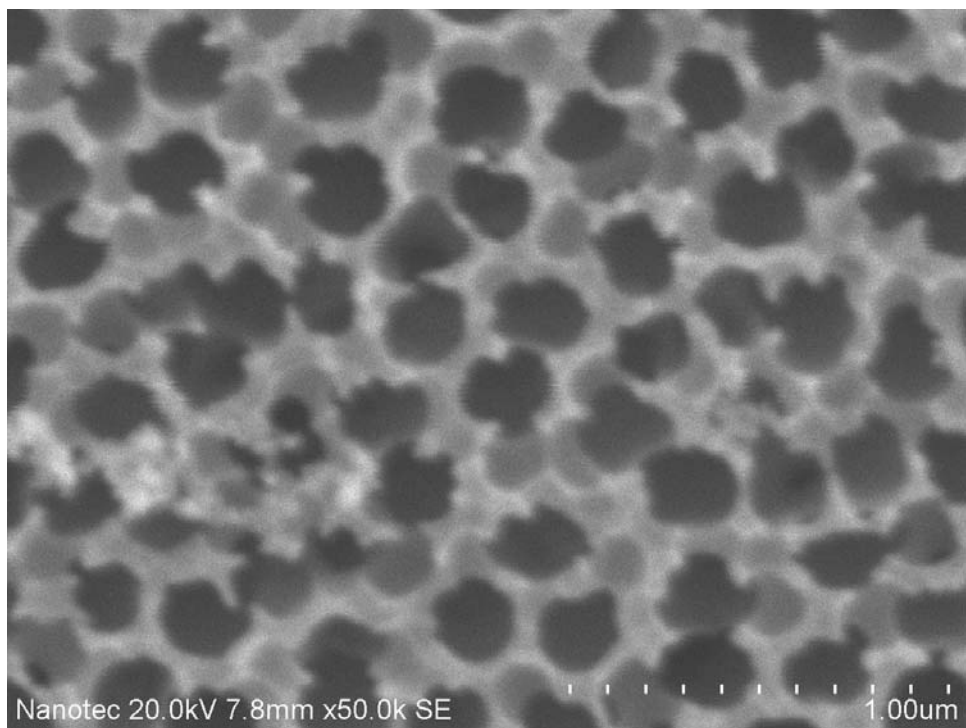
3.2b. High temperature heated membrane

Because we usually observe that templates are curled and rolled up after the synthesis, this situation leads to a question whether there is a significant structural change on the channels of heated membrane during the synthesis or not. To test our supposition, we treated a commercial AAO template which typically used for our CNTs synthesis (average pore diameter = 200 nm) thermally by using the analogue condition that we use for the synthesis. Briefly, the template was heated to 900°C (*Setpoint Temperature* = 1050°C) under 20 ml/min nitrogen flow with heating rate of 10°C/min. After the desired temperature can be read out from the controller, the system was dwelled for 3 h 15 min before allowing to cool down to room temperature under nitrogen ambient.

The surface (Figure 10a-b) and cross section view (Figure 10c-e) E-SEM micrographs, which were performed on a Hitachi S3400 microscope with an accelerated voltage of 20 kV of the membrane, are shown in Figure 10. The low- and high-magnification surface view images (Figure 10a and 10b, respectively) show the variation of pore diameter of the template after heat treatment. The low-magnification cross-section view image (Figure 10c) indicates that the thickness of the template and the array of parallel and straight channels are retained. However, it can be concluded from the high-magnification cross-section view images (Figure 10d and e) that there is partial closure or realignment of the pores at the surface of the specimen.

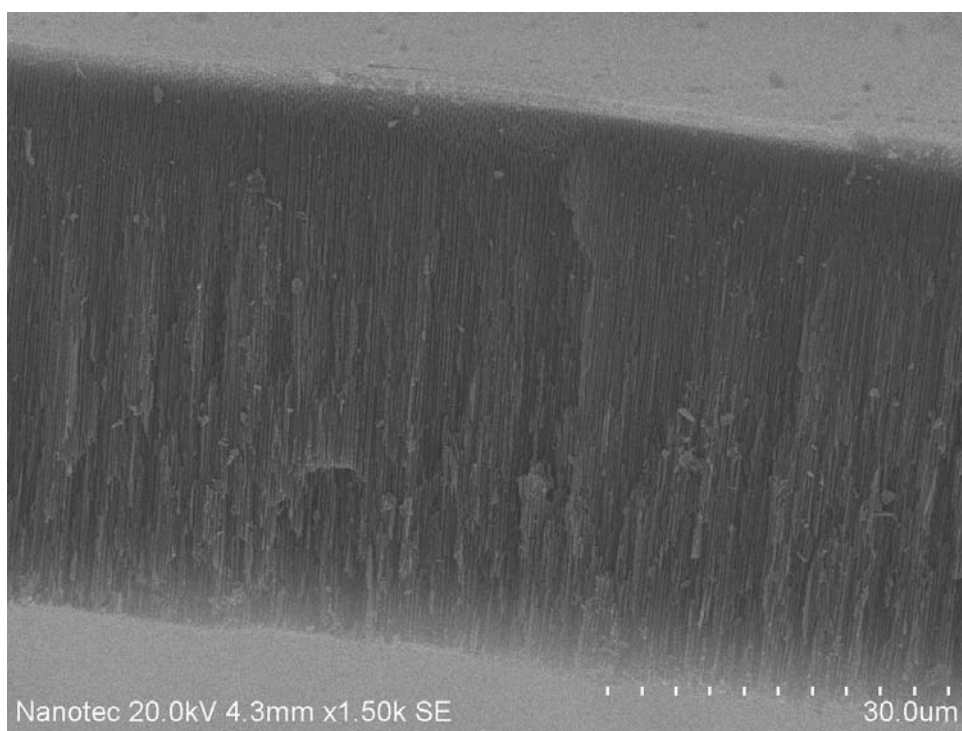


(a)

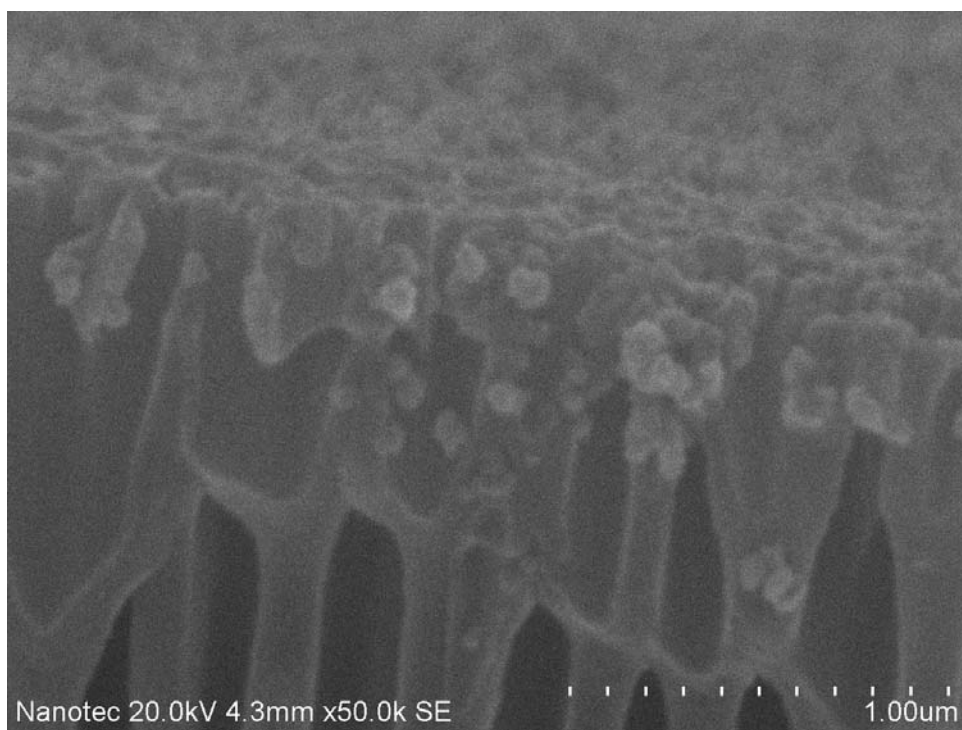


(b)

Figure 10 E-SEM images of heated anodic alumina with nominal 200 nm pore diameter showing the surface (a-b) and cross-section (c-e) view.

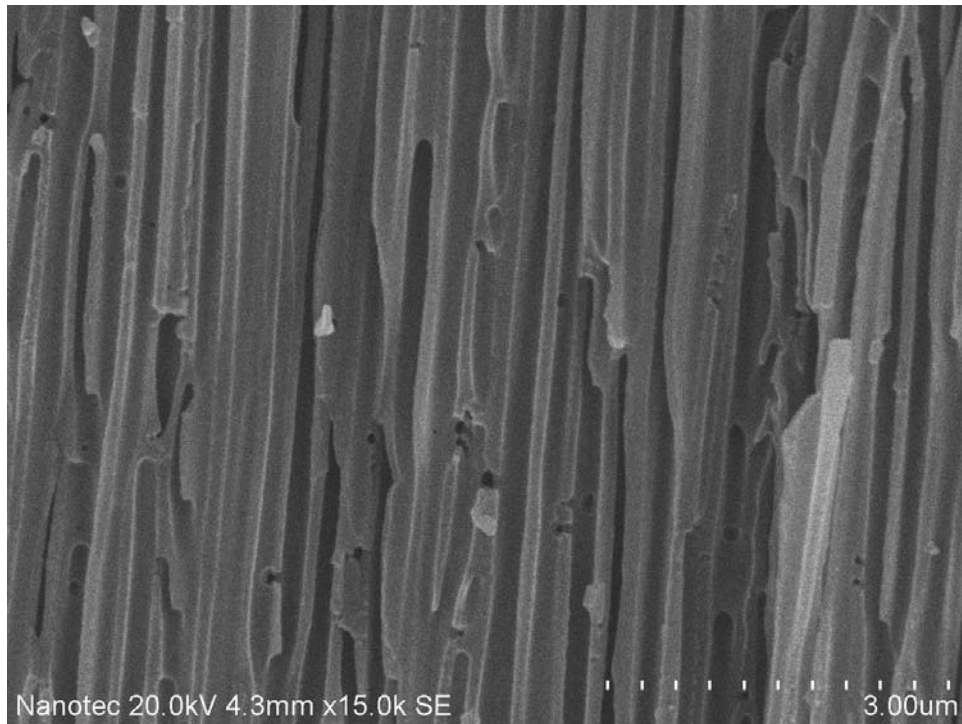


(c)



(d)

Figure 10 (continued)



(e)

Figure 10 (continued)

3.3. Carbon nanotubes synthesized by using the commercial AAO membrane filters with average pore diameter about 200 nm and 20 nm as templates

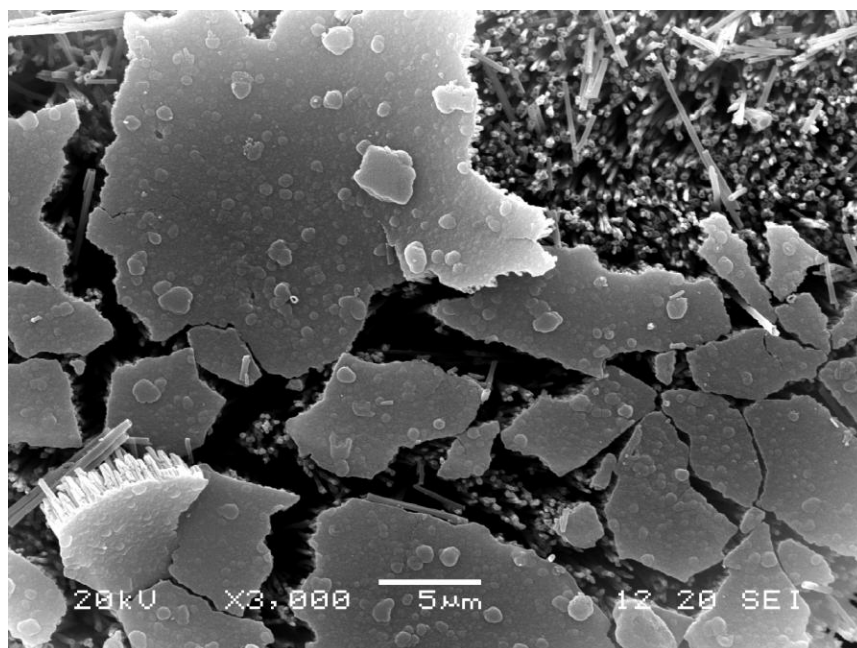
The obtained composite film (CNTs/AAO), which was taken from the work tube after reaction by using a template with pore size 200 nm, was visually observed as Figure 11. The appearance color of the composite is metallic black. In order to dissolve the template, the composite was soaked in an excess amount of 46% HF solution (about 10 ml) at room temperature overnight. However, the CNT growth template was not removed. The original template was readily dissolved in the HF solution. It is known that a non-catalytic CNT growth from a hydrocarbon precursor within a membrane filter is always accompanied by a deposition of amorphous carbon on the membrane surface (Schneider *et al.*, 2006). Then there might be a hard carbon coverage of amorphous carbon deposited on the top of surface. This carbon coverage may prevent the solubilization of the template.



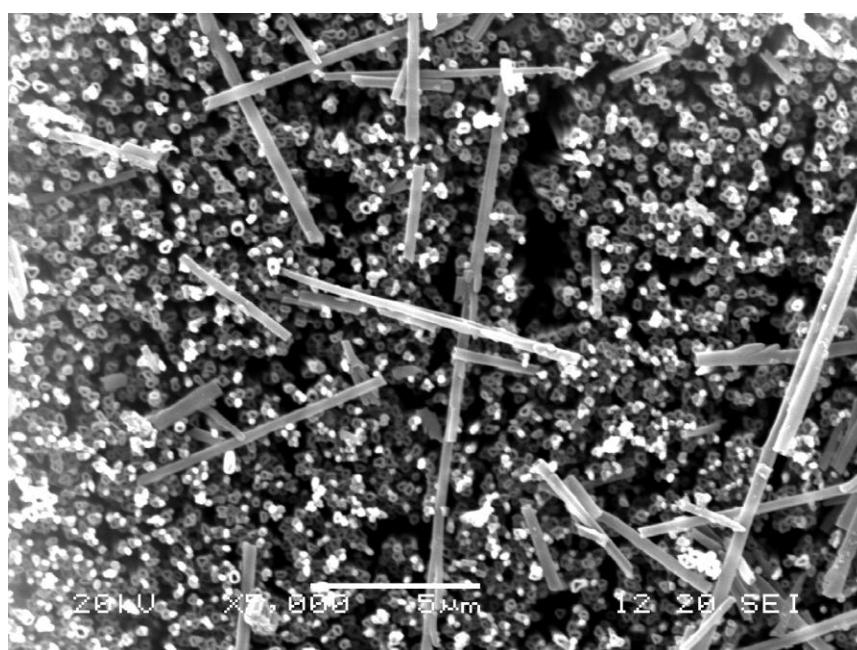
Figure 11 The CNTs/AAO composites obtained from our CVD synthesis.

Scanning Electron Microscopy (SEM) was performed on JSM 5600 LV microscope with an accelerated voltage of 20 kV. Figure 12b notices the opened end nature of synthesized tubes where Figure 12c demonstrates the parallel and straight character of the tubes. Figure 12a and 12c show the dense layer of amorphous carbon on top of the surface of the template. The dissolution problem of the template was solved by crushing the composite to very small pieces before immersed in the 46% HF solution overnight at room temperature.

After centrifugation (10000 rpm, 1 h), particle isolation and rinsing with DI water, drying in an oven at 200°C for 1 h, very light black powders sample was obtained as shown in Figure 13. The total weight of the sample was 0.0337 g. These powers were characterized by Raman spectroscopy. Raman spectroscopy was performed on RENISHAW 2000 Raman microscope with excitation by an Ar laser with excitation wavelength of 514 nm.

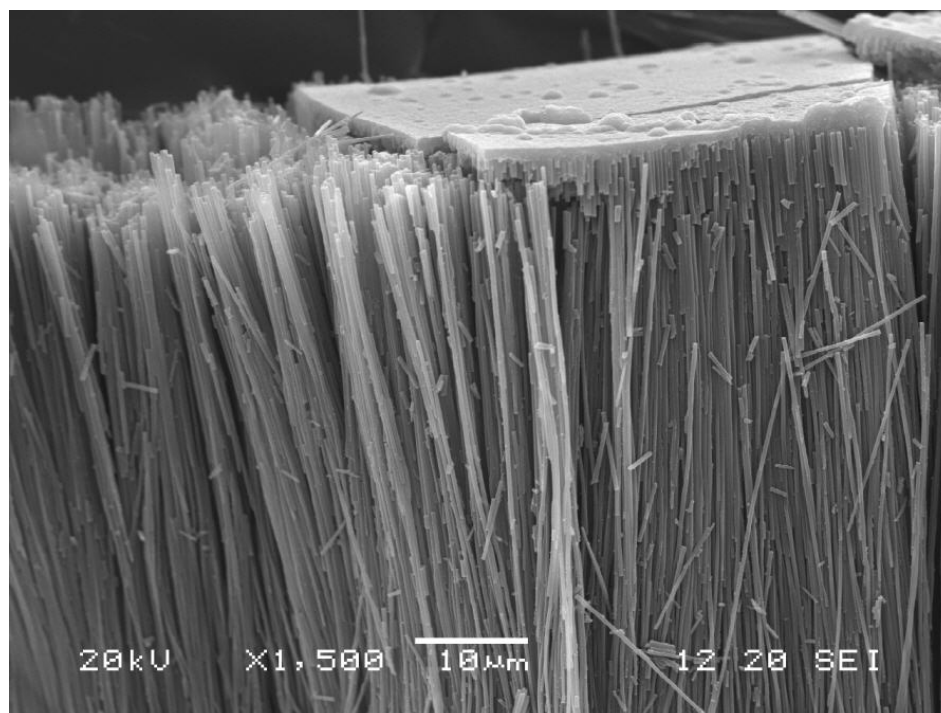


(a)



(b)

Figure 12 Surface view (a-b) and cross-section view (c) SEM images of a specimen taken after synthesis showing a thick carbon overgrowth layer on top of the surface and the opened end nature of synthesized tubes.



(b)

Figure 12 (continued)**Figure 13** Very light black powders obtained after removing template by immersing in HF solution, centrifugation, particle isolation and rinsing with DI water, drying in oven at 200°C for 1 h.

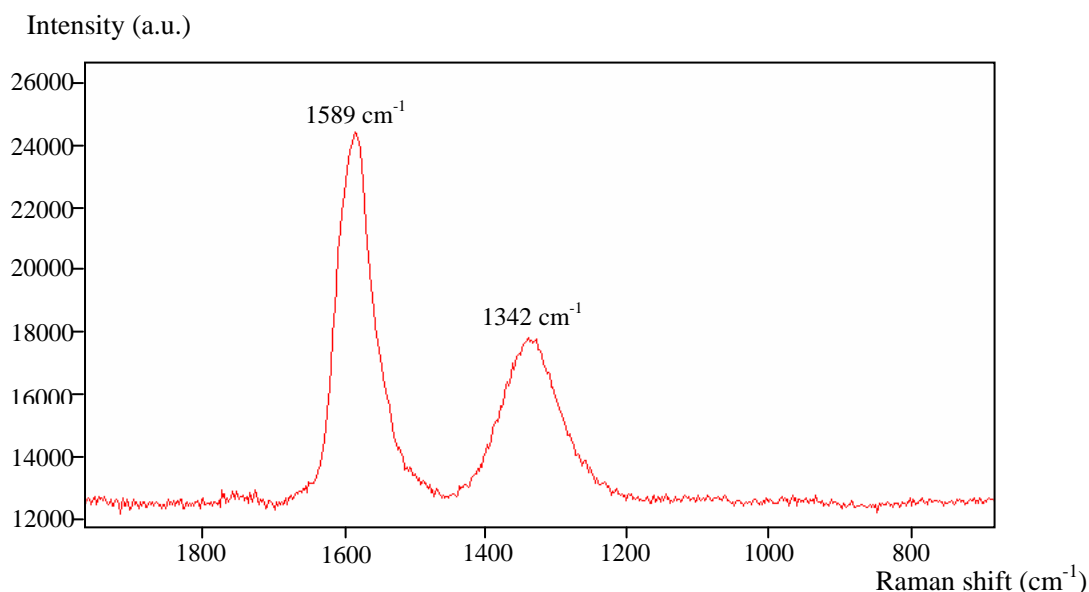


Figure 14 Raman spectrum of CNT sample obtained from the CVD synthesis showing multi-walled structure characteristic.

The Raman spectrum (Figure 14) shows two strong bands at 1342 and 1589 cm^{-1} confirming multi-walled nature of CNT. These bands correspond to fundamental vibration of D_{6h}^4 of graphite (Eklund *et al.*, 1995). The band at 1347 cm^{-1} (D-band) is mainly derived from disordered carbon defects of the MWNTs. This band is one of the in-plane vibrational modes. The band at 1589 cm^{-1} (G-band) corresponds to the Raman allowed optical mode E_{2g} of two-dimensional graphite, i.e. Raman active in-plane vibrational mode for an infinite or finite hexagonal network. As compared to the G-band at 1580 cm^{-1} for the graphitic carbons (Eswaramoorthi and Hwang, 2007), the shift in G-band toward a higher wavenumber (1589 cm^{-1}) suggests a turbostratic structure formation. Raman intensity ratios of two peaks (I_D/I_G) and peak linewidths strongly depend on the crystallinity of carbon materials. A strong D mode corresponds to a lower degree of graphitic ordering (high I_D/I_G) (Kastner *et al.*, 1994). The I_D/I_G value (0.69) obtained here shows that the crystallinity of synthesized CNTs is not high. The low crystallinity of the synthesized CNTs is not expected since the process is without the metal catalyst and would require higher synthesis temperature for obtaining well crystalline CNTs (Jeong, 2004).

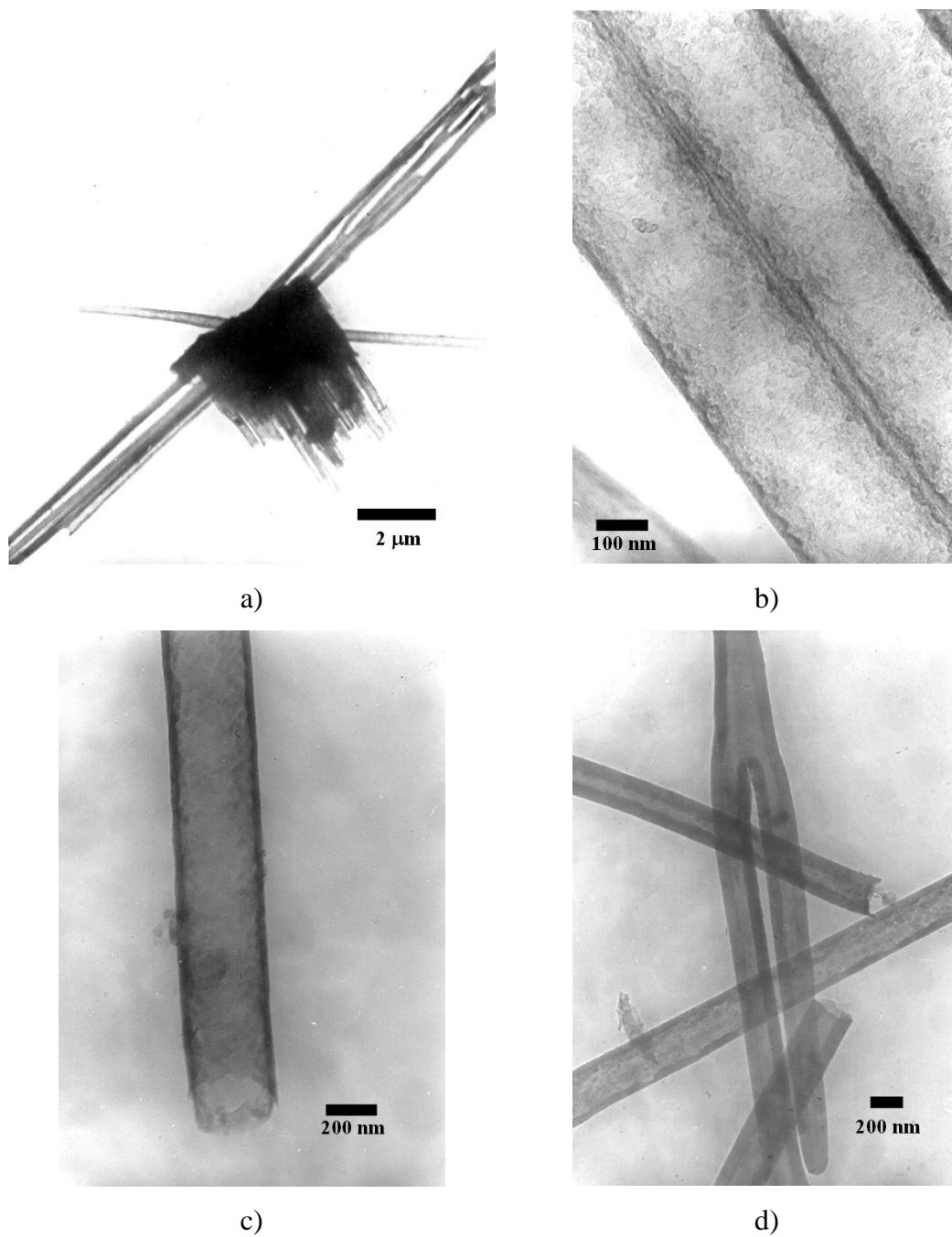


Figure 15 TEM images of CNTs synthesized by the CVD technique showing a) arrays of parallel and straight channels of the synthesized tubes, b) parallel, straight and complete tubes with uniform outer diameter of about 200 nm, c) open ended nature of the synthesized tubes, and d) a synthesized branched tube.

Transmission Electron Microscopy (TEM) was performed on a JEM 1220 microscope with an accelerated voltage of 100 kV. The obtained TEM images were shown in Figure 15. The low-magnification image (Figure 15a) shows arrays of parallel and straight channels of the synthesized tubes. The high magnification image (Figure 15b) reveals the formation of straight and complete tubes with uniform outer diameter of about 200 nm corresponding to the template used. The inner spaces of these tubes are empty. Since the carbon deposits follow the geometry of the AAO template, it is possible to make particularly vary shapes of carbon tubes, depending on the shape of template used.

Figure 15c shows the end of the synthesized tube. The open end structure of the tip is also clearly noticed. This leads the synthetic technique used in this study have many material applications since it is possible to fill the synthesized CNTs by ions and molecules. As previously supposed, the branched tube can also be formed during the synthesis (see Figure 15d) as a copy of the branch channel of the template.

TEM images of the carbon samples obtained with 20 nm diameter size template showed that very few carbon tubes were formed. A typical structure obtained from the synthesis is shown in Figure (16a and 16b). It is found that the tube is not completely formed. The varying of the outer diameter (about 50 nm) of this tube from the average diameter of 20 nm may be explained by a range of diameters in the template itself. The difference of the CNT formation is due to the size different of the template (about 10 times). Due to the much smaller diameter size (20 nm), the entering of gases to the channel is much difficult than that of 200 nm channel diameter. Then the nanotubes can not be formed completely. Increasing carbon source (acetylene) concentration is not expected to increase any the CNTs formation because it will increase the formation of amorphous carbon at the external surface of the template.

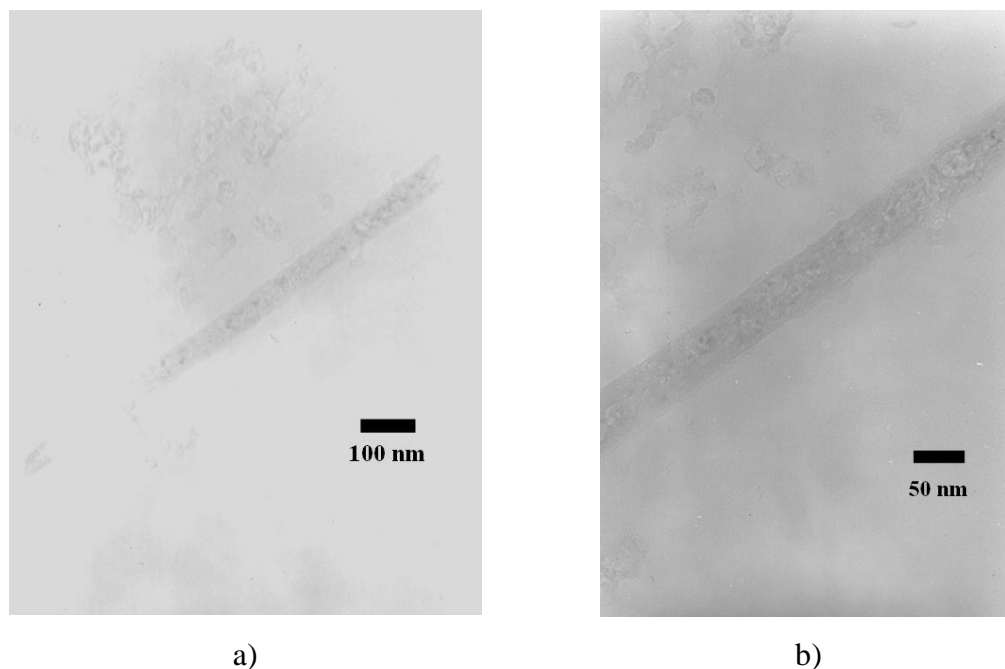


Figure 16 a) Low-magnification and High-magnification TEM image of a typical CNT obtained from CVD synthesis using 20 nm pore diameter template (a commercially available membrane filter of 25 mm o.d. wide, 60 μm thick, average diameter of about 20 nm, ANODISC25, WHATMAN). The growth temperature was 900°C. The reaction time was 3 h. The total gas flow rate was 20 ml/min. The gas mixture composition was 10% acetylene and 90% nitrogen.

4. Conclusion

Using our experimental setup and optimized synthetic system and conditions, carbon nanotubes can be formed by chemical vapor deposition (CVD) method. CNTs here were growth in 200 nm-average pore diameter commercial porous anodic aluminum oxide template with the growth temperature of 900°C, the reaction time of 3 h, the total gas flow rate of 20 ml/min and the gas mixture composition of 10% acetylene and 90% nitrogen. The obtained carbon nanotubes are low crystalline, straight and complete multi-walled carbon nanotubes. Diameter of tubes is uniform corresponding to the pore of the template used. The formation of CNTs inside the AAO pores without any additional metal catalyst is a strong indication of the catalytic

behavior of the internal pore surface of AAO. We supposed that this catalytic activity is uniform and high enough to catalyze the decomposition of 900°C, however, not high enough to produce well-graphitized CNTs. Because synthesized carbon nanotubes produced by this template technique are straight, metal-catalyst free and have an uniform diameter and empty inner space, this technique is expected to be very useful to produce CNTs for many material applications.

By the varying of the average pore diameter template from 200 nm to 20 nm, we found that the structure of 20 nm obtained CNTs differs significantly differs from that of the 200 nm CNTs. The latter are produced as incomplete tubes and the product yield is very low. It can be concluded that if the diameter of the carbon tubes in the range of ten to hundreds of nanometers can easily be controlled by changing the average channel diameter of the anodic oxide film, it is required to reoptimize the synthetic conditions, such as temperature, reaction time or flow rate.

**CHAPTER III. DIELS-ALDER CYCLOADDITION OF SINGLE-WALLED
CARBON NANOTUBES WITH ELECTRON RICH DIENES
: A THEORETICAL STUDY**

1. Introduction

Depending on the structure, the electronic properties of nanotubes become diverse. There are essentially two different types of nanotubes. Single-wall carbon nanotubes (SWCNTs) are the simplest kind. They can be visualized as being formed by rolling a single layer of graphite (called a graphene layer) into a seamless cylinder. Their special properties emerge from the strong one-dimensionality and crystalline perfection of the structure.

Mutiwall carbon nanotubes (MWCNTs), which can be considered as coaxial assemblies of concentric SWCNTs with different diameters, are typically formed with diameters in the range of 2-25 nm (Ajayan, 1999). Due to the geometric constraints in forming the seamless “honeycomb” graphene cylinders, the layers of the MWCNT lack the interlayer structural correlation that prevails in single-crystal graphite (ABAB stacking). Nevertheless, their interlayer distance (approximately 0.34-0.6 nm) is close to that of graphite (0.34 nm). Therefore, MWCNTs tend to exhibit the properties of turbostratic graphite whose layers are essentially uncorrelated. However, we concentrate here on SWCNTs because of their highly ordered structure.

The structure of SWCNTs can be specified by a Bravais lattice vector (see Figure 17) $\overline{C}_h = n\overline{a}_1 + m\overline{a}_2$, where n and m are two integer indices, which depend on the type of nanotube, and \overline{a}_1 and \overline{a}_2 are the primitive lattice vectors of the hexagonal lattice. \overline{C}_h connects two crystallographically equivalent sites, A and A', as shown in Figure 17. The graphene cylinder is formed by connecting together the points A and A' and the cylinder joint is made along the lightly dotted lines perpendicular to \overline{C}_h . The fiber diameter d is defined by

$d = \frac{|C_h|}{\pi} = \frac{a\sqrt{n^2 + nm + m^2}}{\pi}$, where $a = 1.42 \times \sqrt{3} \text{ \AA}$ is the lattice constant. The chiral angle, $\theta = \arctan\left[\frac{-\sqrt{3}m}{2n+m}\right]$, is defined as the angle between $\overline{C_h}$ and the zigzag direction, as shown in Figure 17.

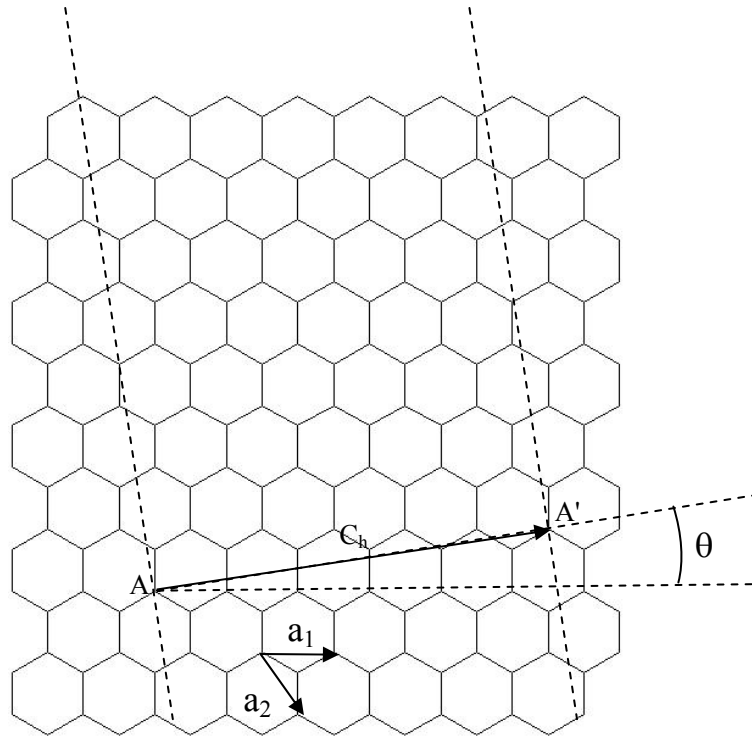


Figure 17 Graphene tubules are made by rolling a graphene sheet into a cylinder. The tubules are uniquely determined by their lattice vectors, $\overline{C_h}$. The chiral angle is denoted by θ , while a_1 , and a_2 , denote the unit vectors of graphite; see text for more details (Saito *et al.*, 1992).

The nomenclature of the various types of SWCNTs is: those with $n = m$ ($\theta = 30^\circ$) are called “armchair”, those with $n \neq 0$ and $m = 0$ ($\theta = 0^\circ$) are called “zigzag”, and all others are called “chiral” because of the arrangement of the hexagons around the circumference (see Figure 18). According to the reference (Saito *et al.*, 1992), an SWCNT will be metallic if it is an armchair one or a zig-zag where $n - m$ is a multiple of three, or a chiral with a specific diameter, as shown in Figure 19. The remaining of SWCNTs are semiconducting.

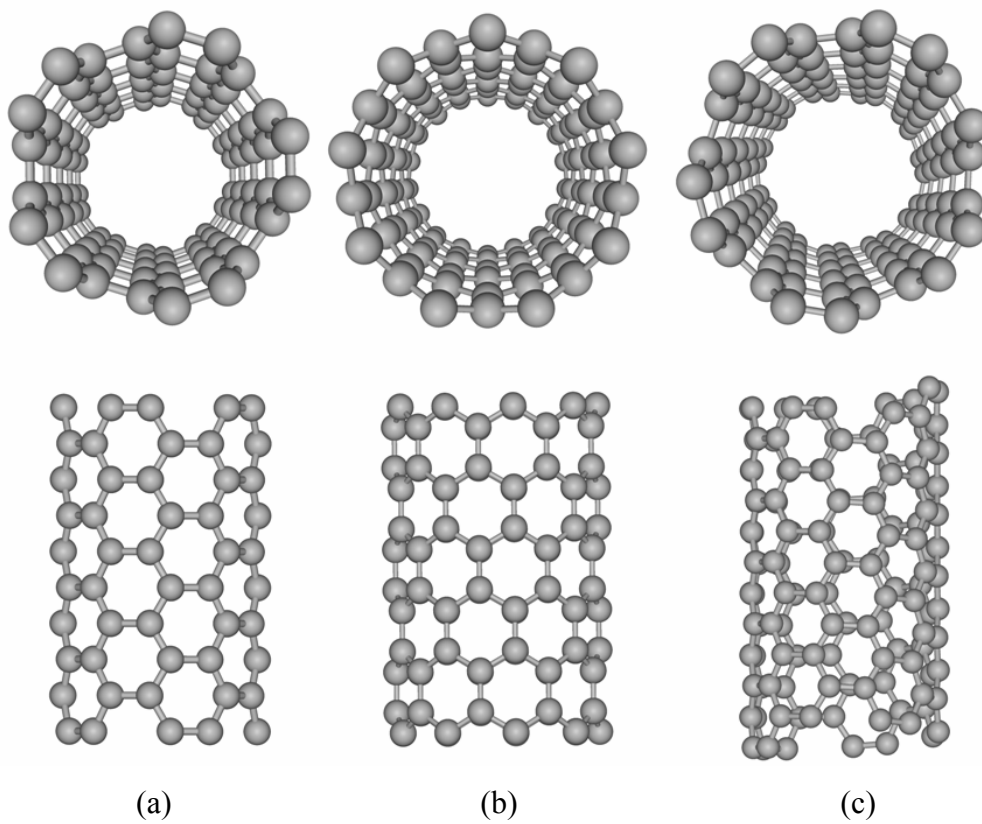


Figure 18 Molecular models of SWCNTs exhibiting different chiralities: (a) armchair configuration ($n = m$ ($\theta = 30^\circ$)), (b) zigzag arrangement ($n \neq 0$ and $m = 0$ ($\theta = 0^\circ$)), and (c) chiral conformation (all other SWCNTs)

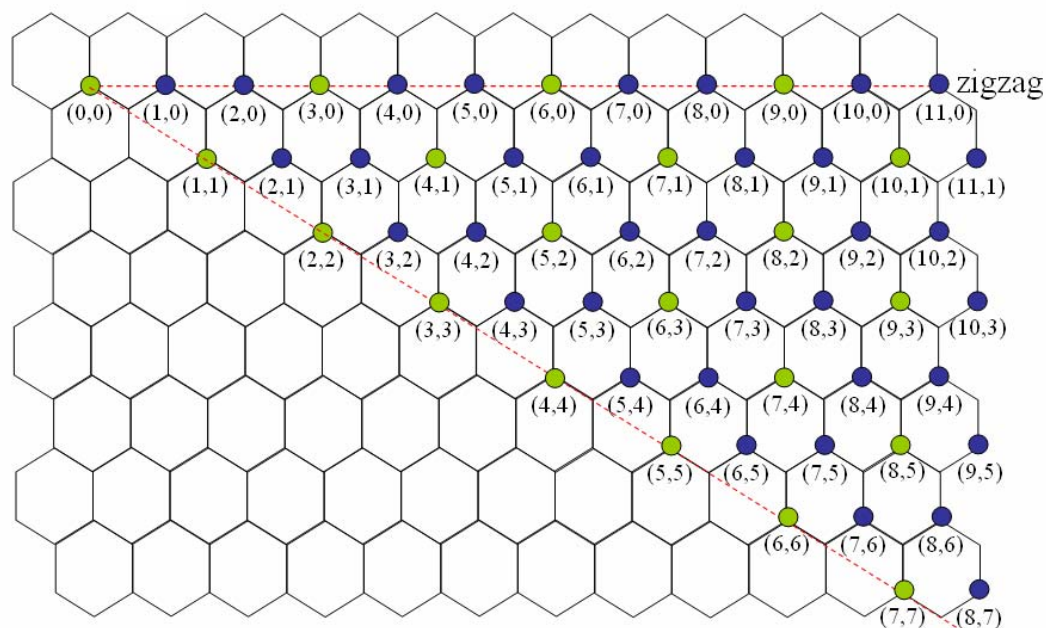
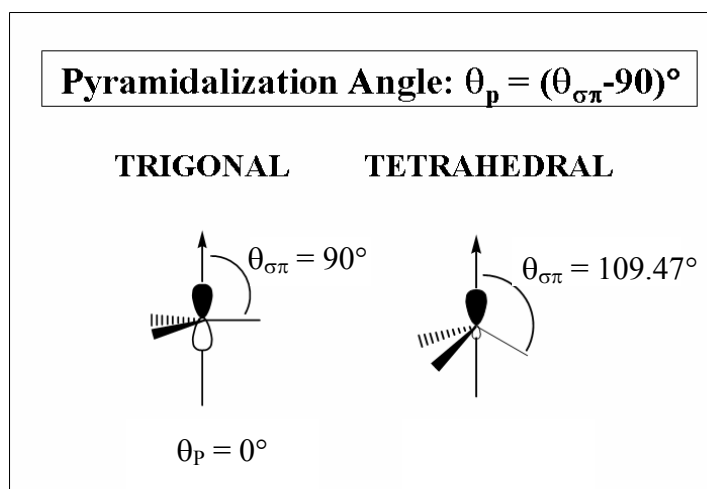
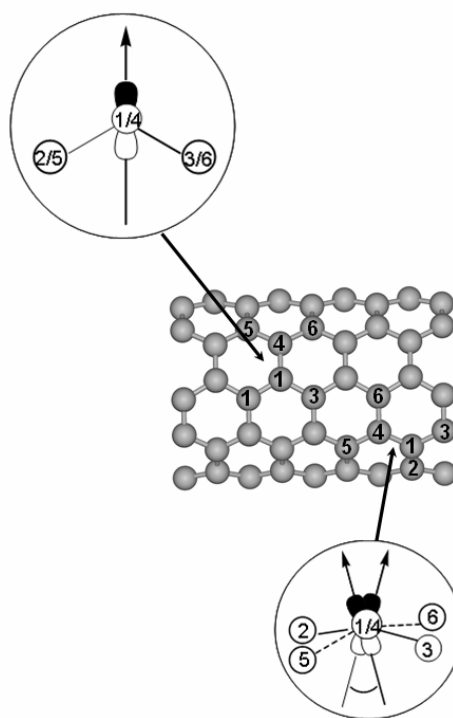


Figure 19 Scheme of the electronic properties of all structures of SWCNTs as a function of their indices (n, m) . The circled dots (●) and dots (●), denote metallic and semiconducting behavior, respectively (Saito *et al.*, 1992).

The strongly covalent sp^2 type of the carbon bonds makes the walls of SWCNTs chemically inert. Consequently SWCNTs are found to be insoluble both in water and organic solvents. This, however, is not always an advantage as it makes it difficult to handle them in industrial processes with current technologies. Another of their features, however, proves helpful here. Their systems are under an enormous strain. This strain, reflected by the pyramidalization angle (θ_p) of the carbon atoms and the π -orbital misalignment between adjacent pairs of conjugated carbon atoms (see Figure 20), can be partially released by the chemical conversion of an sp^2 -hybridized (trigonal) carbon atom ($\theta_p = 6.0^\circ$ for the sidewall of (5,5) SWCNTs) into an sp^3 -hybridized (tetrahedral) carbon atom ($\theta_p = 19.5^\circ$). Various functionalizations on the sidewalls of SWCNTs have taken advantage of this process (Niyogi *et al.*, 2002).



(a)



(b)

Figure 20 Diagram of (a) pyramidalization angles (θ_p) of trigonal and tetrahedral carbon atoms, and (b) the π -orbital misalignment angles between adjacent pairs, the pair perpendicular to the nanotube axis and the pair nearly along the nanotube axis, of conjugated carbon atoms in SWCNTs (Niyogi *et al.*, 2002).

Among these efforts are the solubilization and purification (Chen *et al.*, 2001c; Dyke and Tour, 2004), the derivatization of the tube ends and sides (Bianco and Prato, 2003; Czerw *et al.*, 2001; Lin *et al.*, 2003; Shim *et al.*, 2002; Zhang *et al.*, 2003), the sorting (Zheng *et al.*, 2003), and the assembly (Diao *et al.*, 2002). Such chemical functionalization of nanotubes provides some new physical and chemical properties for several specific applications, including catalysis, catalyst support, sensor, gas storage and component in high performance composites. It has been shown experimentally that covalent sidewall functionalizations of SWCNTs can be reached by means of fluorination (Khabashesku *et al.*, 2002; Mickelson *et al.*, 1998), addition of alkyl radicals (Holzinger *et al.*, 2001), [2 + 1] cycloaddition (Chen *et al.*, 1998; Holzinger *et al.*, 2001), 1,3-dipolar cycloaddition (Georgakilas *et al.*, 2002a; Georgakilas *et al.*, 2002b), arylations (Bahr *et al.*, 2001; Dyke and Tour, 2003a), ozonolysis (Banerjee and Wong, 2002a), and osmylation (Cui *et al.*, 2003).

2. Theoretical approaches

A lot of theoretical studies have been reported in order to predict the reactions on the sidewalls of SWCNTs: ozonization (Lu *et al.*, 2002c), 1,3-dipolar cycloaddition (Lu *et al.*, 2002c; 2003a), [4 + 2] cycloaddition (Lu *et al.*, 2002b), osmylation (Lu *et al.*, 2002a), [2 + 1] cycloaddition (Lu *et al.*, 2003b), and epoxidation (Lu *et al.*, 2003c). These studies demonstrated the plausibility of functionalizing the sidewalls by means of synthetic organic chemistry. In order to determine accurate geometries, mechanisms and energies of SWCNTs functionalizations, where chemical bonds are broken or formed, very accurate quantum chemistry methods are required. However, due to the large number of atoms of the SWCNT, accurate computations with high-level methods are limited by their extreme computational demand, yet the use of any low-level method is not able to describe the bond breaking/forming sufficiently accurately.

The problem can be alleviated by the partitioning of the system into two or more parts or layers, where the interesting or difficult part of the system (the inner layer) is treated at a ‘high’ level of theory and the rest of the system (the outer layer) is described by a computationally less demanding method. This idea is not new and many different implementations can be found in the literature (Bakowies and Thiel, 1996a; 1996b; Maseras and Morokuma, 1995; Gao, 1995; Field *et al.*, 1990; U. Singh and Kollman, 1986).

These hybrid methods differ mainly into two aspects (Dapprich *et al.*, 1999). First, there are different ways to treat the boundary region of the different parts of the molecule. If there is no covalent between the layers, there is no special boundary region. A typical case is a solvated system, where the solvent molecules form the outer layer and the solute is the inner part which is treated by a higher level method. However, if one is interested in the accurate description of a particular region of a large organic molecule or a macromolecule, covalent bonds have to be cut in order to generate the inner model system. This process leaves dangling bonds at the border of the inner layer, which have to be saturated in order to avoid a chemically unrealistic model. The most frequent approach to solve this problem is saturating the dangling bonds of the inner fragment, at the boundary between different levels, with hydrogen as link atoms.

The second crucial aspect in all the hybrid schemes is the interaction between the inner and the outer layer part of the system. If the total energy $E(X-Y)$ of the entire system $X-Y$ (inner region X , outer region Y) is defined as

$$E(X-Y) = E_{interlayer}(X-Y) + E_{low}(X) + E_{high}(X) \quad \dots(1)$$

with $E_{interlayer}(X-Y)$ being a separate interaction energy between the two layers (Gao, 1995), this may be referred to as a “connection scheme”. On the other hand, if the total energy $E(X-Y)$ is calculated according to

$$E(X-Y) = E_{low}(X-Y) - E_{low}(X) + E_{high}(X), \quad \dots(2)$$

then this shall be referred to as an “embedding” or “extrapolation” scheme (Stephane *et al.*, 1996). The latter case has the advantage that there is no necessity for a special interaction ‘coupling’ Hamiltonian, since the interaction between the two layers is consistently treated at the low level of theory, but it has the disadvantage that the low level is also present in the inner layer and might spoil the high-level calculation.

3. Some background on the ONIOM approach

A hybrid implementation that shows a good performance and has a wider applicability, is the ONIOM (abbreviated from “our-Own-N-layered-Integrated molecular Orbital and molecular Mechanics”) method (Svensson *et al.*, 1996). This method is an extrapolation scheme.

In the ONIOM approaches (Dapprich *et al.*, 1999; Maseras and Morokuma, 1995), a molecular system can be divided into onion shell-like layers as shown in Figure 21. Every layer can be treated at an arbitrary level of theory ranging from an MM level for describing the steric and electrostatic effects of the exterior part of the system, some intermediate levels of MO methods describing the electronic effects of functional groups or ligands close to the center of action, and finally, a highly accurate method to deal with the electron correlation at a very high level theory on the most important action center of the system. The selection of the atoms included in the *model* and the level of theory in that part of the system (high-level), as well as the level of theory for the outer layer (low-level), are the limiting factors regarding the accuracy of the results.

The basic idea behind the ONIOM approaches can be explained most easily when it is considered as an extrapolation scheme in a two dimensional space spanned by the size of the system on one axis and the level of theory on the other axis (Dapprich *et al.*, 1999; Maseras and Morokuma, 1995), as shown in Figure 22.

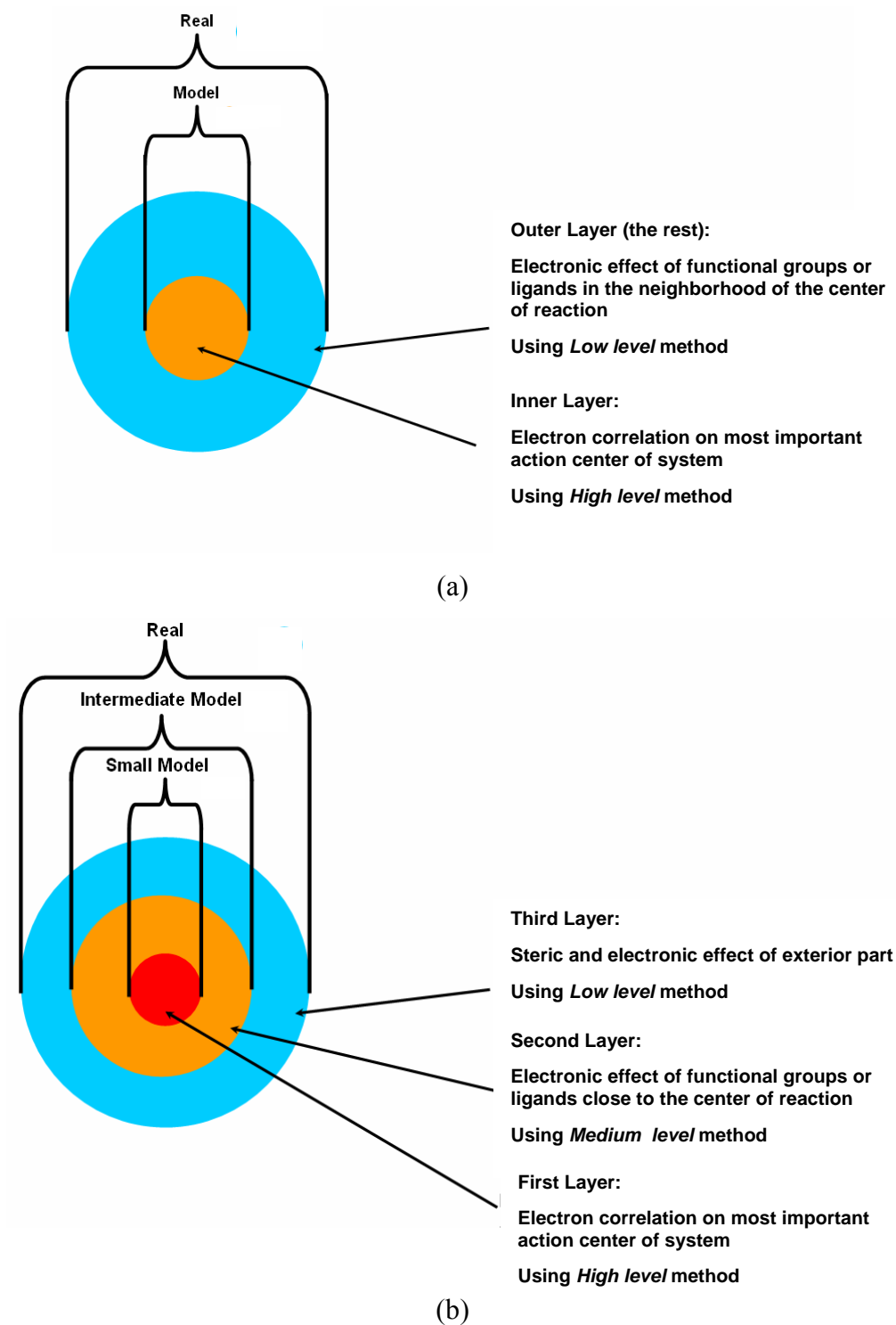


Figure 21 Schematic concept of the ONIOM method: (a) the two-layers ONIOM approach (ONIOM2) (b) the three-layers ONIOM approach (ONIOM3) (Dapprich *et al.*, 1999; Maseras and Morokuma, 1995).

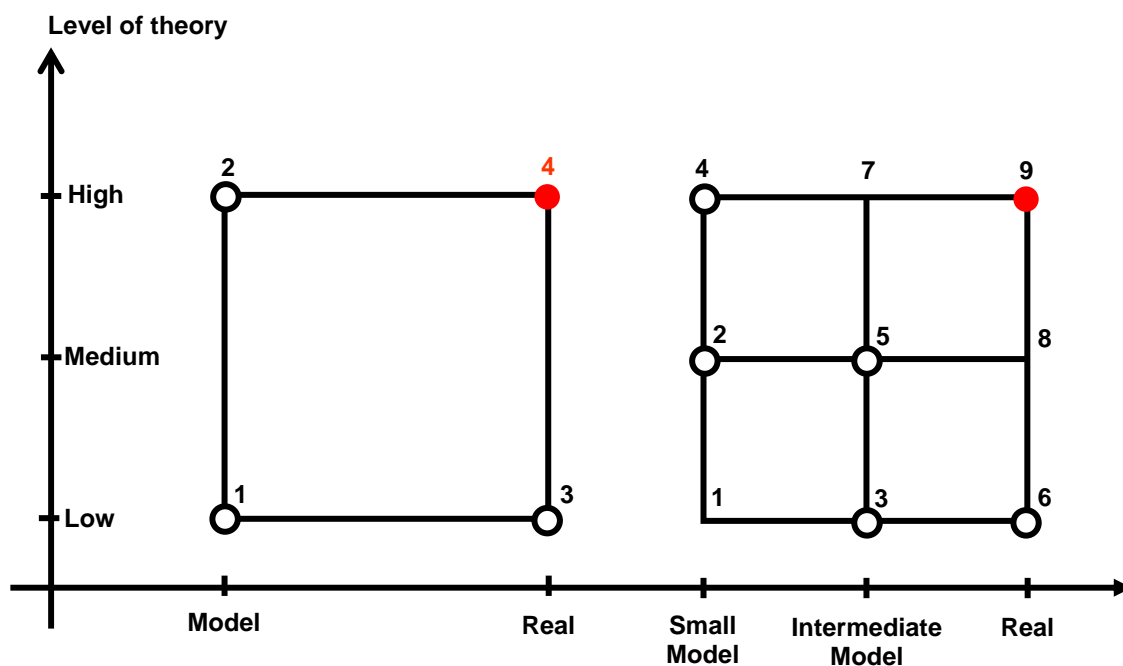


Figure 22 Schematic representations of the ONIOM extrapolation schemes for a molecular system portioned into two (left) and three (right) layers. See text for description (Dapprich *et al.*, 1999; Maseras and Morokuma, 1995).

Figure 22 shows the extrapolation procedure schematically. The target energy, the energy of the real system at a high level can be approximated by a system partitioned into two layers can be considered to have an energy, E_{ONIOM2} , which is defined as:

$$E_{ONIOM2} = E_4 = E_3 - E_1 + E_2 \quad \dots(3)$$

In a system consisting of three layers, the extrapolated energy of the entire system calculated at high level of theory is defined as

$$\begin{aligned} E_{ONIOM3} &= E_9 \\ &= E_6 - E_3 + E_5 - E_2 + E_4 \quad \dots(4) \end{aligned}$$

4. Functionalization of SWCNTs studied by ONIOM

SWCNT functionalizations have been extensively studied by the ONIOM method, mostly the ONIOM2 in which the inner layer was treated by the density functional theory (DFT) with the Becke's hybrid 3-parameter nonlocal exchange functional (Axel, 1992a; 1992b; 1993), with Lee, Yang, and Parr's nonlocal correlation functional (Lee *et al.*, 1988), using the 6-31G(d) basis set (B3LYP/6-31G*) level of theory and the outer layer was treated as the semiempirical Austin model 1 (AM1) (Dewar and Thiel, 1977) approach. Here a middle part of a short tube, mostly C₁₆ cluster of C₁₃₀H₂₀ ((5,5)-armchair) (see Figure 23), was treated as a model (Lu *et al.*, 2002a; 2002b; 2002c; 2003a; 2003b; 2003c). Since it was previously found that the armchair single-walled carbon nanotube is the most thermodynamically stable tube (among all kinds, armchair, zigzag and chiral single-walled carbon nanotubes) (Okotrub *et al.*, 1998) then the armchair single-walled carbon nanotubes, especially (5,5) SWNT, which is considered as a chemically reactive armchair tube because it is small in size and exhibits high curvature (Lin *et al.*, 2005), are typically used as the typical model for studying the SWCNT functionalizations (Lu *et al.*, 2002a; 2002b; 2002c; 2003a; 2003b; 2003c).

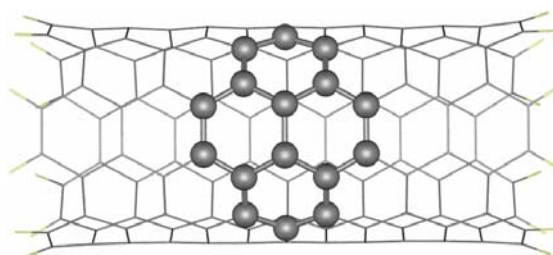


Figure 23 The ONIOM2 model of a CNT that has been extensively used for studying functionalization of SWCNTs ('*Real*' is C₁₃₀H₂₀ cluster (typically treated with B3LYP/6-31G* level of theory) and '*Model*' is C₁₆ cluster (typically treated at the AM1 level of theory, see the highlighted atoms in the figure) (Lu *et al.*, 2002a; 2002b; 2002c; 2003a; 2003b; 2003c).

Based on an idea that studying the properties of the middle part of a relatively short tube leads to the properties which are good approximations to the infinitely long ones (Li *et al.*, 2002), this ONIOM scheme (*Real*: C₁₃₀H₂₀ cluster, *Model*: C₁₆ cluster) provides the possibility to study the properties of the whole tube (SWCNTs have a typical length about 1-50 μm (Hernadi *et al.*, 1996)) which is impossible to simulate. Furthermore, although both the experimental and theoretical investigations confirm that the carbon nanotubes have either open or capped ends and it is suggested that the chemical reactivity of the tip is more active than the sidewall in carbon nanotubes (Slanina *et al.*, 2003), it is reasonable to predict the chemical modifications on the sidewall, which is expected to be a reaction site mainly. This is due to the sidewall area being the majority.

Among SWCNTs functionalizations that have been reported, including cycloaddition (Lu *et al.*, 2002b; 2003b), epoxidation (Lu *et al.*, 2003c), oxidation (Lu *et al.*, 2002a), hydroboration (Long *et al.*, 2003), and ozonizations (Lu *et al.*, 2002c), the Diels-Alder reaction, the [4+2] cycloaddition seems to be one of the most attractive reactions to introduce new functional groups on SWCNTs. This is because it requires only heat or light for initiating the reaction (Fleming, 1976). However, a previous theoretical study on the Diels-Alder reaction of a typical diene, 1,3-butadiene, with SWCNTs (here acts as a dienophile) using the ONIOM(B3LYP/6-31G*:AM1) approach (Lu *et al.*, 2002b) suggested that the reaction is kinetically and thermodynamically unfavorable ($E_a = 32.4$ kcal/mol and $E_r = -1.6$ kcal/mol) compared to the simplest dienophile, ethylene ($E_a = 22.4$ kcal/mol (Rowley and Steiner, 1951) and $E_r = -43.1$ kcal/mol (Uchiyama *et al.*, 1964)). A difference of about 10 kcal/mol in the activation barrier (E_a) and about 40 kcal/mol in the reaction energy (E_r) is very significant and clearly shows that SWCNTs have a low viability for Diels-Alder reactions. Thus, our first objective is to study the possibility to increase the Diels-Alder functionalization viability of SWCNTs by using a reactive diene. The consideration about the reactive dienes (for the Diels-Alder reaction) is discussed in next section.

Some background on the Diels-Alder reaction and the Frontier Molecular Orbitals (FMOs)

The Diels-Alder reaction is an organic chemical reaction (specifically, a cycloaddition) between a conjugated diene (a molecule with two alternating double bonds which are not directly next to each other, but rather separated by a single bond in between them) and a substituted alkene (an unsaturated chemical compound containing at least one carbon-to-carbon double bond), commonly termed the dienophile, to form a substituted cyclohexene system (see Figure 24). Here the three double bonds in the two starting materials are converted into two new single bonds and one new double bond in a single step. Because the diene has four pi-electrons that shift position in the reaction and the dienophile has two, the Diels-Alder cycloaddition is classified as a [4+2] process.

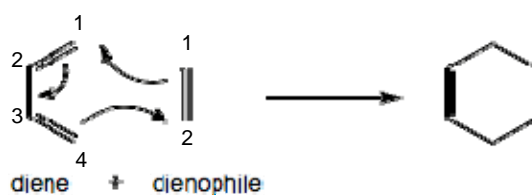


Figure 24 The simplest Diels-Alder Reaction is the reaction of 1,3-butadiene and ethylene to yield cyclohexene.

The simplest Diels-Alder reaction of ethylene with 1,3-butadiene is not efficient and requires high temperatures. Rapid reactions occur when the dienophile has electron-withdrawing substituents (like $-\text{NO}_2$, $-\text{CN}$, $-\text{COR}$, etc) and the diene has electron-donating substituents (like $-\text{OR}$, $-\text{NR}_2$, etc). The reactions here are known as the "normal electron demand" Diels-Alder reactions. Less commonly, rapid Diels-Alder reactions occur when an electron-poor diene and an electron-rich alkene are used; these reactions are called "inverse electron demand" Diels-Alder reactions. In order to understand this pattern of reactivity it is useful to use the Frontier Molecular Orbital (FMO) theory.

As first expressed by Fukui (Fukui, 1971; 1981), the FMO theory continues to be utilized extensively by synthetic organic chemists to help them predict the reactivity and selectivity of many organic reactions (Fleming, 1976). Within this FMO approach, most of the determining factors governing a chemical reaction involve the FMOs, the highest occupied and lowest unoccupied molecular orbitals (HOMO and LUMO) respectively, of the electron donor and electron acceptor pair. The basic quantities here are the molecular orbital coefficients and the intermolecular HOMO-LUMO gap.

The π molecular orbitals of 1,3-butadiene and ethylene and the electron configuration in such orbitals are shown in Figure 25. As pertains to the Diels-Alder reaction, predictions of reactivity and selectivity are normally based on the strength of the FMO interactions, the occupied orbitals of one and the unoccupied orbitals of the other component, either HOMO (diene) and LUMO (dienophile) (normal electron demand type) or HOMO (dienophile) and LUMO (diene) (inverse electron demand type), that having the smaller energy gap (the energy difference between the two orbitals), electrons are thus easily traded (from the occupied orbitals of one and the unoccupied orbitals of the other component). The FMOs which participate in the normal and inverse electron-demand Diels-Alder cycloadditions are shown in Figure 26.

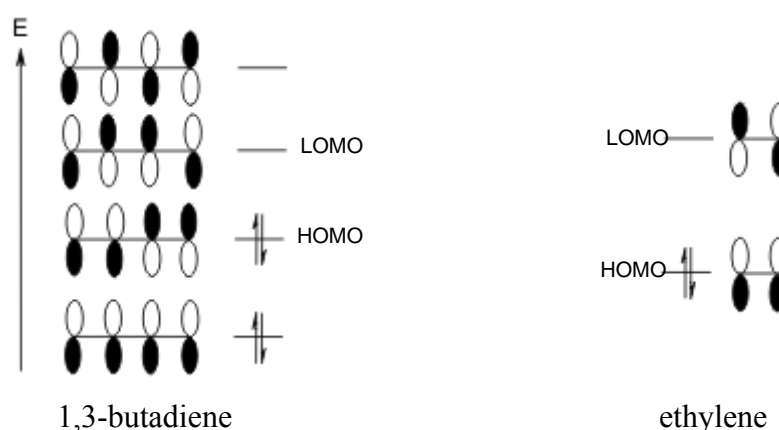
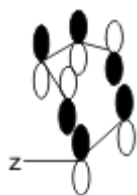


Figure 25 Diagram of the π molecular orbitals of 1,3-butadiene and ethylene and the electron configuration in those orbitals.



Normal electron demand type



Inverse electron demand type

Figure 26 The π molecular orbitals of 1,3-butadiene and ethylene that correspond with the FMOs in the normal and inverse electron-demand Diels-Alder cycloadditions.

If the energy gap between the HOMO (diene) and LUMO (dienophile) is less than that between the HOMO (dienophile) and LUMO (diene) thus, the dominant interaction here is the HOMO (diene) and LUMO (dienophile), the reaction will be rapid when the dienophile has electron-withdrawing substituents (use the ethylene structure as the reference) and the diene has electron-donating substituents (use the 1,3-butadiene structure as the reference). Because the donor substituent (abbreviated as D) increases the energy of the HOMO and LUMO while the acceptor substituent (abbreviated as A) lowers the energy of both FMOs, then finally the energy gap between the HOMO (diene) and LUMO (dienophile) is decreased from that of non-substituted reactants (see Figure 27a). The result being, electrons are readily traded from the HOMO (diene) to the LUMO (dienophile) and the reaction occurs rapidly.

On the other hand, if the energy gap between the HOMO (dienophile) and LUMO (diene) is less than that between the HOMO (diene) and LUMO (dienophile), then the dominant interaction is the interaction between the HOMO (dienophile) and LUMO (diene). Therefore, the reaction will be rapid when the diene has electron-withdrawing substituents and the dienophile has electron-donating substituents because the energy gap between the HOMO (diene) and LUMO (dienophile) is decreased from that of non-substituted reactants (see Figure 27b). As a result, the reaction goes on more readily since electrons are readily traded (from the HOMO (dienophile) and the LUMO (diene)).

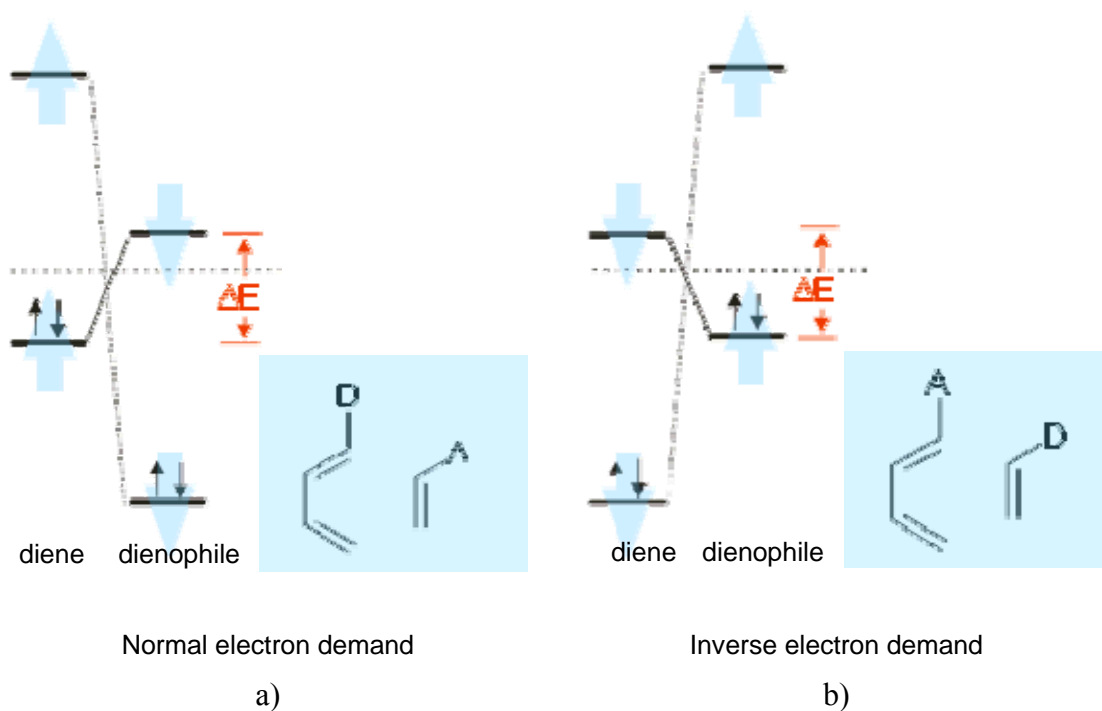


Figure 27 Diagram showing FMOs level and the corresponding electron configuration of diene and dienophile. Blue arrow shows changing in the FMOs in the a) normal and b) inverse electron-demand Diels-Alder cycloadditions when the reaction is facilitated by some substituents group. D and A are abbreviations for a donor substituent and an acceptor substituent, respectively.

As previously mentioned, the viability of the normal electron demand type Diels-Alder reaction is increased when the dienophile has electron-withdrawing substituents and/or the diene has electron-donating substituents, which means that the reaction viability is increased when the dienophile has an electron deficiency character and/or the diene has an electron-rich character. Then, in order to study the possibility to increase the Diels-Alder functionalization viability of SWCNTs, the first way that was expected to have the ability to increase reaction viability, the using of electron-rich diene for the Diels-Alder reaction of SWCNT was studied. For this study the selected diene is a diene of 2,3-dioxy-substitued-1,3-butadienes, 2,3-dimethylene-1,4-dioxane (see structure in Figure 28). The choice of this diene is due to its high reactivity (compared with other dienes in the 2,3-dioxy-substitued-1,3-

butadienes group, an electron-rich dienes group that the Diels-Alder products obtained from this group will be precursors of valuable functionalities like acryloin or diketone derivatives, which can be easily further functionalized (Torres-Garcia and Mattay, 1996)).

Because the previous study of the Diels-Alder reaction of 2,3-dioxy-substitued cis-fixed butadienes with C_{60} (see Figure 28) (Torres-Garcia and Mattay, 1996) showed that the Diels-Alder reactivity has been related to the distance between the carbons in the butadiene moiety ($R_{1,4}$): the reaction rate is higher as the distance is shorter (see Figure 28). This guided us to the conclusion that the Diels-Alder reactivity is not only influenced by the substituents on the diene and dienophile molecule, but also influenced by this $R_{1,4}$ distance.

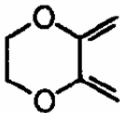
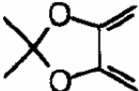
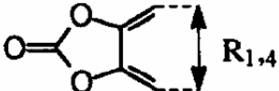
			
Diene	<i>2,3-dimethylene-1,4-dioxane</i>	<i>4,5-dimethylene-2,2-dimethyl-1,3-dioxalane</i>	<i>4,5-dimethylene-1,3-dioxolan-2-one</i>
$R_{1,4}$	322.6	338.5	340.9
Reactivity	high	medium	low

Figure 28 The Diels-Alder reactivity with 2,3-dioxy-substitued cis-fixed butadienes with C_{60} relates as a function of the distance between the carbons in the butadiene moiety ($R_{1,4}$) of the diene (Torres-Garcia and Mattay, 1996).

Then, from this additional important information, we are also interested in studying the influence of the $R_{1,4}$ distance on the Diels-Alder reactivity. Because the influence of substituents on the diene molecule and the influence of $R_{1,4}$ distance have not been compared before and they could competitively have influence on the reaction. We then studied the Diels-Alder reactivity of two additional dienes (the

previous one was *2,3-dimethylene-1,4-dioxane*), the first one is 1,2-dimethylene-1,4-dioxane (this diene has a comparable $R_{1,4}$ distance with that of the previous diene, (see details in Results and Discussion section), and another one is the 4,5-dimethylene-1,4-dioxalane (this is a diene in the 2,3-dioxy-substitued-1,3-butadienes group and is a comparable substituent group with that of the *2,3-dimethylene-1,4-dioxane*) with SWCNT. These studies are expected to allow us to compare the influence of substituents on the diene molecule and the influence of the $R_{1,4}$ distance.

Finally, another way that has the possibility to increase the Diels-Alder functionalization viability of SWCNTs, using the electron-deficiency dienophile, was studied. In order to increase the electron-deficiency character of the SWCNT, the metal cation embedded SWCNT is analyzed. Due to the metal cation introduced in the cavity of the tube that would increase the electron deficiency character to the tube, this cluster is expected to be more reactive than the bare cluster. This hypothesis will be proved by comparing the reactivity of this cation embedded tube with that of the bare tube in the Diels-Alder reaction with *2,3-dimethylene-1,4-dioxane*.

5. Computational Procedure

The ONIOM scheme (B3LYP/6-31G*:AM1), which has been successfully used in previous works on the SWCNTs functionalizations: ozonization (Lu *et al.*, 2002c), 1,3-dipolar cycladdition (Lu *et al.*, 2002c; Lu *et al.*, 2003a), [4 + 2] cycloaddition (Lu *et al.*, 2002b), osmylation (Lu *et al.*, 2002a), [2 + 1] cycloaddition (Lu *et al.*, 2003b), and epoxidation (Lu *et al.*, 2003c) and the ONIOM model, a $C_{130}H_{20}$ model tube, in which the high level part is a C_{16} cluster, together with ten H-atoms as boundary atoms (see Figure 29a), were used here. For armchair SWCNTs, there are two types of bond: the bond perpendicular to the nanotube axis, 1,2-pair site, and the bond nearly along the nanotube axis, 1,3-pair site, as shown in Figure 29. However, the 1,2-pair site, considered to be more dienophile than the 1,3-pair site (Khabashesku *et al.*, 2002), was considered in this study.

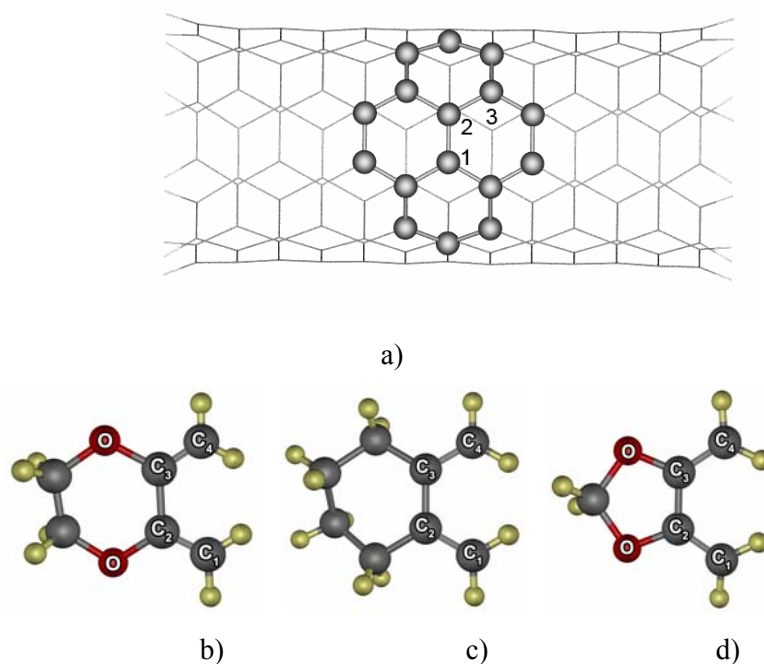


Figure 29 a) ONIOM model of (5,5) SWCNT ($C_{130}H_{20}$ cluster) and three different types of dienes : b) *diene (1)*; c) *diene (2)*; and d) *diene (3)*. Atoms belonging to the quantum cluster (B3LYP/6-31G*) region are drawn as balls and sticks; the rest is treated at the AM1 level of theory.

In order to study the possibility to increase the Diels-Alder functionalization viability of SWCNTs, the addition of a 2,3-dioxy-substitued-1,3-butadiene, 2,3-dimethylene-1,4-dioxane (see Figure 29a), an electron-rich diene, was first studied. The calculated activation energies (E_a) and the reaction energies (E_r) were compared with that of the typical diene, 1,3-butadiene. The influence of the donor substituent on the Diels-Alder reactivity was discussed. Next, in order to compare the influence of substituents on the diene with the influence of $R_{1,4}$ distance on the Diels-Alder reactivity, Diels-Alder reaction of SWCNT with three different dienes: 2,3-dimethylene-1,4-dioxane, 1,2-dimethylene-1,4-dioxane and 4,5-dimethylene-1,3-dioxalane (called as *diene (1)*, *diene (2)* and *diene (3)*, respectively) (see Figure 29) were performed. Because *diene (1)* and *diene (3)*, have comparable substituent units (2,3-dioxy-substituent) and *diene (1)* and *diene (2)* have comparable $R_{1,4}$ distances

(see details in Result and Discussion section) so the influence of the substituent units and $R_{1,4}$ distance on the Diels-Alder reactivity can be compared.

Finally, another possibility to enhance the Diels-Alder reactivity of SWCNT, the increasing of the electron-deficiency character of the dienophile, was studied by performing the Diels-Alder reaction of a SWCNT with Na^+ embedded inside in the tube, called *Na@SWCNT*, with the 2,3-dimethylene-1,4-dioxane. The *Na@SWCNT* was modeled by introducing Na^+ inside the tube, the bare CNT model ($\text{C}_{130}\text{H}_{20}$ model tube, in which the high level part is a C_{16} cluster). Here Na^+ was fixed at the middle of the tube during the calculation. The difference in equilibrium geometry, activation energies (E_a) and the reaction energies (E_r) between *Na@SWCNT* and the bare tube were discussed.

During the structure optimization, only the quantum cluster region (16 carbon atoms for the SWCNT) and the adsorbates are allowed to relax, while the remaining ones are constrained at the configuration obtained from a previous optimization at the AM1 level of theory. All calculations were performed using the Gaussian 03 program. Frequency calculations were carried out to confirm the single imaginary mode for all transition states.

6. Results and Discussions

6.1. The Diels-Alder reaction of the sidewall armchair (5,5) SWCNT ($C_{130}H_{20}$) with different types of dienes

All the reactions considered in this study were found to be a synchronous concerted mechanism. This is due to the symmetry of the dienes and dienophile. The important geometric parameters of the transition states and the products are depicted in Figures 30 and 31, respectively. The synchronous saddle points are characterized as the true transition state structures, possessing only one imaginary frequency. Interestingly, among the derived TSs, the lengths of the forming C-C single bonds are remarkably constant, being in the usual range of 2.0-2.3 Å found in most cycloaddition reactions (Houk *et al.*, 1992a; 1992b; 1995).

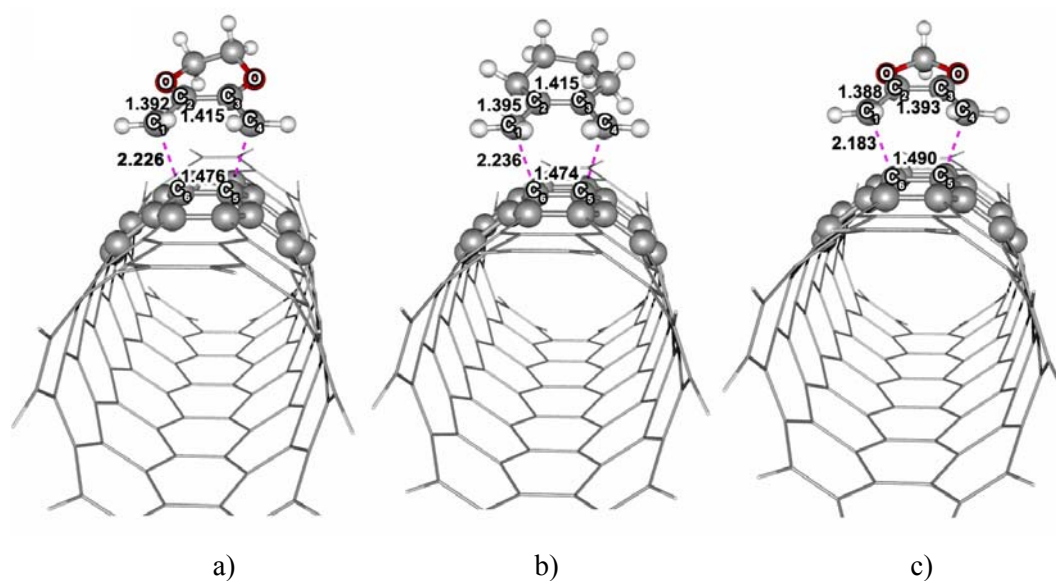


Figure 30 Selected parameters (bond length in Å) obtained at the ONIOM(B3LYP/6-31G*:AM1) level of theory for the transition states of the Diels-Alder reaction of 5,5-armchair SWCNT fragment ($C_{130}H_{20}$) with three dienes: a) *diene (1)*; b) *diene (2)*; and c) *diene (3)*.

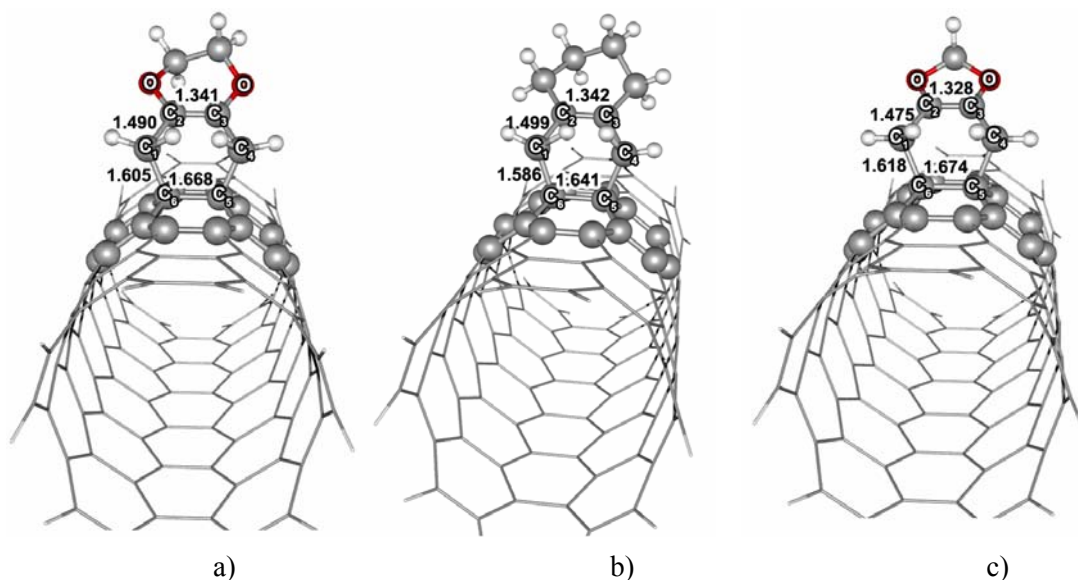


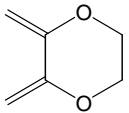
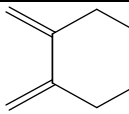
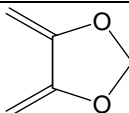
Figure 31 Selected parameters (bond length in Å) obtained at the ONIOM(B3LYP/6-31G*:AM1) level of theory for the products of the Diels-Alder reaction of 5,5-armchair SWCNT fragment ($C_{130}H_{20}$) with three dienes: a) *diene (1)*; b) *diene (2)*; and c) *diene (3)*.

The calculated percentages of bond lengthening and shortening at the TS of the reactions are documented of the SWCNT with different types of dienes studied here are documented in Table 1. It is found that the transition state obtained for *diene (1)* has the smallest percentage of bond alteration. This indicates that the TS for *diene (1)* is the tightest one, the earliest transition state. The derived results agree well with Hammond's postulate (Hammond, 1955), that is, the reaction with a lower activation barrier and a higher exothermicity has an earlier transition state.

The calculated activation energies (E_a) and the reaction energies (E_r) are also documented in Table 1. The activation barriers of three dienes considered in this study are 19.4, 29.4 and 36.6 kcal/mol for *diene (1)*, *diene (2)* and *diene (3)*, respectively. This activation barrier of *diene (1)* is compared with the activation energy of the Diels-Alder reaction of (5,5) SWCNT with the typical diene, 1,3-butadiene, from the previous work calculated from the same model and level of theory (Lu *et al.*, 2002b) of 32.4 kcal/mol. It is conclusively found that *diene (1)* is more reactive than 1,3-

butadiene due to the 2,3-dioxy group substituted on the butadiene moiety that acts as the electron donating group .

Table 1 The distances between the methylene carbons in the butadiene moiety ($R_{1,4}$) of various dienes obtained from the B3LYP/6-31G* level of theory, the computed activation energies (E_a), reaction energies (E_r) and the percentages of bond lengthening and shortening for the Diels-Alder reaction of three dienes considered in this study onto the 1,2-pair site side wall of (5,5) SWCNT ($C_{130}H_{20}$) obtained from the ONIOM(B3LYP/6-31G*:AM1) calculation.

Diene	$R_{1,4}$ (Å)	E_a (kcal/mol)	E_r (kcal/mol)	Shortening at the TS (%) ^a	Stretching at the TS (%) ^a	
				C ₂ -C ₃	C ₁ -C ₂	C ₅ -C ₆
 <i>diene (1)</i>	3.005	19.4	-11.7	46.9	33.6	32.6
 <i>diene (2)</i>	2.966	29.4	-4.7	52.9	32.2	33.2
 <i>diene (3)</i>	3.200	36.6	14.7	56.2	37.9	34.9

^aThe percentage of stretching or shortening of the bond = $((r_R - r_{TS}) / (r_R - r_P)) * 100$

where r_R = bond distance calculated at the reactant

r_{TS} = bond distance calculated at the TS

r_P = Bond distance calculated at the product

Diene (1) and *diene (2)*, have comparable distances between the methylene carbons in the butadiene moiety ($R_{1,4}$) (3.005 and 2.966 Å, respectively), however, the former having an activation energy of 19.4 kcal/mol is more reactive than the latter (29.4 kcal/mol). This is due mainly to oxygen atoms in the *diene (1)* that exhibit an electron donating behavior. We found that in the case of *diene (3)*, the reactivity of the Diels-Alder reaction is significantly lower than the other two cases, even though this diene has similar substituent group, 2,3-dioxy-substituted-1,3-butadiene, like *diene (1)*. This decrease is due mainly to the constraints of the six- and five-membered rings of *dienes (1)* and *(3)*, respectively, that affect the distance between the methylene carbons in the butadiene moiety ($R_{1,4}$) of diene. Thus, the major influence on the reactivity of these dienes comes from the $R_{1,4}$ distance: the reactivity becomes higher as the $R_{1,4}$ becomes shorter.

For the Diels-Alder reaction of *diene (1)*, the most reactive diene considered in this study onto the 1,2 pair site of with (5,5) SWCNT, the ONIOM calculations predicted an activation energy of 19.4 and an exothermic of -11.7 kcal/mol. This result shows conclusively that the diene (1)/SWCNT reaction is more favorable kinetically, but thermodynamically less favorable, compared to the typical butadiene/ethylene reaction ($E_a = 27.5 \pm 2$ kcal/mol (Steiner, 1951) and $E_r = -38.4$ kcal/mol (Uchiyama *et al.*, 1964)). Thus, in order to study possibility to enhance the reactivity of this reaction, the embedded metal cation SWCNT (Na@SWCNT) which behaves as an electron-deficient cluster is examined in the next section.

6.2. The Diels-Alder reaction of Na@SWCNT with 2,3-dimethylene-1,4-dioxane

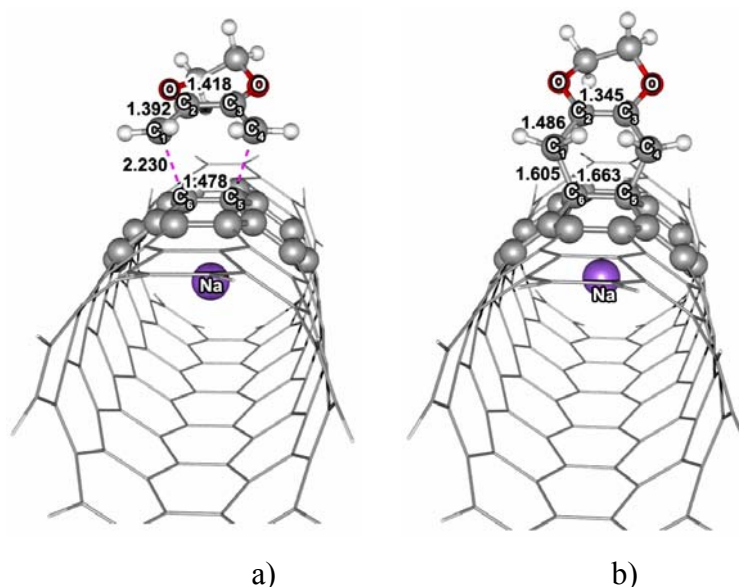


Figure 32 Selected parameters (bond lengths in Å) obtained at the ONIOM(B3LYP/6-31G*:AM1) level of theory for a) the transition state and b) the product of the Diels-Alder reaction of the embedded metal cation SWCNT ($Na@SWCNT$) with the 2,3-dimethylene-1,4-dioxane, *diene* (1).

The complex of the SWCNT with Na^+ embedded inside in the tube, called $Na@SWCNT$, was compared to that of the bare SWCNT. The much results of interest here is that the calculated C=C bond distance onto the 1,2-pair site obtained in the $Na@SWCNT$ complex is slightly longer (1.403 Å) than that in the isolated SWCNT (1.391 Å). A similar finding was reported for the interaction of cations with a double bond of benzene, also yielding a slightly lengthened C=C bond distance (Tan *et al.*, 2001). The reaction was found to be a synchronous concerted mechanism. The important geometric parameters of the transition state and the product are depicted in Figure 32. The length of the forming C-C single bonds (2.230 Å) is in the usual range of 2.0-2.3 Å found in most cycloaddition reactions (Houk *et al.*, 1992a; 1992b; 1995).

The Frontier Molecular Orbital (FMO) energies for the SWCNT and Na@SWCNT are depicted in Figure 33. As we mentioned that the viability of the Diels-Alder reactions can be estimated from the strength of two frontier orbital interactions (Fleming, 1976), the energy gap of HOMO (diene) and LUMO (dienophile) for normal electron demand reaction (ΔE^N) and the energy gap of HOMO (dienophile) and LUMO (diene) for inverse electron demand reaction (ΔE^I), then the strength of two FMOs interaction, ΔE^N and ΔE^I are calculated as follows:

$$\Delta E^N (\text{diene/SWCNT}) = E_{LUMO}^{SWCNT} - E_{HOMO}^{diene} : \text{Normal electron demand type}$$

$$\Delta E^I (\text{SWCNT/diene}) = E_{LUMO}^{diene} - E_{HOMO}^{SWCNT} : \text{Inverse electron demand type}$$

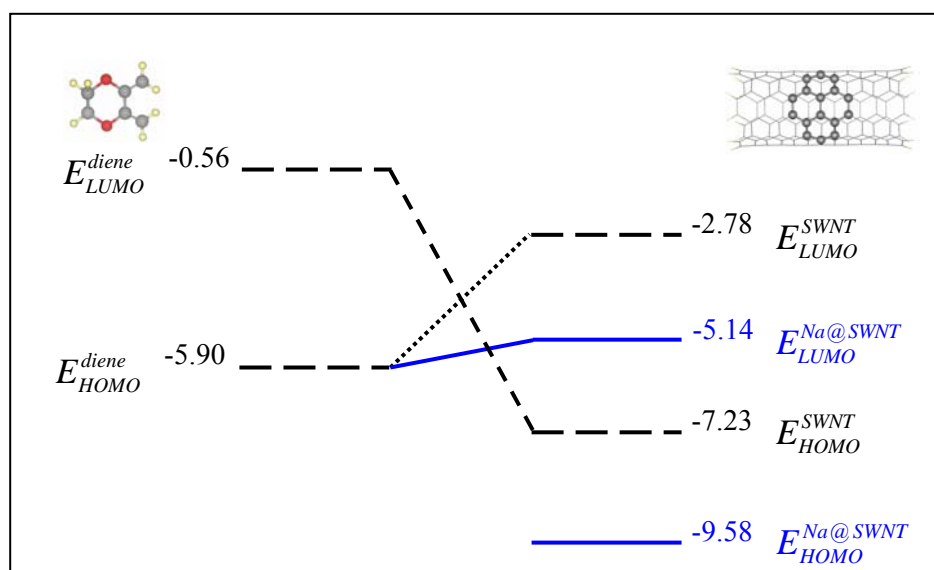


Figure 33 The Frontier Molecular Orbital (FMO) energies (E_{HOMO} and E_{LUMO} , in eV) of SWCNT and Na@SWCNT, obtained from ONIOM(B3LYP/6-31G*:AM1) calculations and of 2,3-dimethylene-1,4-dioxane, diene (*I*), obtained from the B3LYP/6-31G* level of theory.

The calculations revealed that the presence of Na⁺ inside the SWCNT stabilizes its lowest unoccupied molecular orbital (LUMO) considerably (-2.78 eV vs. -5.14 eV) and further leads to the tubular structure acting as an electron-deficient cluster. The interaction of the LUMO of the SWCNT with the HOMO of diene

dominates the reactivity of Na@SWCNT since the energy difference between these two molecular orbitals, ΔE^N , is much smaller than ΔE^I , the corresponding difference between E_{HOMO}^{SWNT} and E_{LUMO}^{diene} . The electron deficiency character of the SWCNT is reflected in the lower activation energy barrier E_a of -13.4 kcal/mol compared to the SWCNT without Na^+ ($E_a = -19.4$ kcal/mol), accounting for an increased Diels-Alder reactivity.

During the product formation via the transition state, the presence of Na^+ in the tube of SWCNT stabilized the resonance ring, thus the reaction energy of Na@SWCNT ($E_r = -16.5$ kcal/mol) is exothermically higher than that of the bare SWCNT ($E_r = -11.7$ kcal/mol). The results obtained in this study suggest the plausibility of functionalizing SWCNT materials for organic reactions.

7. Conclusion

Diels-Alder cycloadditions of SWCNT with the different outer-ring dienes have been studied using the two layer our-Own-N-layered-Integrated-molecular Orbital and molecular Mechanic (ONIOM) approaches (B3LYP/6-31G*:AM1). Structure-activity relationships for a series of different outer-ring dienes interacting with armchair (5,5) single wall carbon nanotube (SWCNT) were established. The calculations revealed that the reactivity of the Diels-Alder reaction is related to the distance between the methylene carbons in the butadiene moiety ($R_{1,4}$) of these dienes. The reactivity is higher as the $R_{1,4}$ becomes shorter. As for *diene (1)* and *diene (2)*, which have comparable $R_{1,4}$ distances, the effect of the oxygen atoms, which exhibit an electron donating behaviour, plays a dominant role on an enhancing the reactivity.

To enhance further the reactivity of the Diels-Alder reaction at the sidewall of SWCNTs, a metal cation, Na^+ , was introduced into the SWCNT. The presence of this ion in the cavity increases the kinetic and thermodynamic reactivity due to the pronounced electron deficiency of the central double bond of SWCNT, and further the LUMO orbital stabilized by the metal cation.

CHAPTER IV. CONTROLLED PURIFICATION, SHORTENING AND DISPERSION OF CARBON NANOTUBES

1. Introduction

The commercial available CNTs are normally severely contaminated with other carbonaceous impurities such as amorphous carbon, fullerene nanocrystalline graphite and metal catalysts. These impurities limit the performance of CNTs because the physical and chemical properties of such samples are modified. This results in a serious impediment to their application to new functional materials and devices. To take advantage of CNTs in applications, an effective purification strategy, which should maintain as far as possible their original properties, must be addressed first.

A variety of purification methods have been reported in the literature, depending on nanotube morphology (single-walled or multi-walled structures) and growth process. Chemical or physical methods or a combination thereof can be used to remove the undesired carbonaceous phases and metal catalysts. The physical methods reported in the literature are mainly based on ultrasound treatment followed by centrifugation or filtration (Bandow *et al.*, 1997; Holzinger *et al.*, 2000; Shelimov *et al.*, 1998), size-exclusion chromatography (Duesberg *et al.*, 1999; Duesberg *et al.*, 1998; Holzinger *et al.*, 2000), flocculation followed by selective sedimentation (Mamalis *et al.*, 2004) and extraction with solvent (Li *et al.*, 2000).

Chemical methods include mainly oxidation and reduction treatments (Rinzler *et al.*, 1998; Chiang *et al.*, 2001; Colomer *et al.*, 1999; Ebbesen *et al.*, 1994; Fonseca *et al.*, 1996; Hernadi *et al.*, 2001; Holzinger *et al.*, 2000; Shi *et al.*, 1999; Tohji *et al.*, 1996). They take advantage of the differences in reactivity, e.g. the oxidation rate (Ebbesen *et al.*, 1994), between the nanotubes and the impurities and can thus separate the synthesis products.

Although the majority of the impurities can be effectively eliminated by chemical methods, these processes tend to damage the structural integrity of the nanotubes by creating defects on the graphene layers (Monthieux *et al.*, 2001). On the other hand, the physical methods, which take advantage of the size differences, provide non-damaged tubes. However, they are more complex and less effective procedures leading to a lower purity. In order to attain a final product with good purity without material loss, the combination of chemical and physical methods should be used (Salernitano *et al.*, 2007).

Due to the substantial van der Waals attraction between the tubes, CNTs tend also to form undesirable aggregates that are insoluble in most solvents. This lack of solubility prevents CNTs from practical applications due to the difficulty in manipulation. To resolve these issues, various strategies have been developed, relying either upon functionalization (Chen *et al.*, 2001a; Chen *et al.*, 1998), oxidations (Bahr *et al.*, 2001; Boul *et al.*, 1999; Mickelson *et al.*, 1999), and/or attachment of soluble polymers (Riggs *et al.*, 2000) in order to suspend CNTs in organic solvents. This point has been considered from a theoretical standpoint in Chapter III.

Despite these shortcomings, water-soluble CNTs, which have important applications in fields such as biochemistry and biomedical engineering, have attracted great interest. Most recently, they started to become available by two main approaches, covalent functionalization and noncovalent functionalization. The covalent attachment of functional groups to the sidewalls (Dyke and Tour, 2003b; Hu *et al.*, 2003; Hudson *et al.*, 2004) produces defects on the perfect structure of the sidewall and alters the intrinsic properties of SWNTs, e.g. the electron transport. The noncovalent functionalizations typically include wrapping by polymers (Star *et al.*, 2002; Numata *et al.*, 2005; Zorbas *et al.*, 2004), encapsulation by supramolecular systems of small molecules, e.g. surfactant micelles (Abatemarco *et al.*, 1999; Matarredona *et al.*, 2003; O'Connell *et al.*, 2002), and π -stacking by rigid, conjugated macromolecules (Chichak *et al.*, 2005; Paloniemi *et al.*, 2005; Wu and Hu, 2004) or polymers (Chen *et al.*, 2002; Keogh *et al.*, 2004; Star *et al.*, 2003; Star and Stoddart, 2002; Steuerman *et al.*, 2002). In contrast to the covalent method, the noncovalent

functionalization of the sidewall can immobilize functional molecules on the surface of SWNTs while maintaining their geometric structure (Chen *et al.*, 2001b). Nevertheless, these noncovalent methods usually suffer from some disadvantages, such as the specific complex and synthetic reagents for the functionalization, a long period of sonication (Hu *et al.*, 2006a) or simply the price like for CNTs solubilized by adsorption of DNA (Zheng *et al.*, 2003).

Apart from high purity and dispersion, the length control is another prerequisite for the utilization of CNTs in many fields, e.g. the building of transistors, biological, imaging and sensing devices (Ziegler *et al.*, 2005a; Ziegler *et al.*, 2005b). Therefore many length-control processes, such as cuttings, have been proposed. Cutting CNTs to uniform undamaged short tubes can either be induced by chemical or mechanical methods, or by a combination of these (Kang *et al.*, 2006; Lustig *et al.*, 2003; Maurin *et al.*, 2001; Stepanek *et al.*, 2000). The chemical methods were developed by using concentrated strong acids (Chen *et al.*, 1998; Liu *et al.*, 1998; Ziegler *et al.*, 2005a) and fluorination (Gu *et al.*, 2002; Ziegler *et al.*, 2005b) while the mechanical methods use mostly sonication techniques (Yudasaka, 2000; Zhang, 2002) and grinding or milling techniques (Maurin *et al.*, 2001; Stepanek *et al.*, 2000). Recently, soft cutting methods, by a combination of chemical and physical methods, were also developed, for example, CNT grinding in cyclodextrins (Chen *et al.*, 2001a). Nevertheless, most papers about mechanical grinding, acid cutting, fluorine cutting, etc., report difficulties in length control. Furthermore they give only very few details about length control.

New techniques, like the lithographical method (Lustig *et al.*, 2003) and the low-energy electron beam cutting technique, were recently reported (Yuzvinsky *et al.*, 2005). The lithographical method is, however, limited in the length control because of a lack of alignment of nanotubes during this process. The electron beam cutting technique for length control can only be conducted within SEM or TEM instruments. The scale-up is thus very difficult.

Recently, an easy, highly efficient and “non-covalent” way to purify, solubilize and functionalize CNTs was reported (Fei *et al.*, 2006). It uses the versatile polyoxometalates (POMs). POMs are inorganic metal-oxygen cluster compounds that are outstanding in their topological and electronic versatility (Pope and Müller, 1991). These compounds can be used in various applications in catalysis (Hill and Brown, 1986) and molecular materials (Ouahab, 1997), which is due to their interesting redox behaviour, unique molecular structure, electronic versatility, and, last but not least, easy availability.

There are many different classes of POMs and among them Keggin and Wells-Dawson structures (Barton *et al.*, 1999; Li *et al.*, 2007a; Pope and Müller, 1991; Mizuno and Misono, 1998) are very well studied in the literature (Li *et al.*, 2007a; Pope and Müller, 1991). The Keggin structure is roughly spherical and gives a general formula of XM_{12} , where X is the heteroatom and M is the d^0 metal. Each corner of the heteroatom tetrahedron is associated with an M_3O_{13} unit. The Dawson type structure is ellipsoidal, of formula X_2M_{18} . This structure consists of two heteroatoms stacked one atop the other, and each end is composed of an M_3O_{13} cap, with two six-metal belts circling the molecule.

A POM with Keggin structure, $([\text{PMo}_{12}\text{O}_{40}]^{3-})$, has been used to disperse carbon black to highly dispersed colloid carbon nanoparticles (Garrigue *et al.*, 2004). This process is most likely driven by the strong chemisorption of POMs on carbon surfaces. Stable suspensions of graphene layers from highly oriented pyrolytic graphite (HPOG) (Rohlfing and Kuhn, 2006) were also prepared by this way. It was also possible to solubilize CNTs in water together with a removal of impurities (Kulesza *et al.*, 2006). Uniform short carbon nanotubes (200 nm in length) can be obtained by using the hydrothermal (high-temperature aqueous solutions) process, assisted by POMs (150°C, 72h). Unfortunately, the role of POMs in the cutting process was not demonstrated (Kang *et al.*, 2006).

In this study, we developed an analogue procedure of the previous studies, the combination of using POM and sonication, which was successfully used for the

preparation of either a stable suspension of carbon nanoparticles or layers of graphene from a carbon black sample or HOPG, respectively (Garrigue *et al.*, 2004; Rohlfing and Kuhn, 2006), and the solubilization of carbon nanotubes (Kulesza *et al.*, 2006), to shorten and solubilize CNTs. The purity of the obtained CNTs in aqueous solution was characterized. The role of POMs in the process was demonstrated. The obtained solution was used as a starting point for modification of the carbon nanoobjects with a metal layer in Chapter V.

2. Experimental section

Guided by the work on the preparation of the stable suspension of highly dispersed colloid carbon nanoparticles (Garrigue *et al.*, 2004), we established an analogue procedure to purify, shorten and solubilize carbon nanotubes in a controlled way. The idea behind this attempt is that the procedure, which had been able to attack carbon black, presumably by strong chemical adsorption of POMs on the carbon surface, should be able to work in a similar way for CNTs.

The details of the work on purification, shortening and solubilization of carbon nanotubes are given schematically in Appendix A. Briefly, the experiment was performed typically as follows. The raw sample of carbon nanotubes used for this study was multi-walled carbon nanotubes produced by catalytic chemical vapor deposition (ARKEMA). About 0.1 mg of MWNTs was added to a POM solution (10 mM $\text{H}_3\text{PMo}_{12}\text{O}_{40}/0.1\text{M H}_2\text{SO}_4$). This solution was prepared from phosphomolybdic acid hydrate, $\text{H}_3\text{PMo}_{12}\text{O}_{40}\cdot x\text{H}_2\text{O}$ (FLUKA) in 0.1M H_2SO_4 . The optimized condition, that means using of 0.1mM H_2SO_4 to be a solvent for POMs instead normal water, is discussed in next section. The suspension was sonicated by a high intensity ultrasonic processor. After 1 hour of sonication, the suspension was divided into two parts (*solution A and B*). The formed precipitate was separated from the supernatant solution by addition of concentrated sulfuric acid to *suspension A* followed by centrifugation. The precipitate obtained from this part was washed twice by diluted aqueous acid solution and *ultrapure water* (the distilled water which is filtered by 0.2 μm cellulose acetate filter, WHATMAN). The final precipitate was redispersed in

ultrapure water by sonication in an ultrasonic bath for a few minutes. The typical result, the purity of the sample obtained after a 1 hour treatment using this combined technique (chemical treatment and sonication), is illustrated in next section. The influence of this combined technique on the purification and the dispersion of CNTs is revealed by the analyzed feature and chemical composition of the obtained solution characterized by TEM and energy dispersive x-Ray (EDX) analysis included in a high-resolution scanning electron microscopy (HRTEM).

The second part (*suspension B*) was exposed to sonication for an hour. Next, this suspension was forced to precipitate by adding acid and performing centrifugation. The supernatant was removed. New POM solution (10 mM $\text{H}_3\text{PMo}_{12}\text{O}_{40}/0.1\text{M H}_2\text{SO}_4$) was added to the remaining sample. The sonication was continuously performed for two hours. After the sonication (finally duration of 4 hours), the precipitation of the suspension was induced. The precipitate was washed with diluted aqueous acid and *ultrapure water*. The final precipitate was redispersed in *ultrapure water*. The obtained stable aqueous suspension (called *CNT/WATER*) was characterized by TEM, Zetasizer, and HRTEM. The resulting features like the length of the dissolved carbon nanotubes influenced by a 4 hour treatment, are shown and discussed in next section.

3. Results and Discussions

3.1. The optimized condition: the POM solution

In this work, we used the $[\text{PMo}^{\text{VI}}_{12}\text{O}_{40}]^{3-}$ polyoxometalate for two reasons. The first reason is that this POM has a Keggin structure, $[\text{XM}_{12}\text{O}_{40}]^{n-}$ where M is an ionic metal core of corner- and edge-sharing pseudo-octahedrally coordinated MO_6 units (usually d^0 or d^1 , commonly called *addenda* or *peripheral* element, typically W^{VI} , Mo^{VI} , and V^{V} because their ionic radii and charge are suitable for combining with O^{2-}) and X is a main group element or a transition-metal ion, which is easy to obtain (synthesize) (Hill and Brown, 1986; Ouahab, 1997). The second reason is that POM has the Mo^{6+} addenda elements which has highest electron affinity among all addenda

element. The relative energy and composition of the LUMO correlates quite well with the electron affinity of each *isolated* M^{n+} ion that is in the order $Mo^{6+} > V^{5+} > W^{6+} > Nb^{5+}$ (Lopez *et al.*, 2002).

Attempting to purify and shorten carbon nanotubes, disperse and solubilize them in the aqueous solution was first done by using the sonication technique together with the using of an aqueous POM solution (10 mM $H_3PMo_{12}O_{40}$ /*ultrapure water*). First trials using 3 h sonication in 10 mM $H_3PMo_{12}O_{40}$ /*ultrapure water* provided a stable quite-homogeneous grey suspension of carbon nanotubes (CNTs were here redispersed in water after treatment and washing procedure). However, the TEM images taken from this sample (see Figure 34) show a film layer of POM formed on the tubes surface during the treatment. The formation of a POM-film (when CNT were added to POM aqueous solution, and sonicated) was reported in the literature (Fei *et al.*, 2006; Pan *et al.*, 2006). Nevertheless, the mechanism of the film formation has not been discussed before.

Because the prepared material will be used as starting material for the gold deposition experiment (seen details in Chapter V) we expected that gold particles, which will be generated from an electrochemical process, will prefer to attach on these films instead on CNTs directly. This hypothesis was proved by a gold deposition experiment. This deposition was done by using the POM-film layer solubilized-CNTs as starting material. TEM images taken from the obtained sample are shown in Figure 35. These images clearly indicate that gold deposition preferentially happens on the film than on bare tubes. Therefore the aqueous POM solution prepared by using *ultrapure water* as a solvent is not suitable for CNT elaboration (purifying, water-solubilizing, dispersing, cutting) because it leads to POM layer formation on CNTs and then finally this film will significantly influence on the further gold decoration procedure. The objective to make the gold deposition dissymmetrical (this point will be further considered in Chapter V) thus can not be achieved. In order to avoid the formation of such films in the next experiments, we use a diluted acid solution (0.1M H_2SO_4) to be a solvent for POM solution instead of water.

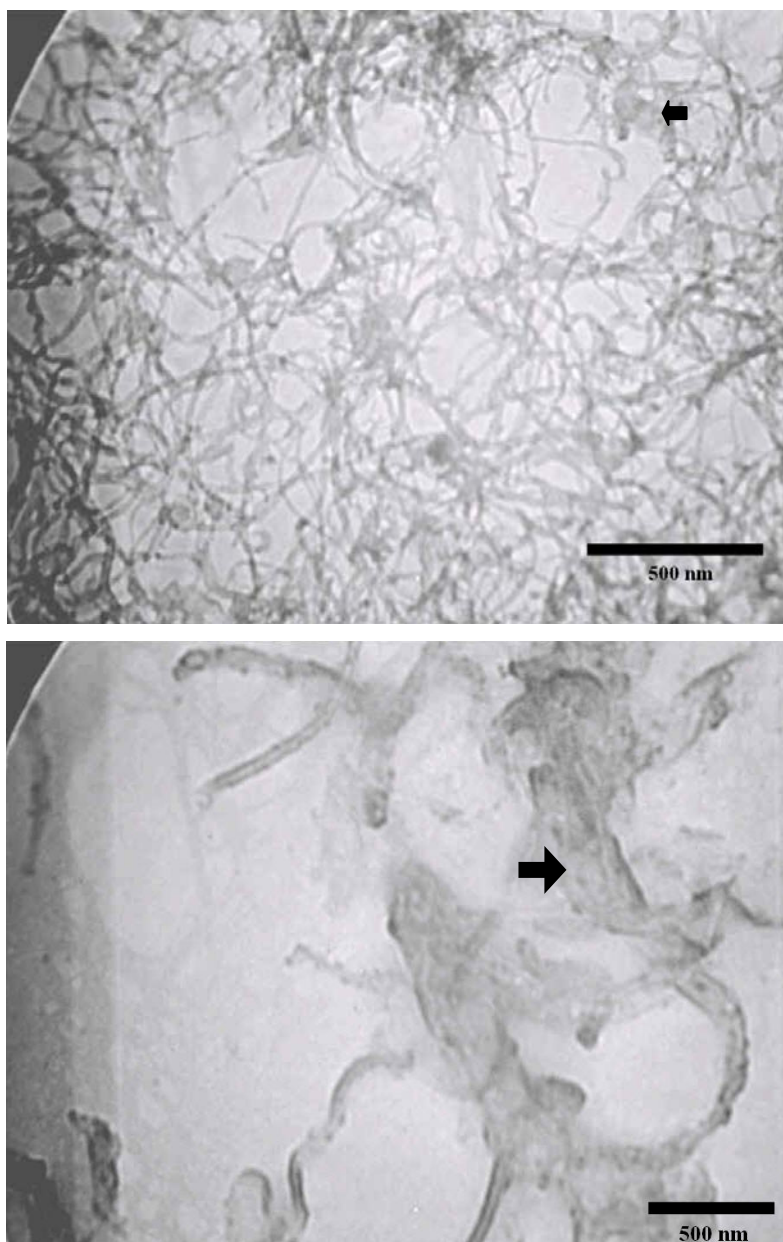


Figure 34 TEM micrographs of POM solubilized-CNTs after the treatment, 3 h sonication in an aqueous POM solution (10 mM $\text{H}_3\text{PMo}_{12}\text{O}_{40}$ /ultrapure water) showing a POM-film formed on the tube surface (see black arrow) during the treatment.

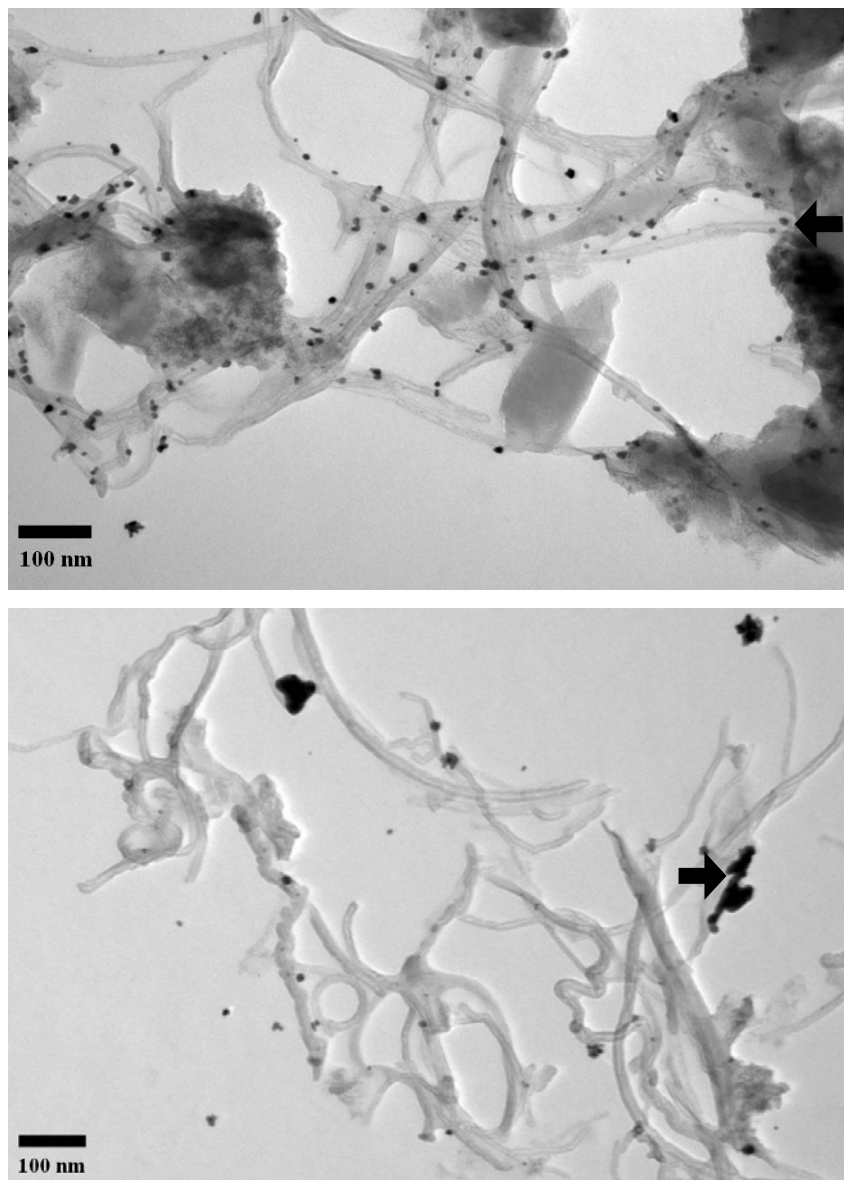


Figure 35 TEM micrographs of gold modified-POM solubilized CNTs obtained by an electrochemical reaction (30kV, 2 min) of the POM-solubilized CNTs in 1 mM HAuCl_4 . These images show that the gold decoration prefers to take place on the POM-film on the tube surface (see black arrow) instead on bare tubes.

3.2. The purification, dispersion and water-solubilization of carbon nanotubes

Before sonication with POM solution (prepared by using 0.1 M H₂SO₄ as a solvent), the CNTs in water appeared as heterogeneous aggregates (see Figure 36a). With the sonication proceeding in an aqueous POM solution (10 mM H₃PMo₁₂O₄₀/0.1M H₂SO₄), a suspension of carbon nanotubes changes its color from yellow to green, indicating that POMs are not only adsorbed on the tube surface but also oxidize carbon surface and diffuse back into solution as reduced heteropolyblue species. The addition of electrons leading to the partial oxidation and the mixed-valence (Mo^{VI,V}) heteropolyblue species is shown as follows (Kulesza *et al.*, 2006):



Since the heteropolyblues species in the used POM solution can be recovered back to the fully oxidized state (Mo^{VI}) with the addition of a small amount of H₂O₂ solution, this approach can be considered as a green and renewable chemical strategy, which will be valuable for research in the field of nanoscience and nanotechnology.

After 1 hour of sonication in the POM solution, the obtained suspension has a black-green color (see Figure 36b). This color is supposed to originate from the color mixing of treated CNT and the used green POM solution. The black-green suspension was stable with only very slow sediment of carbon particles. One part of this suspension was taken and centrifuged in order to remove the supernatant POM rich phase. Due to the absence of ions that could shield the electrostatic repulsion between the attached POM anion, the suspension was stable. A subsequent prolonged centrifugation (15000 rpm, 1h) can lead to a partial sedimentation. The particle sedimentation can be increased by adding sufficient H₂SO₄ in order to screen the electrostatic repulsion. After sediment isolation and rinsing with diluted sulfuric acid and *ultrapure water* twice, the remaining precipitate was finally redispersed in *ultrapure water*. The quite homogeneous grey suspension was stable for a few weeks (see Figure 36c). Because of the adsorption of POM anion, the modified tubes sufficiently solubilize in water. Simultaneously, this adsorption also results in stability

of the solution due to electrostatic repulsion between attached POM anion leading to CNTs with an overall negative charge.

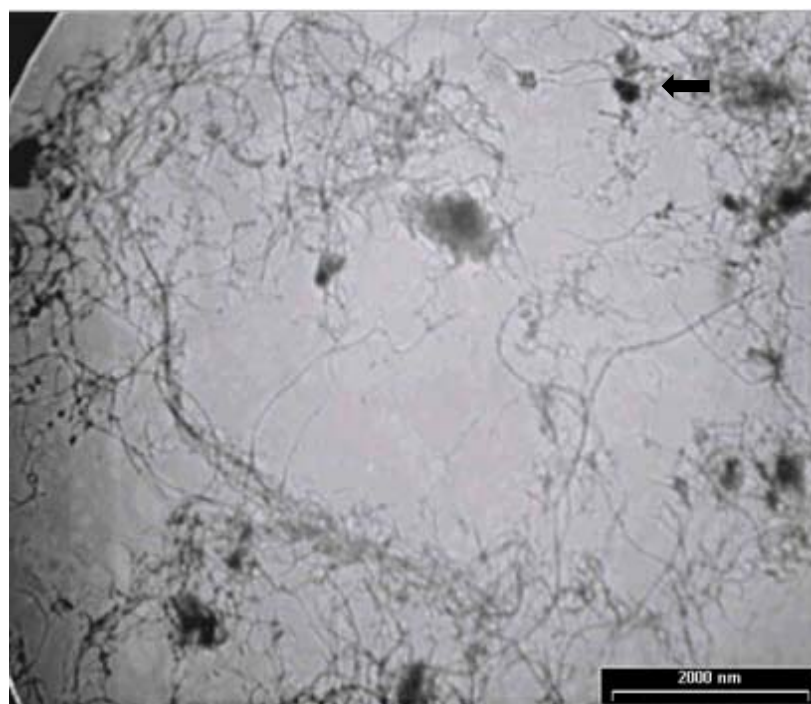


Figure 36 Photographs showing (a) untreated CNTs aggregated in water, (b) the black-green suspension of CNTs (treated CNTs still suspended in the used POM solution), and (c) the stable quite homogeneous grey aqueous CNTs suspension (treated CNTs suspended in water). The treatment was performed by 1 hour of sonication in the POM solution.

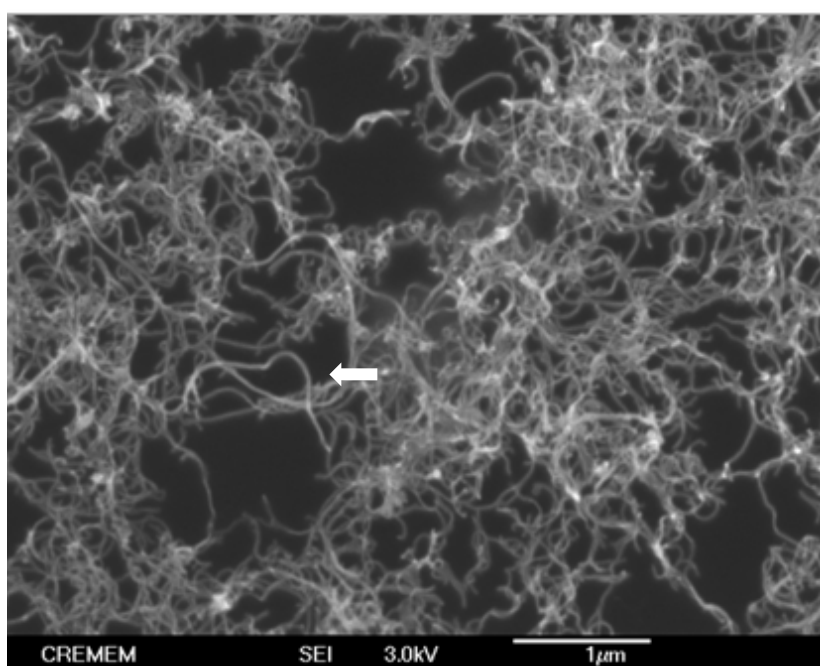
A few droplets of the suspension were dried on TEM grids. The deposits on TEM grids were analyzed by TEM and HRTEM in order to visualize the particles and check their purity. As a control, the raw carbon nanotubes were examined by TEM. Figure 37a shows that the as-produced CNTs are bound into intractably entangled macroscopic ropes and aggregate seriously. Because both ends of tubes can not be observed from the image, we supposed that length of the nanotubes here is very long,

of the order of several micrometers. The image also shows that the sample contains many impurities. After 1 h sonication with POM solution, the SEM images of CNTs cast from the suspension (Figure 37b) shows that most of the impurities have been removed after treatment leading to purified tubes. The image also shows that some CNTs were shortened from several micrometers to a few micrometers. An example of shortened CNTs is indicated by a white arrow in Figure 37b.

Because the catalytically prepared carbon nanotube sample contains various kinds of by-products e.g. amorphous carbon, catalyst particles (mainly Fe in this case) there is a difference in the oxidation reactivity in carbon nanotubes and impurities. During oxidative purification, competitive oxidation always takes place: carbon nanotubes and other impurities react simultaneously, with different oxidation rates. The impurities which have a reactive edge structure, are exposed directly to oxidizing agents, resulting in faster oxidation compared to carbon nanotubes (Hernadi *et al.*, 2001). Therefore, we supposed that with the short treatment (1 h sonication in the POM solution), the POM anion clusters adsorb preferentially on impurity surfaces (on their reactive edges) and oxidize that surface more rapidly than that of CNTs. As a consequence almost all impurities are much better dissolved in the solution than carbon nanotubes. Using fractionated precipitation by centrifugation and adding acid to the solution, the impurities contained in the supernatant can be removed by decanting the supernatant from the solution. The sediment left at the bottom of the tube contains POM-modified CNTs.



(a)



(b)

Figure 37 (a) TEM image of raw CNTs (black arrow points a position of impurities contained in the sample) and (b) SEM image of purified and dispersed CNTs (treated with 1h sonication in 10 mM $\text{H}_3\text{PMo}_{12}\text{O}_{40}/0.1\text{M H}_2\text{SO}_4$) (white arrow indicates a shortened tube).

Of course, the structures of different carbon nanotubes have a certain effect on their oxidation rate. The reactivity of carbon nanotubes presents some unique features determined by the combination of topology and strain. The oxidation reaction rate of the end cap of a perfect structure, which is strained by pentagons at the end cap, is definitely higher than of the sidewall. So the straight carbon nanotubes can be oxidized only from the ends. In the imperfect tubes, structural defects become the sites of preferential reaction during oxidation (Hernadi *et al.*, 2001).

In our case, raw CNTs are randomly oriented (spaghetti-like) with defects like tube bending and twisting (Wong *et al.*, 2004). These defects will be favorable sites for a chemical attack. Therefore it is not surprising that several shortened carbon nanotubes are also observed after the treatment as seen in Figure 37b. This indicates that the length-controlled CNTs could be obtained by optimizing the conditions, e.g. sonication time, POM solution concentration, of this treatment.

Chemisorption of POM molecules on the surface of MWCNTs has been reported (Kang *et al.*, 2004; Kulesza *et al.*, 2006) and described as strong and irreversible bonding (Garrigue *et al.*, 2004). The attachment of POM molecules on the CNTs was elucidated by FTIR measurement. The corresponding results showed that the spontaneous and strong chemisorption of POM on CNTs surface may lead to the formation of CNTs-POMs composites through Mo-O-C bond (Pan *et al.*, 2006). The presence of POM on the carbon surface of the POMs solution-treated CNTs and the purity of those tubes after 1h treatment were studied by TEM-EDX qualitative analysis.

TEM-EDXS results are shown in Figure 38. As Mo was found on the tubes, this implies that the POM clusters are adsorbed on the tube surface. Because we found Fe just at the position of the tubes it is reasonable to conclude that 1 h sonication treatment in the POM solution is sufficient to remove the metal catalyst impurities which are not trapped inside of the tubes. Due to the multi-layer structure of the tubes used in this study, it is normal that this purification technique could not remove the metal catalyst which was trapped inside the as-synthesized tubes.

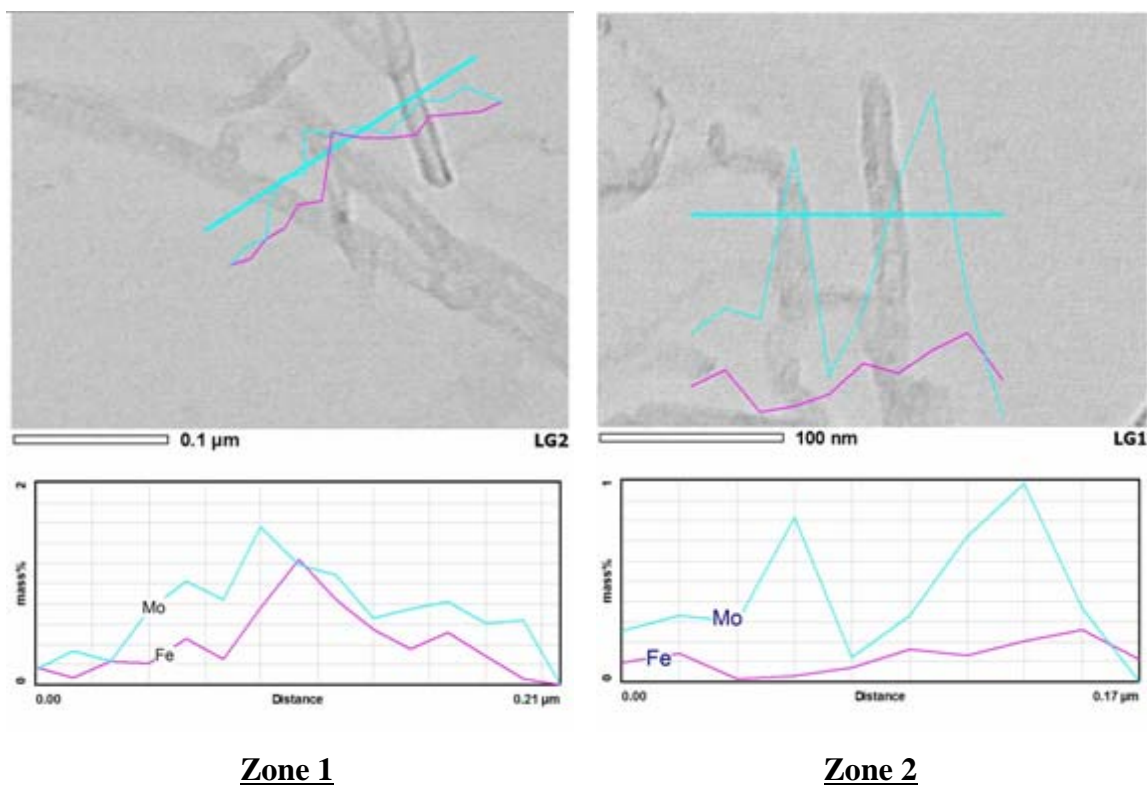


Figure 38 TEM images of the obtained carbon nanotubes and corresponding energy dispersive X-ray spectroscopy (EDXS) spectra showing Mo and Fe compositions of the selected zones of POM treated CNTs.

After sonication in the POM solution (final duration of 4 h), CNTs sample were isolated, washed and redispersed in *ultrapure water*. The obtained homogeneous grey suspension was stable for many weeks. This high stability is essentially due to irreversible chemisorption of negatively charge POM clusters on the carbon surface similar to that obtained from 1 h treatment. The length of CNTs contained in this suspension was roughly estimated by a light diffusion experiment (Zetasizer). Because this technique assumes a spherical shape of the analyzed objects, which is definitely not the case for the highly anisotropic CNTs, only a rough evolution of the size distribution with the treatment can be obtained. The size distribution of treated tubes compared with that of raw CNTs is shown in Figure 39. The measurement shows that before treatment (sonication in the POM solution) the CNT sample is characterized by a polydisperse size distribution. This covers a broad range of values between several tens of nanometers to several thousand nanometers (micrometers).

We supposed that very small particles (tens nanometers size) which we found here are impurities (small carbon particles or catalyst particles) contained in the solution whereas the very big particles (thousands of nanometers) we found here are big CNTs aggregates. Light diffusion also illustrates roughly a shift of the extremely broad distribution (nanometers to micrometer) to a significantly more narrow distribution with lower values (nanometers) indicating that CNTs in solution are shortened during the treatment. However, as we mentioned that the structure of the particles (spherical) assumed in this analysis is different from CNTs structure (tubular), the statistic evaluation of the tube length of the treated CNTs was performed by counting and measuring the CNT length obtained from TEM images.

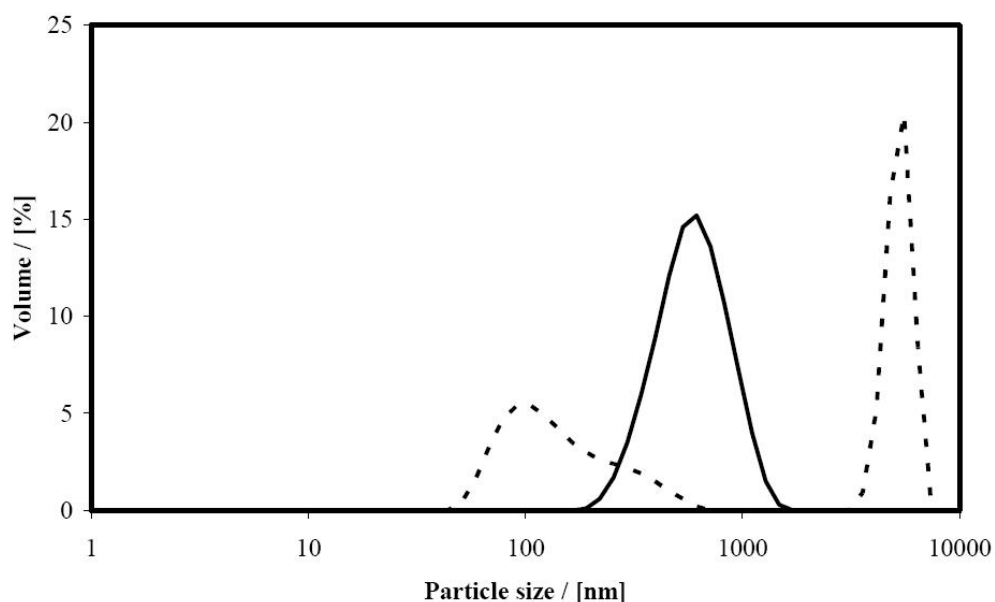


Figure 39 The size distribution in terms of volume fraction of raw CNTs (dashed line) and shortened CNTs (solid line) (obtained after 4 h sonication in POM solution) suspended in water.

The TEM study was performed on the grid where a few droplets of the homogeneous and stable suspension of CNT sample were put and dried in air. By counting and measuring the CNT length from the TEM images (Figure 40), the lengths of treated tubes are in the range of 90-1300 nm and the average length is 463 nm. These values are in good agreement which that obtained by light diffusion (see Figure 39). Following our series of experiment (1 h and 4 h sonication time), it is

suggested that the length of obtained short carbon nanotubes is largely depending on sonication time (POM amount is in excess). Increasing the sonication time leads to a decrease in length. In the present conditions, the obtained short CNTs are cut from several micrometers down to tens or hundreds of nanometers in a controllable way.

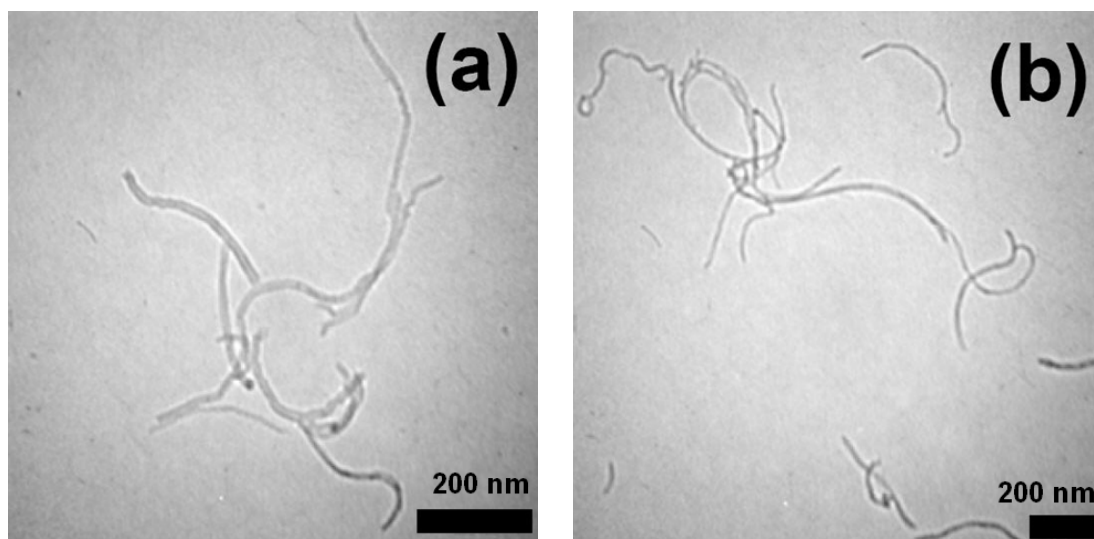


Figure 40 TEM images of shortened CNTs (treated with 4h sonication in 10 mM $\text{H}_3\text{PMo}_{12}\text{O}_{40}/0.1\text{M H}_2\text{SO}_4$).

The particles on the grid were further characterized by HRTEM. For HRTEM study we concentrated only on the cut edges of the shortened CNTs. HRTEM image of a typical cut of shortened CNTs is shown in Figure 41. It is found that the shortening of carbon nanotubes by using sonication technique together with POM leads to very neat cuts on the tubes. Because of their ability to purify, water-solubilize, disperse and shorten CNT by neatly cutting, this combined technique is considered to be an effective method to purify, water-solubilize, disperse and shorten carbon nanotubes in one single approach.

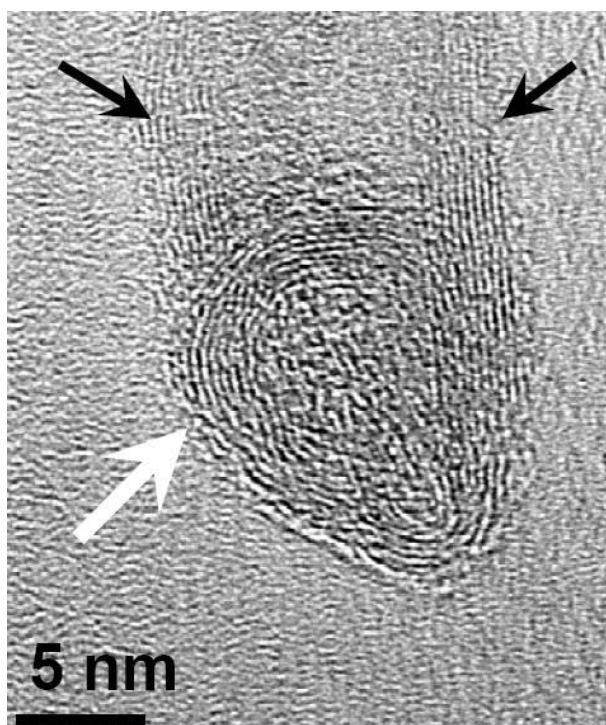


Figure 41 HRTEM image showing a typical cut of the shortened CNTs (treated by 4h sonication in 10 mM $\text{H}_3\text{PMo}_{12}\text{O}_{40}$ /0.1M H_2SO_4). Black arrows indicate the nanotube wall with an aligned multilayer of graphene sheets. The white arrow indicates the cut section showing circular arranged graphene sheets.

4. Conclusion

In this work we propose an extremely simple method to purify, water-solubilize, disperse, and shorten CNTs. The combination of POMs and sonication technique, that previously has been used to prepare a stable suspension of carbon nanoparticles or of layers of graphene from a carbon black sample and HOPG, respectively (Garrigue *et al.*, 2004; Rohlfing and Kuhn, 2006), a similar procedure can also be used to elaborate pure carbon nanotube samples with a controlled length. Because of its ability to purify, water-solubilize, disperse and shorten CNTs using a single experimental approach this combined technique is considered as an important step forward for many applications using CNTs.

CHAPTER V. METAL DECORATION OF CARBON NANOTUBES

1. Introduction

A number of different approaches have been proposed for the attachment of metal or semiconductor nanoclusters to nanotubes in order to obtain nanotube/nanoparticle hybrid materials with useful properties that might improve their performances or extend their applications (Ellis *et al.*, 2003; Jiang *et al.*, 2003a; Jiang and Gao, 2003; Jiang *et al.*, 2003b; Kong *et al.*, 2001; Liu *et al.*, 1998; Satishkumar *et al.*, 1996). Among others this opens up the application of carbon nanotubes in the area of nanoelectrodes in the next generation of high performance fuel cells and batteries, nanoscale electronic devices, biosensors, nanoprobe in scanning probe microscopy, chemical sensors, electromechanical actuators, memory elements for molecular computing and field emitters for flat panel display applications (Baughman *et al.*, 1999; Dai *et al.*, 1996b; de Heer *et al.*, 1995; Kong *et al.*, 2001; Liu and Lin, 2006; Moghaddam *et al.*, 2004; Rueckes *et al.*, 2000; Wang *et al.*, 2002; Wu and Hu, 2005).

Several semiconductor nanoparticles, such as e.g. SiO₂ (Fu *et al.*, 2002), TiO₂ (Banerjee and Wong, 2002b), CdS (Shi *et al.*, 2004), CdSe (Ravindran *et al.*, 2003) and CdTe (Banerjee and Wong, 2003), have been bound to the surfaces of CNTs. Several metal nanoparticles such as Pd (Lim *et al.*, 2005), Ag (Guo and Li, 2005), Pt (Yu *et al.*, 1998) and Au (Liu *et al.*, 2003) have also successfully been immobilized on CNTs. These metal introductions have been carried in view of heterogeneous catalysis (Lordi *et al.*, 2001; Lu, 2007; Xing, 2004) or chemical and biomolecule sensing (Lim *et al.*, 2005; Liu *et al.*, 2005; Tang *et al.*, 2004; Yang *et al.*, 2006b; Zhu *et al.*, 2005)

The modifications of CNTs with metal nanoparticles were first carried out by direct immobilization of metal on carbon nanotubes (Ayala *et al.*, 2006; Bradley *et al.*, 2005; Chen *et al.*, 2005; Chen *et al.*, 2000; Rahman, 2005; Jitianu *et al.*, 2004; Lee *et al.*, 2006; Lim *et al.*, 2005; Liu *et al.*, 2003; Liu *et al.*, 2006; Ma *et al.*, 2006;

Ma *et al.*, 2005; Oh *et al.*, 2005; Sainsbury *et al.*, 2005; Sun *et al.*, 2006; Yang *et al.*, 2006a). This has been achieved by self-assembly of nanoparticles at the CNT surface, heterogeneous coagulation and direct hydrolysis, inorganic reactions in supercritical CO₂-methanol solutions, physical vapour deposition, bipolar electrodeposition, electrodeposition, electroless plating technique, and the sol-gel techniques. Unfortunately, due to the highly hydrophobic nature, the chemical inert character and very regular structure of carbon nanotubes, it is not easy to modify the outer surface of carbon nanotubes (Ellis *et al.*, 2003; Fasi *et al.*, 2003). Furthermore, decorating nanotubes with well-dispersed metal clusters of nanometric dimensions adhering to the nanotubes was also inhibited because of their tendency to aggregate and difficulty to suspend them in solution. Therefore activating their surface is an essential prerequisite for linking nanoparticles to them (Jiang and Gao, 2003).

Activation of carbon nanotube surfaces is usually achieved by covalent functionalization or acid treatments (Han *et al.*, 2004; Jiang *et al.*, 2003b; Lordi *et al.*, 2001; Satishkumar *et al.*, 1996; Showkat *et al.*, 2007; Yu *et al.*, 1998; Zanella *et al.*, 2005). However, these processes normally change the electronic properties of the carbon nanotubes (Ramanathan *et al.*, 2005). An extension of this strategy is the adsorption of surfactant and dispersing agents on the carbon nanotube surface (Jiang *et al.*, 2003b; Jiang and Gao, 2003; Kim and Sigmund, 2004; Zhang *et al.*, 2006) and wrapping of carbon nanotubes with polymer (Carrillo *et al.*, 2003).

In the present study the activation of the carbon nanotube surfaces is a direct and automatic consequence of the purification, solubilization and cutting of carbon nanotubes by the procedure described in Chapter IV. A key element of this strategy is the generation of adsorbed POM anions on the carbon nanotube surface. Therefore in this study the suspension obtained from the purifying and cutting step was used as the starting solution to attach gold nanoparticles to nanotubes without any further surface activation step.

Recently noble metal nanostructures, particularly gold nanoparticles, become the focus of many researchers among others because of their special optical properties (Dirix *et al.*, 1999), electronic properties including conductivity (Terrill *et al.*, 1995) and catalytic activity (Haruta and Daté, 2001). Although bulk gold has been regarded as inert and less active as a catalyst due to its completely filled 5d shell and the relatively high value of its first ionization energy (Bailar *et al.*, 1973), gold begins to show interesting behaviors when its size is reduced to the nanoscale, opening up applications in the field of nanotechnology including nanoelectronic devices, nanoarchitecture, non-linear optics, catalysis, etc. (Daniel and Astruc, 2004; Haruta and Daté, 2001). The melting point of gold, which is in the bulk form 1,060°C, can be as low as 940°C when it is prepared as nanoparticles, as a result of the huge increase in surface area of gold nanoparticles (Inasawa *et al.*, 2005). In the bulk form gold has a familiar yellow color, which is caused by a reduction in the reflectivity of light at the blue end of the spectrum. However, if we subdivide the gold into smaller and smaller particles, there comes a point at which the particle size is smaller than the wavelength of incident light. New modes of interaction between the radiation and the gold become prominent, in particular interactions involving electronic oscillations called surface plasmons lead to variations in color (Alvarez *et al.*, 1997).

Attaching gold nanoparticles (GNP) to nanotube sidewalls is of great interest for obtaining GNP/CNT hybrids which are promising for novel, highly efficient photoelectrochemical cells and sensor device (Hu *et al.*, 2006b). Several approaches of depositing metals onto carbon nanofibers and carbon nanotubes were reported, including the metal decoration of acid-treated (Satishkumar *et al.*, 1996) or phase transfer agent treated CNTs (Qin *et al.*, 2003), the self-assembly of gold nanoparticles on functionalized SWNTs with free thiol ends (Dai *et al.*, 1996b) or also the anchoring of gold colloids to CNTs through the adsorbed polyelectrolyte on the surface of CNTs and the nanoparticle (Jiang *et al.*, 2003b). All these methods have their advantages and also problems and so far no ideal method exists for the highly controlled and eventually site selective metal deposition on CNTs. In order to improve the control over the metal deposition and also its efficiency two complementary methods, the electroless and electrochemical deposition were

developed and extensively studied in the frame of this thesis. It will be shown that these methods allow the generation of original hybrid nanoobjects with a rich structural diversity opening up many potential applications, among others also in the field of analytical chemistry.

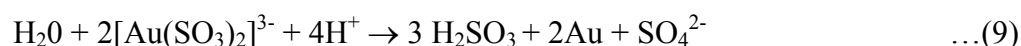
2. Electroless chemical deposition of gold nanoparticles on carbon nanotubes

2.1. Introduction

Previous work of the Bordeaux group reported the synthesis of gold microspheres from a commercial gold plating solution (Li *et al.*, 2007b). Under acidic conditions, gold(I) sulfite complex $[\text{Au}(\text{SO}_3)_2]^{3-}$ in the solution is decomposed and precipitates in the form of metallic gold. The related equations are



The total reaction can be expressed by the following equation



In the present work we tried to adapt this method in order to deposit gold on carbon nanotubes. The key idea is using CNTs as nucleation sites for the gold(I) reactant. The metal layer on CNTs was expected to be obtained in a homogeneous way. Since the size and surface roughness of gold nanoparticles generated in the solution can be easily controlled by varying the acid concentration (Li *et al.*, 2007b) this approach was expected to be easily implementable and a useful procedure allowing controllable modification of CNTs with gold, leading finally to new functional materials.

2.2. Experimental section

A commercial gold plating solution (ECF60) was purchased from Metalor SAS France. The suspension of shortened CNTs in ECF60 (*CNT/ECF60*) was prepared from the stable aqueous suspension of shortened CNTs (*CNT/WATER*) by the detailed experimental procedure shown in Figure 42. The prepared *CNT/ECF60* solution was used to be a starting reagent to form CNTs/golds composites. Details of the experimental method for the electroless gold deposition on CNTs are shown in Table 2.

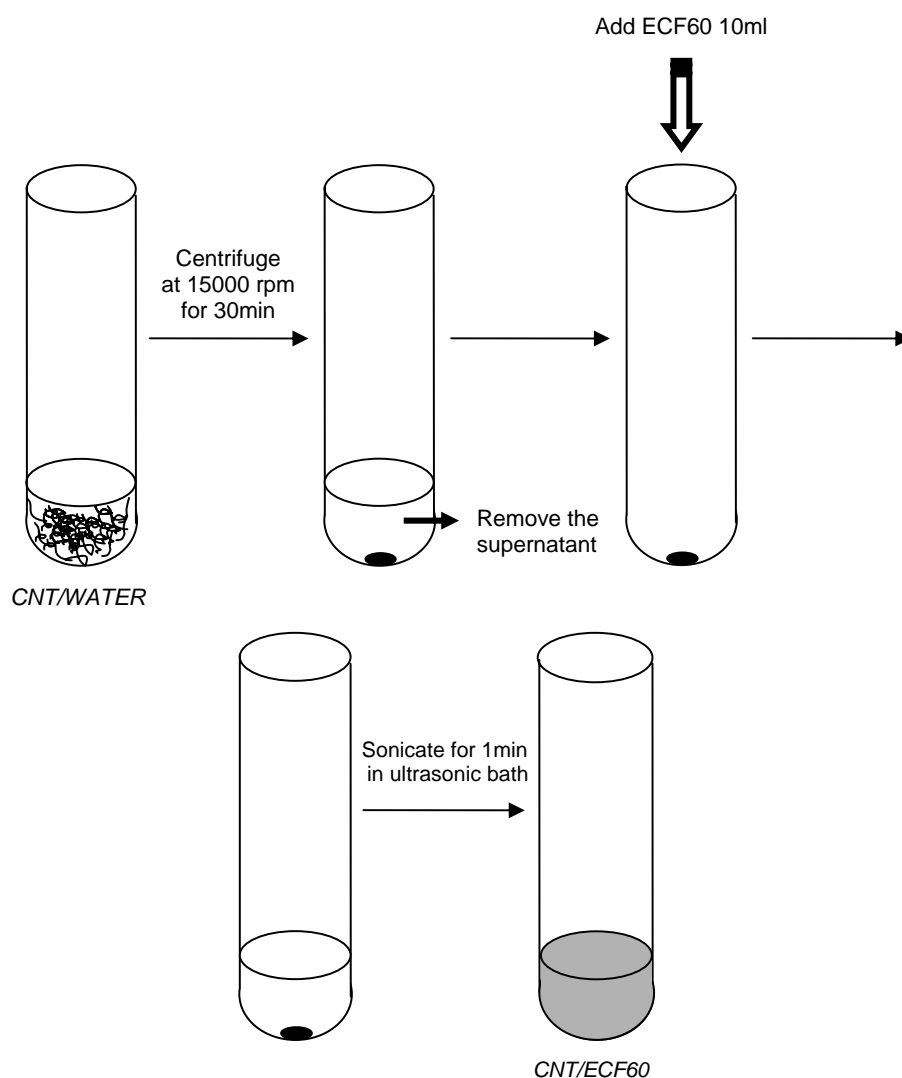


Figure 42 Schematic illustration of experimental procedure for preparation of a suspension of shortened CNTs in the ECF60 solution (*CNT/ECF60*).

Table 2 Detailed experimental method of the electroless gold deposition on CNTs by using the prepared *CNT/ECF60* solution as a starting reagent.

Step	Details	Name	Purpose
1	Prepare 0.5, 1, 2, 3 and 6M HCl		Electroless gold deposition
2	Pipette 1ml of HCl solution (0.5, 1, 2, 3 or 6 M) to glass vial (5ml)	<i>Solution A</i>	
3	Pipette 0.5 ml <i>CNT/ECF60</i> solution and add to <i>Solution A</i>		
4	Wait for 5 minutes		
5	Centrifuge at 10000 rpm for 5 minutes		Purification of CNTs/golds composites
6	Remove supernatant		
7	Add 5ml of <i>ultrapure water</i> to the precipitate		
8	Repeat 4 th , 5 th and 6 th step twice		
9	Add 1 ml of <i>ultrapure water</i>	<i>Solution B</i>	Redisperse the composites in water
10	Deposit one drop of solution B on TEM grid and let the composite dry		Characterization of the composites
11	Repeat 10 th step		
12	Characterize the composites by SEM		

2.3. Results and Discussions

The influence of the HCl concentration on the CNT/gold composite formation was studied by using 0.5, 1, 2, 3 or 6 M HCl. However, we only found gold deposition on CNTs when using 6 M HCl as the reagent. Therefore it can be primary concluded that HCl concentration plays an important role in gold formation on CNTs. The low- and high-magnification HRSEM images of the CNTs/golds composites synthesized by using 6 M HCl are shown in Figure 43. The low magnification images (Figure 43a-c) show that spherical gold clusters were formed as aggregates of gold nanoparticles. These clusters have non-uniform size on the micrometer scale as shown in the previous study (Li *et al.*, 2007) which used ECF60 and 6 M HCl as reagents (CNTs were not involved in the reaction). The high-magnification image (Figure 43d) shows that the gold clusters were formed around the CNTs. This supports our expectation that the gold formation starts preferentially on CNTs as nucleation sites. Since the size of the gold microclusters is significantly different from that of carbon nanotubes the composites is not expected to be useful for applications e.g. as heterogeneous catalysts.

Decreasing the size of the gold spheres was attempted by adding citric acid or water in order to stop the growth of gold particles on carbon nanotubes. This experimental step was performed by adding citric acid and water 30s after the deposition reaction had started (after 3rd step in Table 2). At that moment the gold nanoparticle formation can already be observed by the appearance of an orange color (in contrast to the transparent and colourless starting solution) as shown in Figure 44. However, we found that CNTs were not modified with gold under these experimental conditions. This clearly shows that the formation of gold particles on CNTs is strongly affected by the composition and concentration of the solution. Increasing the concentration of CNTs in *CNT/ECF60* solution is suggested for future work in order to decrease the size of the gold clusters formed on CNTs.

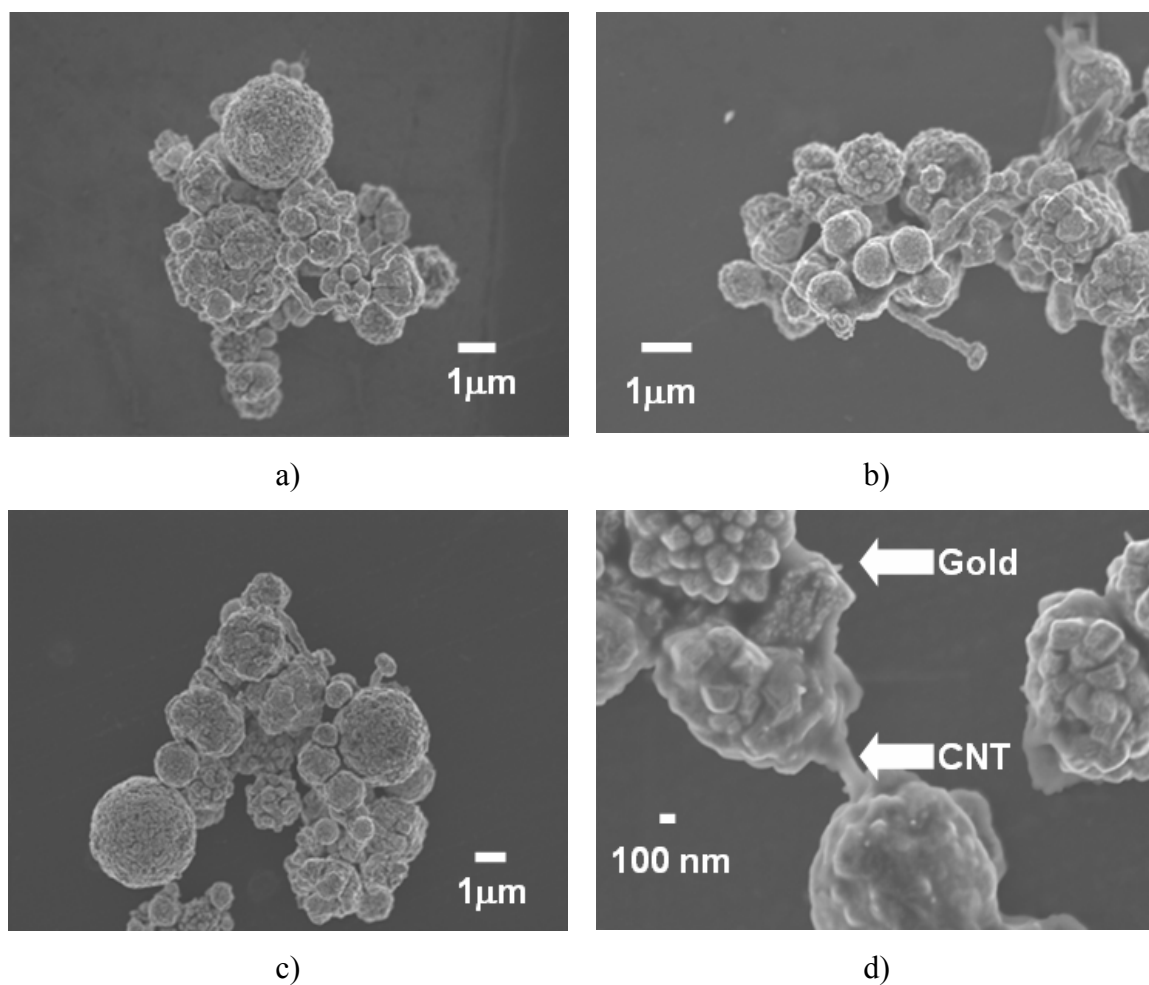


Figure 43 Low-magnification (a-c) and high-magnification (d) HRSEM images of CNT/gold composites synthesized by electroless chemical deposition (the reagent was 6M HCl).



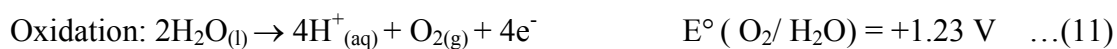
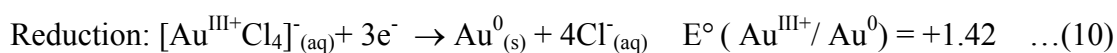
Figure 44 Orange color appearance of the treated solution demonstrates the gold nanoparticle formation 30s after adding the *CNT/ECF60* solution to 6M HCl.

3. Electrochemical deposition of gold nanoparticles on carbon structures by bipolar electrochemistry

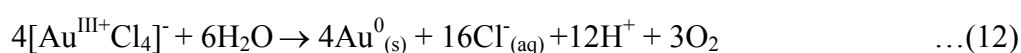
3.1. Introduction

Since dissymmetry brings an additional degree of freedom to systems it can be used to increase the complexity of targeted micro/nano-materials (Hugonnot *et al.*, 2005). Such a strategy could be very promising for self-assembly (Lehn, 1995), chemical sensing (Himmelhaus and Takei, 2000), drug delivery (Mathiowitz *et al.*, 1997), or micro-optics (Ito *et al.*, 1998). It seems therefore very attractive to design a procedure allowing the deposition of gold on the carbon nanotubes in a controlled dissymmetric fashion. One possibility to achieve this goal is using an electrochemical method.

In conventional electrochemistry, electrochemical reactions occur on separated electrodes that are directly connected to the power supply. The modification of an object using a normal gold salt solution is obtained by the reduction of gold ions from the solution at the surface of the object that has to be physically connected to the cathode. In the case of HAuCl_4 as the gold ion source, the electrochemical reaction can be expressed by the following equations occurring at the cathode and the anode respectively:



The total reaction can be expressed by the following equation



Looking at the standard potentials one can conclude that from a pure thermodynamic point of view this reaction should occur spontaneously because Au^{III} ions are such strong oxidants that they can oxidize water. In the present case the real potential is

lower because we use millimolar solutions and therefore according to the Nernst equation we can calculate in a first order approximation:

$$E = 1.42 + 0.059/3 \log 10^{-3} = 1.36 \text{ V} \quad \dots(13)$$

However an analogous calculation can also be made for the second redox couple which has a redox potential of +1.23 V under standard conditions, that means a proton concentration of 1 M. A change in pH will considerably influence this potential and a typical proton concentration of 1 mM would lead to a real potential of 1.05 V.

As the pH locally varies during the experiment no precise prediction about the spontaneous or non-spontaneous character of the reaction can be made, however experimental observation indicates that there is no spontaneous decomposition of the gold salt, at least at the time scale of the experiment. As a consequence an external driving force seems to be necessary to drive the reaction from the left side to the right side. This means that the reaction as written can occur when the cathode (where reduction occurs) potential is more negative than the potential for Au^{III} reduction and the anode (where oxidation occurs) potential more positive than the one calculated for water oxidation.

In our case, the situation is even more complicated because the gold deposition has to take place on the CNTs which are suspended in aqueous solution and therefore not in direct contact with the electrode. We would like to deposit gold on one side of the shortened and purified CNTs which are dispersed in the prepared *CNT/WATER* solution. Therefore a conventional electrodeposition method can not be used and an alternative route has to be taken. Such a method allowing an electrochemical reaction to occur on an isolated object, which is not in ohmic contact with a power supply, falls in the field of “bipolar electrochemistry” (Fleischmann *et al.*, 1985; Bradley *et al.*, 1998).

In bipolar electrochemistry, when an object is placed between two electrodes in an electrolyte (a substance containing free ions that behaves as a conductive medium) and the conductivity of this electrolyte is less than that of the object, the electric field will induce an important potential difference between the poles of the object in line with the field. The induced potential difference, field intensity, and length of the object are related by the following equation:

$$V_d = E \times L \quad \dots(14)$$

where V_d is the potential difference between the poles of the object, L is the length of the object and E is the applied electric field.

Electrochemical reactions can be carried out at the poles of the object when the induced potential difference is sufficient to drive a reduction and oxidation reaction on the two opposite sides of the object with respect to their redox potentials. Oxidation will occur at the side of the object which has an induced partial positive charge. Reduction will take place at the opposite side (where the induced partial negative charge is located). We have chosen the gold/ H_2O couple because in this case the necessary driving force in terms of potential drop quite small or even (see above calculations) and applying a global electric field should easily result in gold deposition. The schematic gold deposition on a tubular object by bipolar electrochemistry in AuCl_4^- solution is shown in Figure 45.

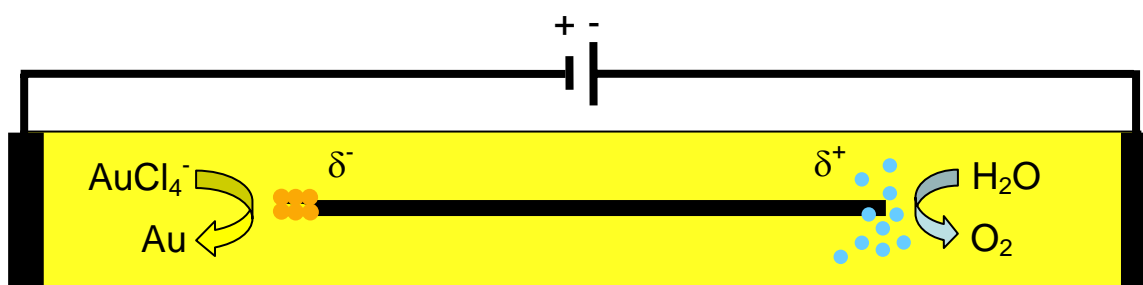


Figure 45 Scheme of the electrochemical reaction occurring on a tubular object in AuCl_4^- solution (See details in text).

The lowest global voltage needed to induce a potential difference sufficiently high to drive the redox couples involving AuCl_4^- and H_2O in the electrolyte (HAuCl_4 solution) on carbon nanotubes was primarily estimated by an analogue electrochemical experiment using a normal carbon fiber on the millimetre scale. This experimental setup used for bipolar electrochemical metaldeposition on a carbon structure is detailed in next section. After the estimated lowest global voltage was obtained, the bipolar electrochemical experiment on carbon nanotubes will be performed.

3.2. Electrochemical deposition of gold nanoparticles on carbon fiber by bipolar electrochemistry

3.2.1. Experimental materials and method

Materials

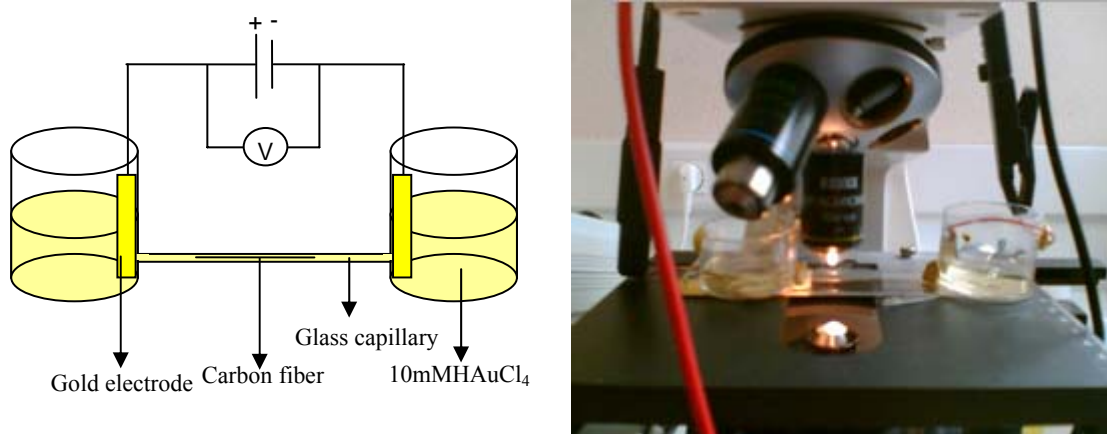
Equipments

1. DC power supply (CONSORT E332)
2. Voltmeter (Multimeter)
3. Inverse light microscope with image display on computer (microscope AXIOVERT 25, camera AxioCam MRc25, and software)
4. Transparent glass capillary (Borosilicate glass capillary, HARVARD apparatus, 1.2 mm O.D., 0.94 mm I.D. and 10 cm long)
5. Plastic vials (to be reservoirs of the solution)
6. Commercial gold coated slide (to be electrodes) (gold plate A.C.M., 50×25×1 mm)
7. Forcep
8. Resin
9. Ultrasonic bath (BIOBLOCK 88154)

Chemicals

1. 10 mM HAuCl_4 (prepared from gold (III) chloride trihydrate $\text{HAuCl}_4 \cdot 3\text{H}_2\text{O}$, SIGMA-ALDRICH)
2. Ethanol (absolute ethanol, SCHARLAU)
3. Substrate: Carbon fiber

Details of the experimental method for the bipolar electrochemical gold deposition on a carbon fiber are shown in Appendix B. In order to illustrate the method, the experimental set up for the bipolar electrochemical experiment is shown in Figure 46.



a)

b)

Figure 46

- a) Schematic illustration of the experimental set up of *VIALS/CAPILLARY*. A carbon fiber was introduced in the glass capillary from a 10 mM HAuCl_4 suspension. Two segmented gold coated slides separated by a distance of 10 cm were used as electrodes. The electrodes were connected to a high voltage DC power supply and voltmeter (V). The reaction occurring on the fiber in the capillary was observed under the microscope.
- b) The experimental setup of *VIALS/CAPILLARY* under the microscope.

3.2.2. Results and discussions

The lowest voltage needed to induce a sufficiently high potential difference which can drive gold deposition on a carbon fiber with 1.3 mm length in 10mM H_{AuCl}₄ was 70V. The distance between the two gold electrodes was about 10 cm. Therefore the induced potential difference between the tips of the fiber is roughly 0.9 V. Then lowest voltage needed to drive gold deposition in 10 mM H_{AuCl}₄ solution onto tubular carbon structures that are oriented parallel to the field lines is estimated as $\frac{9z}{y} \times 10^6$ where the length of that carbon nanostructure is y nm and the electrodes are separated with distance of z cm (see details of calculation in Appendix C).

Optical micrographs that show gold deposition on the carbon fiber are presented in Figure 47. The field application time varied from 0-80 min. The length of the fiber was measured under the microscope to be approximately 1.3 mm. The images show gold deposition only on one end of the fiber as expected, the other end of the fiber will be the anode. A direct correlation between the amount of deposited gold and the time of the experiment can clearly be observed. As shown in the figure the gold deposit is concentrated mainly on the tip of the fiber. The gold continues to deposit on previously deposited gold cluster. This is in agreement with the fact that when a carbon fiber is placed in an electric field, the effect of the electric field at the carbon fiber/solution interface extends along the entire length of the fiber. When the fiber is straight and parallel to the field lines, the maximum potential field difference will be at the tips of the fiber, which are closest to the electrodes.

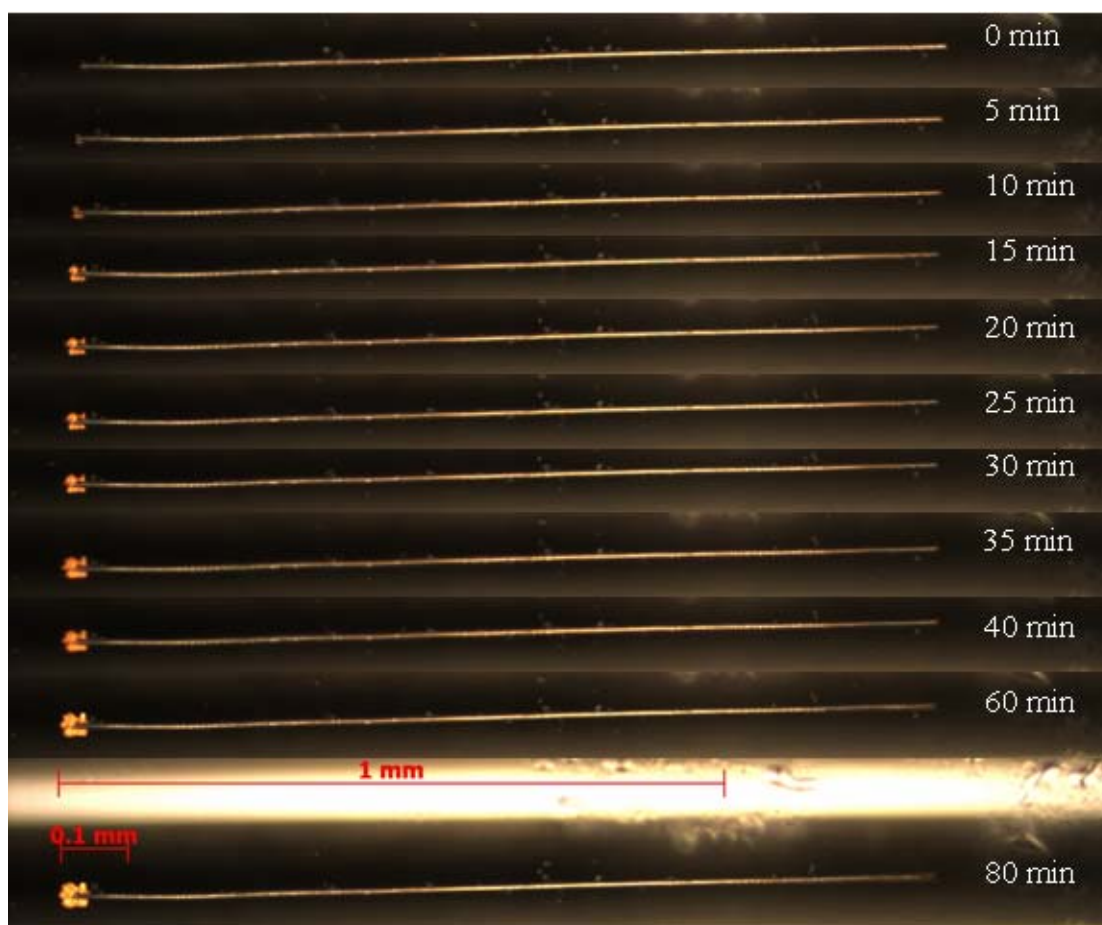


Figure 47 Optical micrographs at the same magnification of a carbon fiber (length about 1.3 mm) with gold deposited by bipolar electrochemistry (70V, 10 mM HAuCl_4) as a function of time.

After 80 minutes of deposition, the gold cluster was found to be of 0.05 mm length along the fiber axis. It should be noted from Equation (11) that the oxygen bubble formation should be observed on the right hand side, cathode side, of an optical micrograph taken during the electrochemical process if the process is rapid. However, we do not see any bubbles in this series of pictures (Figure 47). We assumed this is to be because the electrochemical process is slow and then the formed oxygen has enough time to dissolve in the electrolyte. This expectation was proven by performing an additional electrochemical experiment with much higher voltage of 300 V (the field application time was 30 S.) on a carbon fiber (1.2 mm length). We observed that a big oxygen bubble was formed on the right hand side, the anode side

(see Figure 48). Since the electrochemical process happened here is now much more rapidly than in the previous experiment shown in Figure 47. The solution becomes locally saturated with the formed oxygen which forms a big bubble.

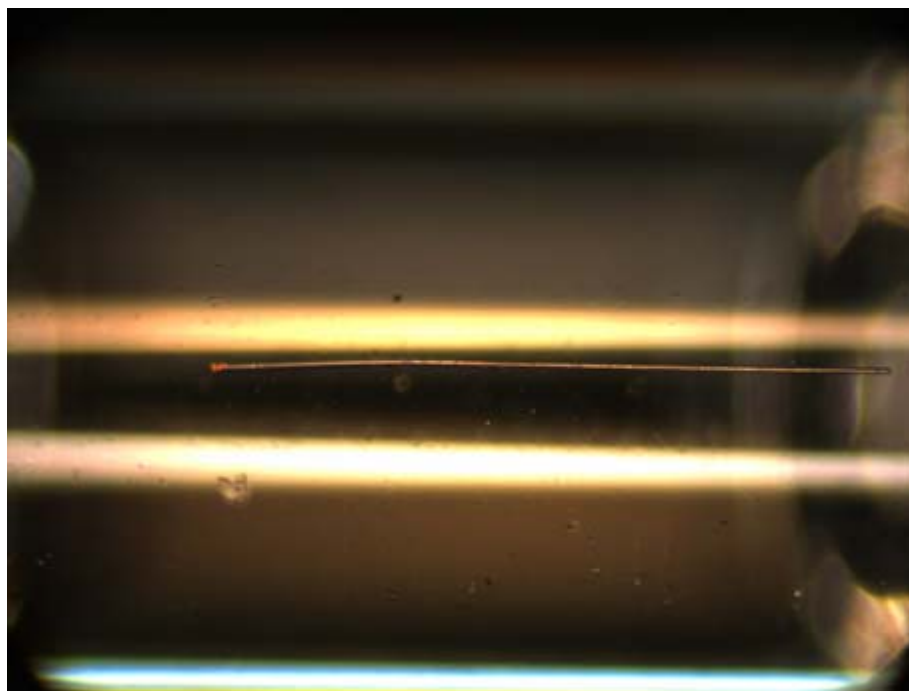


Figure 48 Optical micrograph of a carbon fiber (length about 1.2 mm) with gold deposited by bipolar electrochemistry (300V, 30 S, 10 mM H_{AuCl}₄).

Low- and high-magnification SEM micrographs of a carbon fiber (length about 1 cm) with a gold cluster deposited on one tip by bipolar electrochemistry (the applied voltage was 40V, the electric field application time was 30S and the used electrolyte was 10 mM H_{AuCl}₄) are shown in Figure 49.

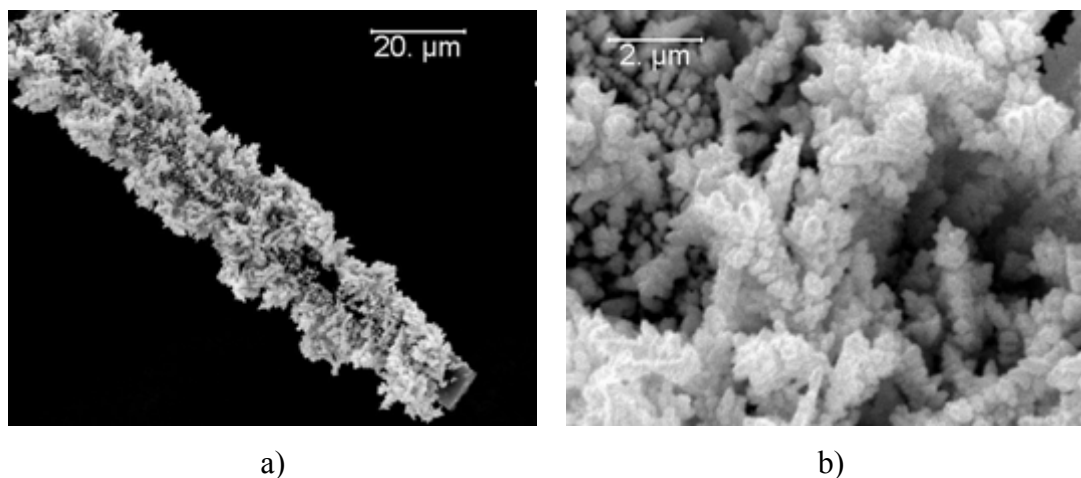


Figure 49 a) Low- and b) high-magnification HRSEM picture of a carbon fiber with gold deposited by bipolar electrochemistry (40V, deposition time 30s, 10 mM HAuCl₄).

Structural details of gold deposition on carbon structures by normal gold salt solution are revealed by the high-magnification SEM image (Figure 49b). The gold deposit on the fiber is composed of gold nanoclusters and thus exhibits a high surface area. This rough surface, however, is not always an advantage. For some applications, especially for the analytical applications planned in this project, a smooth surface would be better. Therefore replacing HAuCl₄ by a commercial gold plating solution is considered in next section. Since the commercial plating solution contains additives such as surfactants this plating solution, it is expected to give a smooth surface gold layer on carbon structures.

3.3. Electrochemical deposition of gold nanoparticles on carbon nanotubes by bipolar electrochemistry

3.3.1. Experimental section

The carbon nanotube/water suspension obtained from the purifying and cutting step was used as a starting solution to attach gold nanoparticles to nanotubes by a bipolar electrochemical process. After analysing its composition the *CNT/WATER* suspension (about 20 ml) was divided into two parts (10 ml per each). To the first part was added 0.59 g of gold (III) chloride trihydrate ($\text{HAuCl}_4 \cdot 3\text{H}_2\text{O}$) (SIGMA-ALDRICH). To the second part was added 5.9 g $\text{HAuCl}_4 \cdot 3\text{H}_2\text{O}$. The concentrations of HAuCl_4 in both solutions were 1 mM and 10 mM, respectively. We called the obtained suspensions *CNT/HAuCl₄*. The bipolar electrochemical process of *CNT/HAuCl₄* suspension was first performed by using a simple experimental setup. The simple equipment which was used here is a disposable cuvette, a DC power supply, two gold electrodes (prepared from gold coated glass slides, A.C.M.). This experimental setup is schematically shown in Figure 50. Details of this experimental setup are shown in Table 3.

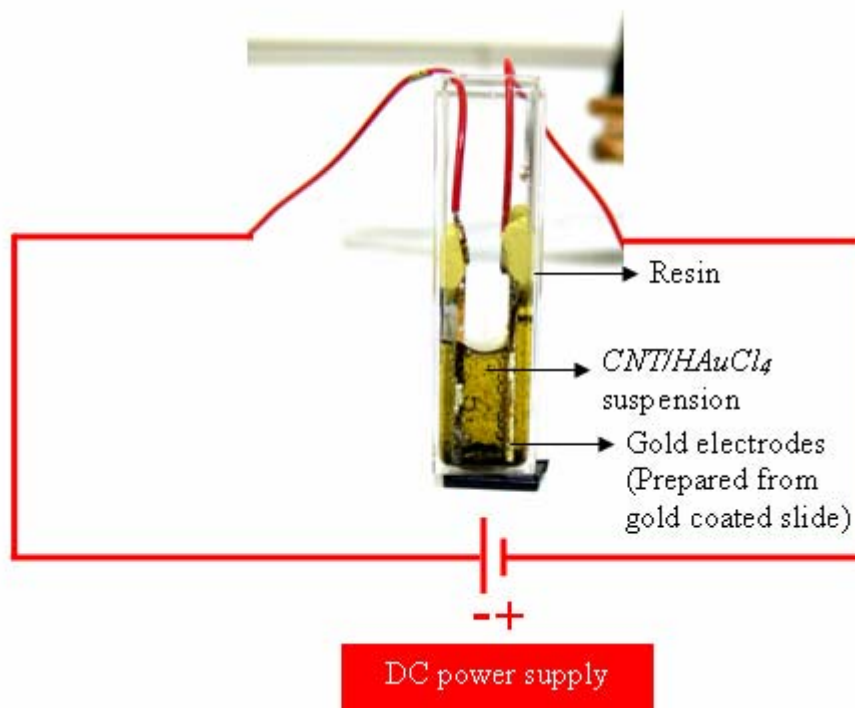


Figure 50 Schematic illustration of our first experimental setup for bipolar electrochemical gold deposition of CNTs. The electrochemical reaction was performed in a disposable cuvette by using the *CNT/HAuCl₄* suspension as a starting suspension. Two segmented gold-coated glass slides were used as electrodes. These electrodes were fixed on the wall of the cuvette by resin. Applied voltage from a DC power supply was used to drive the electrochemical reaction.

Table 3 Detailed experimental method of the bipolar electrochemical gold deposition on CNTs by using the prepared *CNT/HAuCl₄* solution as a starting reagent.

Step	Details	Purpose
1	Place two gold electrodes (about 0.6 cm×3cm) prepared from the gold-coated glass slides vertically in a disposable cuvette. Fix the gold electrodes at wall of the cuvette with resin (see Figure 50).	Bipolar electrochemical gold deposition on CNTs
2	Connect the electrodes to DC power supply without applying electricity.	
3	Fill the cuvette slowly with <i>CNT/HAuCl₄</i> suspension (about 2 ml).	
4	Apply voltage from DC power supply (see details of the applied voltage and the field application time in the next result and discussion section).	
5	Stop voltage after desired field application time has been reached.	
6	Transfer the suspension from the cuvette to an eppendorf (1.5 ml).	Purification of CNTs/golds composites
7	Centrifuge the suspension at 10000 rpm for 5 minutes.	
8	Remove supernatant.	
9	Add 1.5 ml of <i>ultrapure water</i> to the precipitate.	
10	Repeat 7 th , 8 th and 9 th step twice.	Redisperse the composites in water
11	Add 1.5 ml of <i>ultrapure water</i> . Shake the suspension gently.	
12	Deposit one drop of the suspension on TEM grid and let the composites dry	
13	Repeat 10 th step	Characterization of the composites
14	Characterize the composites by HRSEM	

3.3.2. Results and discussions

The carbon nanotubes contained in the *CNT/WATER* suspension which is used as the starting solution have lengths in the nanometer range (about 90-1300 nm, see Chapter IV). The distance between the electrodes was approximately 1 cm. Therefore the lowest voltage needed to drive gold deposition in 10 mM HAuCl₄ solution onto carbon nanotubes, can be estimated from the bipolar electrochemical gold deposition experiment on a carbon fiber (with 10 mM HAuCl₄). Depending on the length it should be in the range of 6.9 kV to 100 kV (calculated from Equation (15), Appendix C). However, because of the different physico-chemical character of a carbon fiber, which is a straight composite and amorphous material, and a carbon nanotube which is a carbon allotrope and has a non-straight morphology the critical voltage might vary. Therefore the lowest overall potential needed to drive gold deposition in the solution onto carbon nanotubes can only be roughly estimated from the results obtained with the carbon fiber.

The maximum voltage of the available DC power supply (CONSORT E332) was 300 V. Therefore we first used that maximum applied voltage of 300 V for the electrochemical reaction. After 30 s of field application we observed bubble formation in our electrochemical system, indicating that some electrochemical reaction had occurred. After a field application time of 5 min the field application was stopped. The composites in the suspension were isolated by centrifugation and purified twice with *ultrapure water*. This suspension was dried on a TEM grid and characterized by HRSEM.

HRSEM images of the obtained particles (see Figure 51) show the gold deposits on CNTs. These gold deposits completely cover the CNTs. This indicates that the voltage of 300 is enough to drive the bipolar electrochemical gold deposition onto CNTs in 10 mM HAuCl₄ and the field application time of 5 min is enough or even too much for growing gold onto the CNTs. In order to reach the objective to get dissymmetric gold deposition onto individual tubes it was necessary to decrease the

field application time to 1 min and the applied voltage to 100 V in a subsequent experiment.

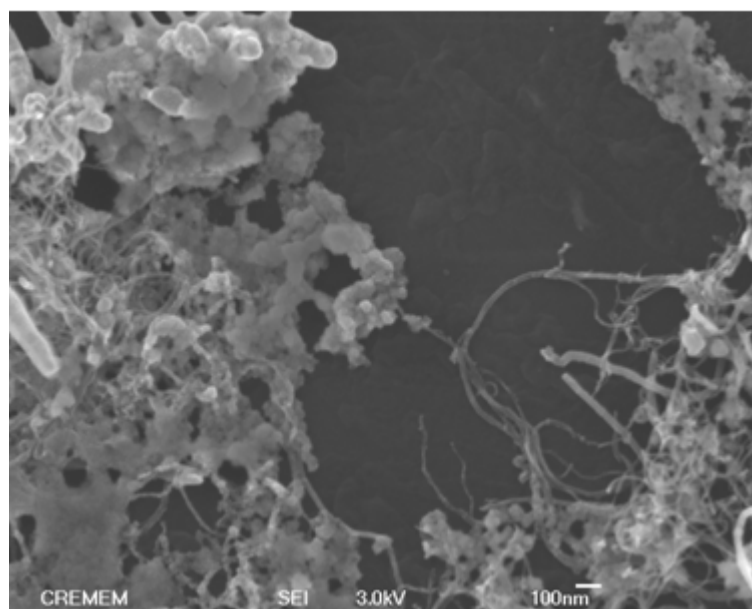


Figure 51 HRSEM image of the carbon nanotubes, which were completely covered by gold deposits during bipolar electrodeposition (300V, 5 min and 10 mM HAuCl_4).

A HRSEM image of the gold deposition onto CNTs in 10 mM HAuCl_4 with a field application time of 1 min and an applied voltage of 100 V is shown in Figure 52. The image shows that the applied voltage of 100 V is still enough to drive gold deposition reaction onto carbon nanotubes in 10 mM HAuCl_4 solution and the field application time of 1 min is still too long. This gold amount is less than what we obtained from the previous experiment (300 V and 5 min), however it is still too high for our selective dissymmetrical deposition. Thus we used a voltage of 100 V and decreased the field application time to 30 s for the next experiment. In this experiment, we also used a more diluted gold solution (1mM $\text{CNT}/\text{HAuCl}_4$ suspension) in order to decrease the amount of gold deposited on CNTs.

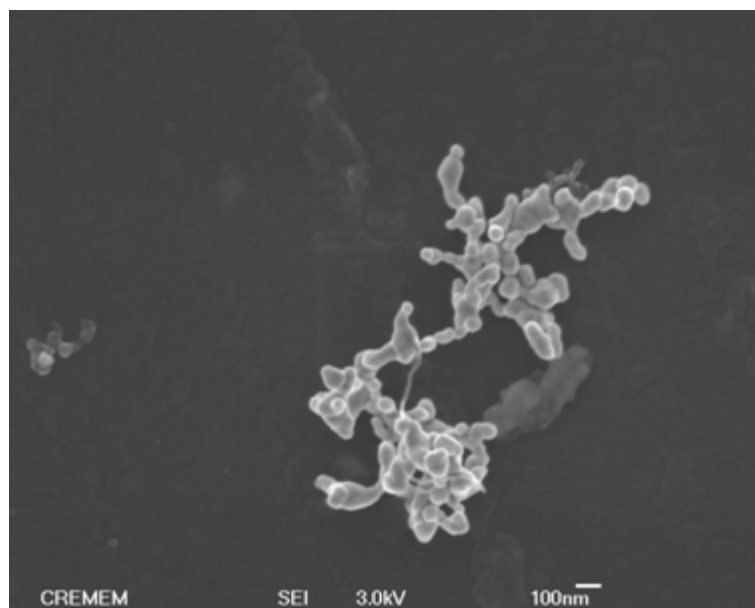


Figure 52 HRSEM image of the carbon nanotubes with gold deposits obtained by bipolar electrochemistry (100V, 1 min and 10 mM H_{AuCl}₄).

HRSEM images of individual tubes with gold deposits obtained by bipolar electrochemical reactions (100V, 30 s and 1 mM H_{AuCl}₄) are shown in Figure 53. These CNTs were almost completely covered by gold. Some of them show the dissymmetric characteristics that we expect from bipolar electrochemistry. The diameter (along tube diameter axis) of the gold deposits here are in range of 100-350 nm. These are still very much compared to a normal carbon nanotube diameter (less than 40 nm). Therefore milder experimental conditions (a decreased voltage and/or a decreased field application time and/or a decreased gold salt concentration) were used for further experiments performed with this simple setup.

We observed that a lot of bubbles were produced during this experiment. This causes CNTs in the suspension moving around very quickly. Therefore they do not have a preferential orientation with respect to the electrical field and thus the final dissymmetric nature can not be obtained using this setup. It was therefore necessary to change the experimental set-up in a way to avoid the bubble formation and the resulting convection in the CNT suspension. One trick to eliminate this problem is to

use capillary electrophoresis. The details of this technique will be discussed in the next section.

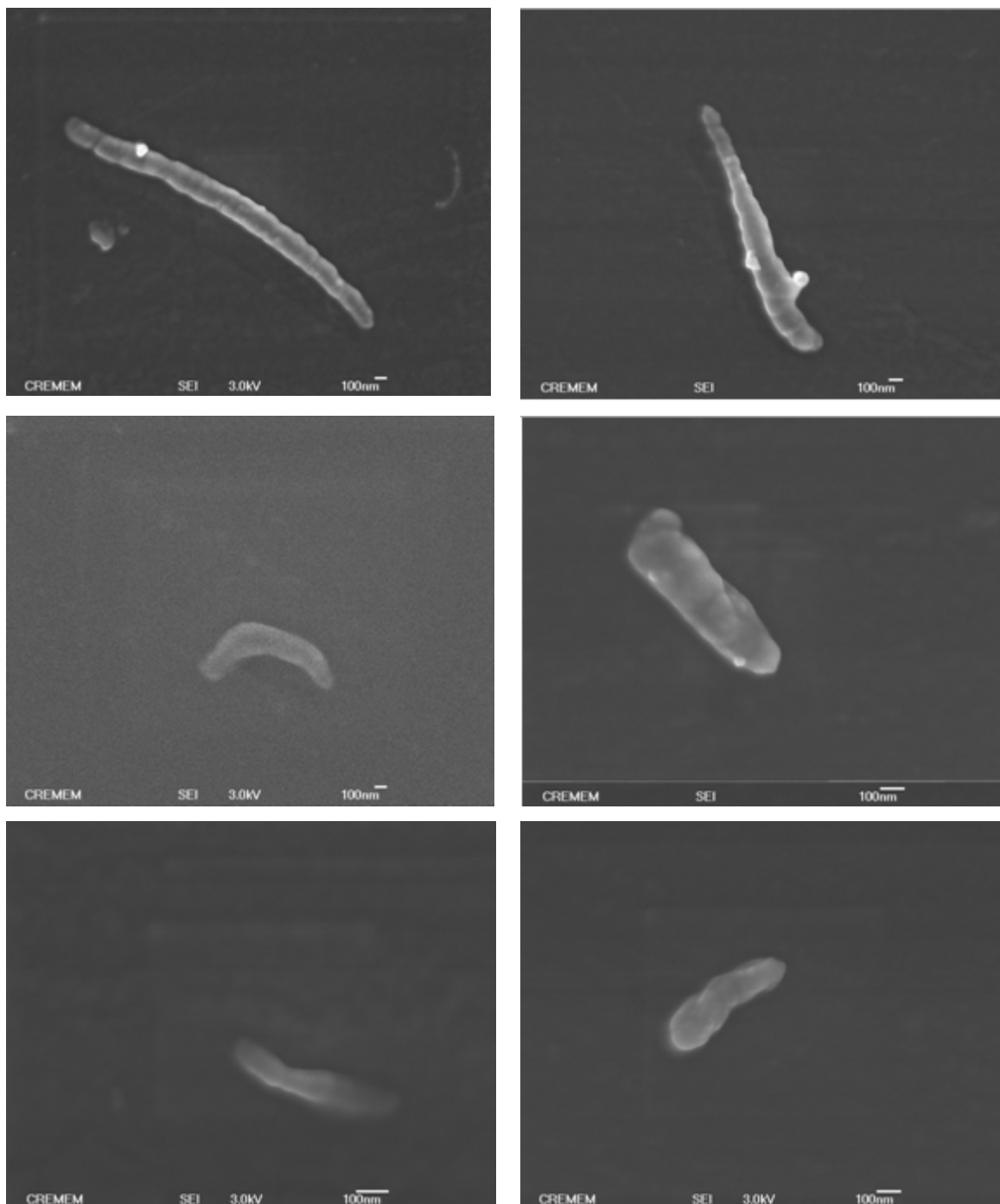


Figure 53 HRSEM images of carbon nanotubes modified with gold deposited by bipolar electrochemistry (100V, 30 s and 1 mM HAuCl_4).

3.4. Bipolar electrochemical deposition of gold nanoparticles on carbon nanotubes by capillary electrophoresis

3.4.1. Introduction

Electrophoretic methods have shown a great potential for purification of nanotubes. Bulk electrophoresis has been used for alignment of nanotubes and is capable of separating nanotubes from particular impurities (Yamamoto *et al.*, 1998). The use of capillary electrophoresis (CE) was reported as an alternative method for separating carbon nanotubes by size (Doorn *et al.*, 2002). Capillary electrophoresis separations are based on charge and size-dependent mobility of solution phase species under the influence of an applied electric field. The rapid, high-resolution separation available with CE has the potential to separate a nanotube sample into discrete fractions of uniform size tubes. The principle of this technique is described as follows.

Basic principle of capillary electrophoresis

Capillary electrophoresis belongs to a family of techniques used to separate a variety of compounds. The separation of the compounds is here driven by an electric field. The operation in a narrow tube, capillary, results in the rapid separation of many hundreds of different compounds. A CE instrument usually consists of two buffer reservoirs, a very long (10-100 cm in length) and small diameter (10-100 μm i.d.) capillary tube (which normally is a fused silica capillary), a high voltage power supply (10-60 kV), a detection system (typically UV absorbance detector). Separation is performed in the electrolyte filled capillary where a current is applied (see Figure 54). The charge of the inner wall of the capillary causes the flow of electrolyte from the anode (where the sample is applied) to the cathode (where the sample is analyzed). The flow of electrolyte through the capillary is called an electro-osmotic flow (EOF). It drives positively charged, neutral and negatively charged analytes through the capillary to the detector. A second force which is electrophoresis, relates to the charge and size of the analyte. An analyte will have a high electrophoretic

mobility when its charge is high and its size is low. This force enhances EOF for cations and opposes EOF for anions, resulting in their further separation.

Adjusting the pH of electrolyte can control the balance between EOF and electrophoresis. At pH above 5, the silanol groups on the inner wall of the silica capillary are ionized, giving the negative charge wall and then resulting in an EOF. At pH below 5, the capillary wall loses its charge, causing the EOF disappear and making electrophoresis become the dominant force (Linhardt and Toida, 2002).

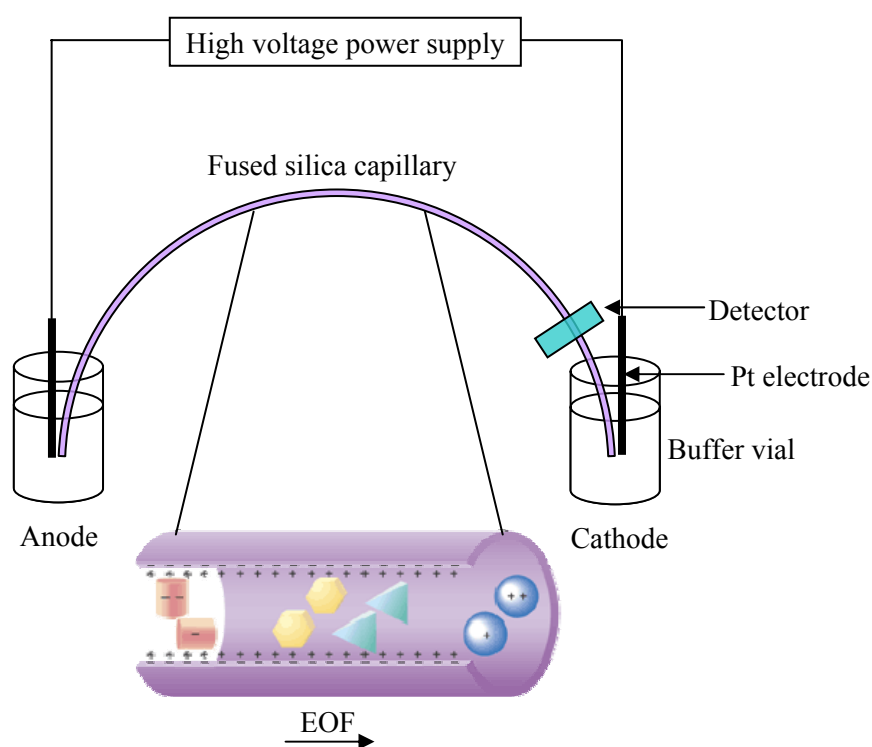


Figure 54 Schematic illustration of a capillary electrophoresis apparatus. An open-end capillary (purple) is placed between two buffer reservoirs. A high voltage is applied across this capillary. This voltage causes the migration of analytes (red, yellow, and blue shapes) from the anode side (+) to the cathode (-) (through detector). Electrophoresis speeds up the migration of cations and retards the migration of anions through the capillary (Linhardt and Toida, 2002).

The analytes separate as they migrate due to EOF flow and electrophoretic mobility. These analytes are detected by a detector near the outlet end of capillary. The output of the detector is sent to a data output and handling device such as an integrator or computer. The data are then displayed as an electropherogram, which reports detector response (typically UV absorbance) as a function of time. Separated chemical compounds appear as peaks with different retention times in an electropherogram.

As we mentioned earlier a bipolar electrochemical process can be carried out at the polarized ends of the object, which is placed between electrodes in an electrolyte when the induced potential difference across this object is sufficient to drive reduction and oxidation reactions. Therefore CE is expected to allow bipolar electrochemical gold deposition on CNTs without disturbing the CNT alignment by bubble formation because the electrodes are located outside of the capillary. Due to the high electric field and rapid operation (separation), this technique is expected to provide the dissymmetrical gold deposits onto carbon nanotubes and the gold deposits should concentrate mainly on the tip of the tubes. The separation ability (based on charge and size) is also expected to facilitate the homogeneity of the obtained tube size for a given retention time. In this study the possibility of bipolar electrochemical gold deposition on carbon nanotubes performed by capillary electrophoresis will be reported. The details of the experimental method are shown in next section.

3.4.2. Experimental section

The starting suspension of CNTs used for the CE experiment is the *CNT/HAuCl₄ (1 mM)* suspension. For CE experiments, all solutions or suspensions were introduced into the capillary by pulling 1 ml of them with a syringe manually. The capillary used here is a fused silica capillary with 46 cm length and 100 μm inner diameter, respectively. The distance from the entrance (the capillary inlet end) to the detection window in this case was 41 cm. The applied voltage was 30 kV. The temperature was maintained at 25°C. The CE experiment was first performed by rinsing of the capillary with *ultrapure water*. When the capillary was clean, the

diluted aqueous suspension of the shortened, POM-modified carbon nanotubes (suspended in the *CNT/WATER* suspension) was introduced into the capillary. The reason for using a diluted suspension for the CE experiment is due to the narrow capillary (100 μm). Introducing a solution containing concentrated particles will lead to clogging of the capillary. The capillary was conditioned with 30 kV. The migration characteristic of shortened, POM-modified CNTs moving in the capillary was determined by recording the variation in the UV absorbance (254 nm) as a function of time. This feature is characterized by the time when CNTs start to leave the capillary and the necessary time for all CNTs to leave completely the capillary. Next, we start the bipolar electrochemical gold deposition of CNTs by introducing the *CNT/HAuCl₄* (1 mM) suspension into the capillary. Because the addition of acid (HAuCl₄ here) can result in the aggregation of the POM-modified CNTs so, the suspension has to be sonicated for 1 minute in ultrasound bath in order to maintain the dispersion of CNT in the solution before introducing it into the capillary.

The particles coming out from the capillary were collected at the outlet of the capillary by replacing slowly the suspension in the capillary with *ultrapure water*. By using a syringe, one drop of the suspension was replaced by injected water at the inlet. This collected sample drop was put on a TEM grid and dried. Because the suspension contains mainly the gold salt (AuCl₄⁻), drying of the suspension on the grid will lead to gold salt crystallization which will extremely disturb the further TEM analysis, therefore after the suspension was dropped onto TEM grid, the solution (HAuCl₄) was dragged through the grid by placing a cleaning tissue under the grid. The process moves the solution towards the cleaning paper and then leaves the modified particles on the grid. After that, the particles on the grid, were washed three times with *ultrapure water*. This washing step was again performed by dropping one drop of *ultrapure water* on the grid and then dragging the liquid through the grid by using cleaning paper. The washed particles were characterized by TEM.

3.4.3. Results and discussions

The capillary was first rinsed by *ultrapure water*. The cleanness of the capillary is demonstrated by the recorded electropherogram. The electropherogram, which shows no significant variation in the absorbance with the time (see Figure 55), demonstrates that the capillary is very clean.

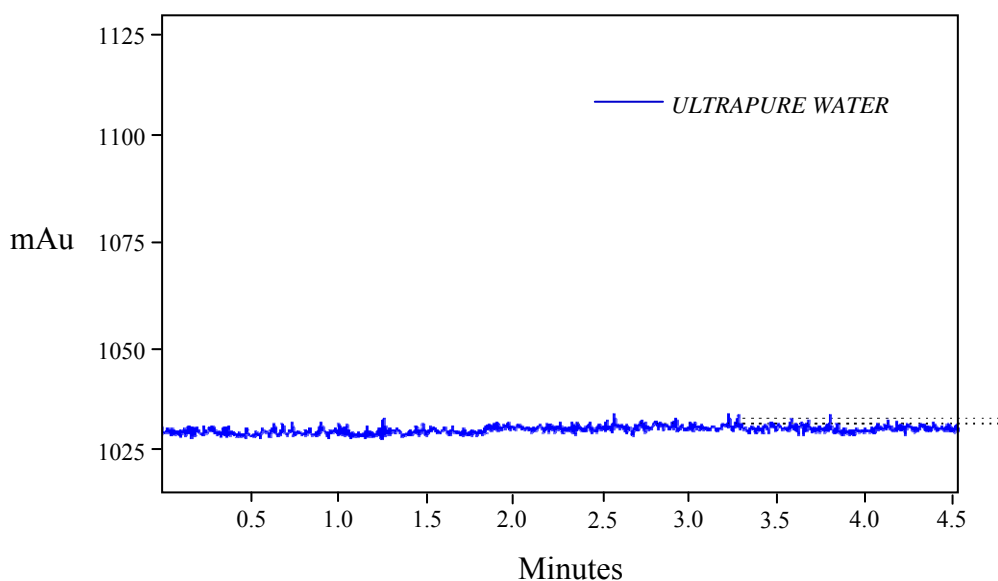


Figure 55 Electropherogram of *ultrapure water* passing through the capillary as a function of time (at 30 kV). Insignificant variations in the UV absorbance (254 nm) with time show that the capillary is clean (there is no other species except water passing in front of the detection window).

After the capillary was cleaned, the characteristic migration of shortened, POM-modified CNTs in the capillary was determined. The electropherogram of shortened carbon nanotubes suspended in water is presented in Figure 56. The large variation in the absorbance at 254 nm during 2-4 min after the capillary was conditioned (30 kV) shows that 2 min after the conditioning of the capillary, the CNTs start to leave the capillary and all CNTs have left the capillary after 4 min. We therefore have chosen to collect samples of modified nanotubes 2 min after the

capillary was conditioned. We expect that the gold modified-CNT will start leaving the capillary at this time.

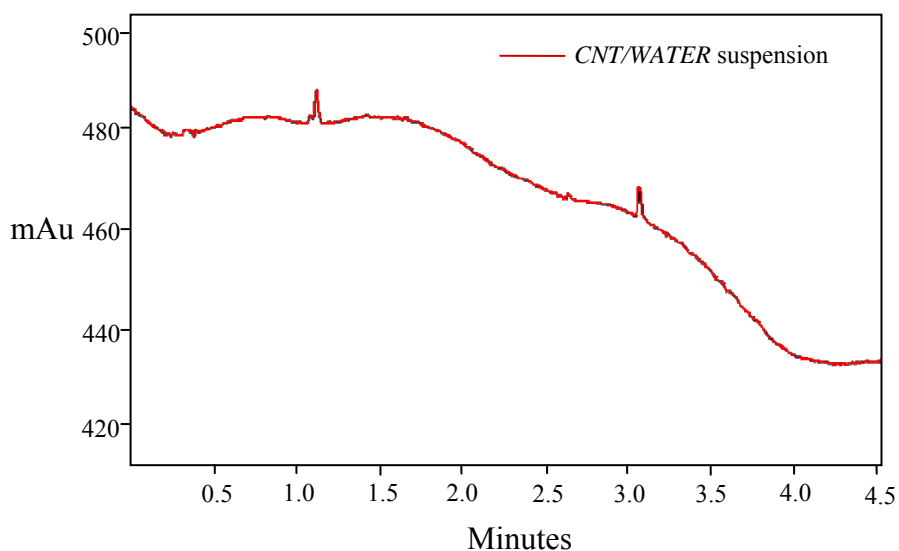


Figure 56 Electropherogram of the CNT/WATER suspension showing the large variation in the UV absorbance at 254 nm between 2-4 min after the capillary was conditioned at 30 kV. This variation indicates that the CNTs start to leave the capillary at about 2 min after the capillary conditioning and all CNTs have left 4 min after the capillary conditioning.

The starting suspension of CNTs used for the bipolar electrochemical CE experiment, the *CNT/HAuCl₄ (1 mM)* suspension, was introduced into the capillary after sonication in ultrasound bath for 1 min. The capillary was conditioned at 30 kV. After 2 min, the application of the electric field was stopped. The modified particles were collected and put on a TEM grid. After washing of these particles by *ultrapure water* three times, the particles were characterized by TEM.

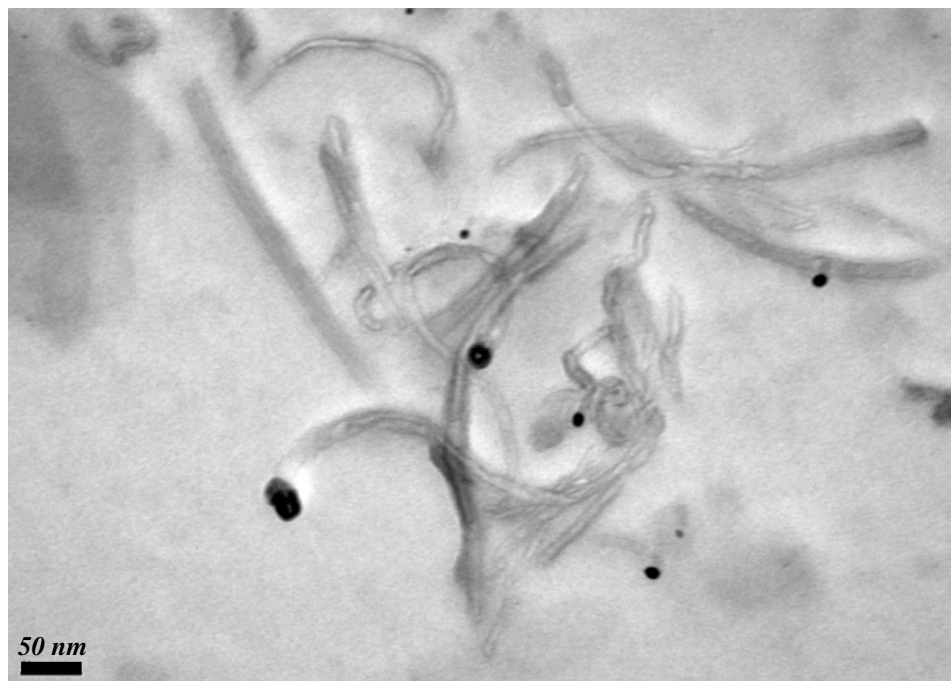


Figure 57 High-magnification TEM image of shortened, POM-modified CNTs taken after the CE experiment (30 kV, 2 min). Some of the tubes are modified with gold concentrating only on the tip.

Following the interruption of the field application at 2 min (after conditioning the capillary), many carbon nanotubes (tube length in the range of 200-800 nm) were modified by gold (diameter about 20-50) (see Figure 57-61). Figure 57 shows many carbon nanotubes staying close together and some of them are modified with gold. The gold deposit concentrates only on the tip of the tubes due to the dissymmetric character of the bipolar electrochemical reaction. This implies that the capillary electrophoresis technique is capable to align some of the carbon nanotubes parallel to the field and the potential gradient in the capillary (30 kV/41 cm) is enough to drive the bipolar electrochemical reaction on both sides of the aligned tubes. Furthermore the field application time of 2 min is enough to lead to a visible gold deposit locally at the CNT tips. Therefore our objective to deposit gold locally on the tips of carbon nanotubes, can be reached using the CE experiment. However as can be seen from the image, not all nanotubes are modified with gold. There might be two different reasons for this:

First, some nanotubes are most likely too short so that the potential drop during the CE is not high enough to trigger the electrochemical reaction. Second, if the orientation of the CNT is not parallel to the field this also will lead to an insufficient potential drop. Finally nanotubes exist in conducting, semiconducting and isolating forms as a function of their molecular structure. The bipolar electrochemical reaction can only occur on conducting nanotubes, eventually on semi-conducting ones, but certainly not on isolating ones. Therefore the unmodified nanotubes might belong to the latter two categories of CNTs. This finally gives an additional interesting feature to this CE procedure, because it might allow to sort nanotubes as a function of their electrical conductivity, a topic of increasing interest (Doorn *et al.*, 2003).

Figure 58 shows individual carbon nanotubes which are modified with gold localized at the tips. The gold deposit here clearly leads to dissymmetric objects due to the features of the bipolar electrochemical process.

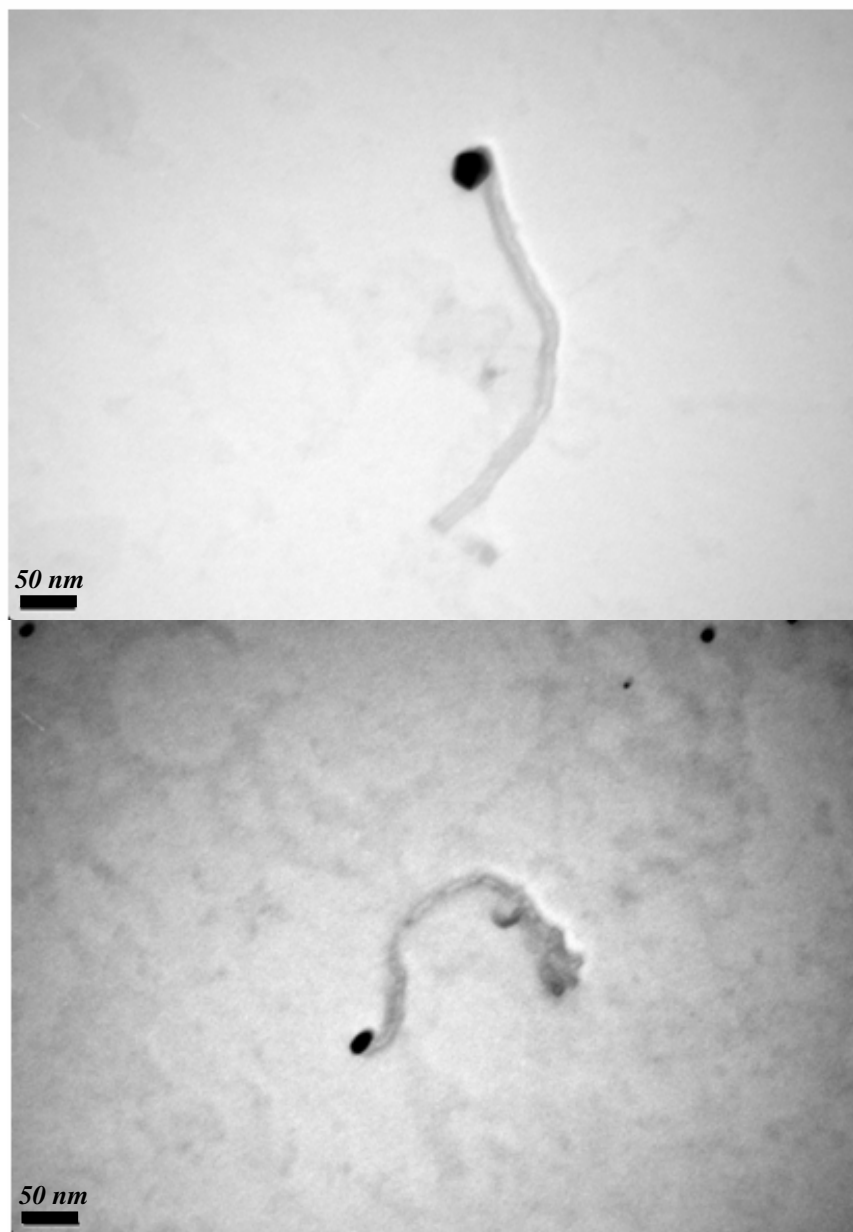


Figure 58 High-magnification TEM image of shortened, POM-modified CNTs taken after the CE experiment (30kV, 2 min). The CNTs here are modified by gold locally on the tip.

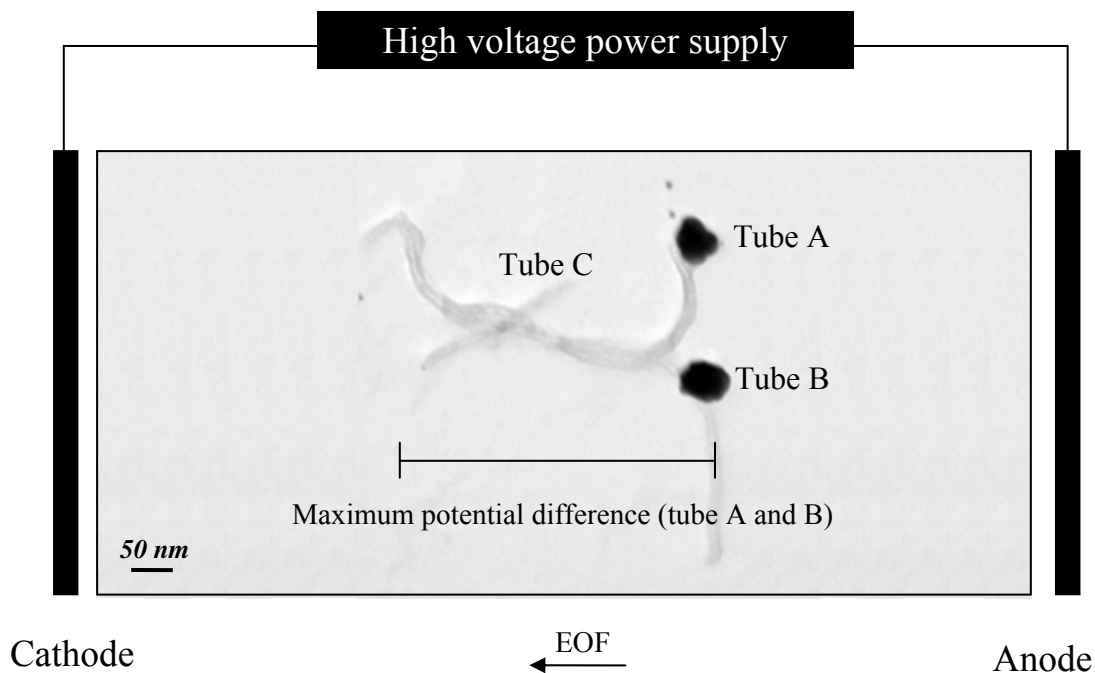


Figure 59 High-magnification TEM image of CNTs (obtained by the CE experiment (30 kV, 2 min) and the supposed alignment of the tube A and B (see details for tube C in the text) in the field. These alignments are deduced from the obtained gold structures. The locations that give maximum potential difference (parallel to the field) of the tubes are supposed to be almost at the tips of tube A and closest to the electrodes for tube B. For tube C, this potential is supposed to be not high enough to drive an electrochemical reaction because gold deposition on tube C was not found.

The TEM image of a group of CNTs containing inhomogeneous features of gold deposition is shown in Figure 59. It is found that two tubes are modified with gold at different locations (on the tip of tube A and on the tube wall of tube B) and one tube is not modified with gold. Based on the principles of bipolar electrochemical deposition, this means the fact that the maximum potential drop will occur across the part of the object that is in a direction parallel to the field, we should observe for an object which is straight and parallel to the field, that the deposition occurs at the tip of the object. For an irregularly shaped object or an object which is not aligned parallel

to the field, the maximum potential difference will be between the locations that are closest to the electrodes. As a consequence the electrochemical reaction will happen at those positions instead of the tips of the object. Based on these arguments, the alignment in the field for tubes A and B is supposed to be at locations that are almost on the tips of tube A and nearest to the electrodes for tube B. For tube C, gold deposition onto the tube was not observed. As already explained above there are at least three reasons why there is no gold deposition. First, the tube is not aligned with the electric field and therefore only a very small potential drop occurs between the both ends of the CNT. Second, even if this tube is aligned parallel to the direction of the electric field the induced potential difference is most likely not enough to drive the electrochemical reaction because tube C is much shorter than tube A and B. Then this tube would require a much higher overall voltage to drive the electrochemical reaction and 30 kV is not enough. The third possibility is that this tube is an isolator/semiconductor and therefore no charge transfer can take place between the two ends of the CNT.

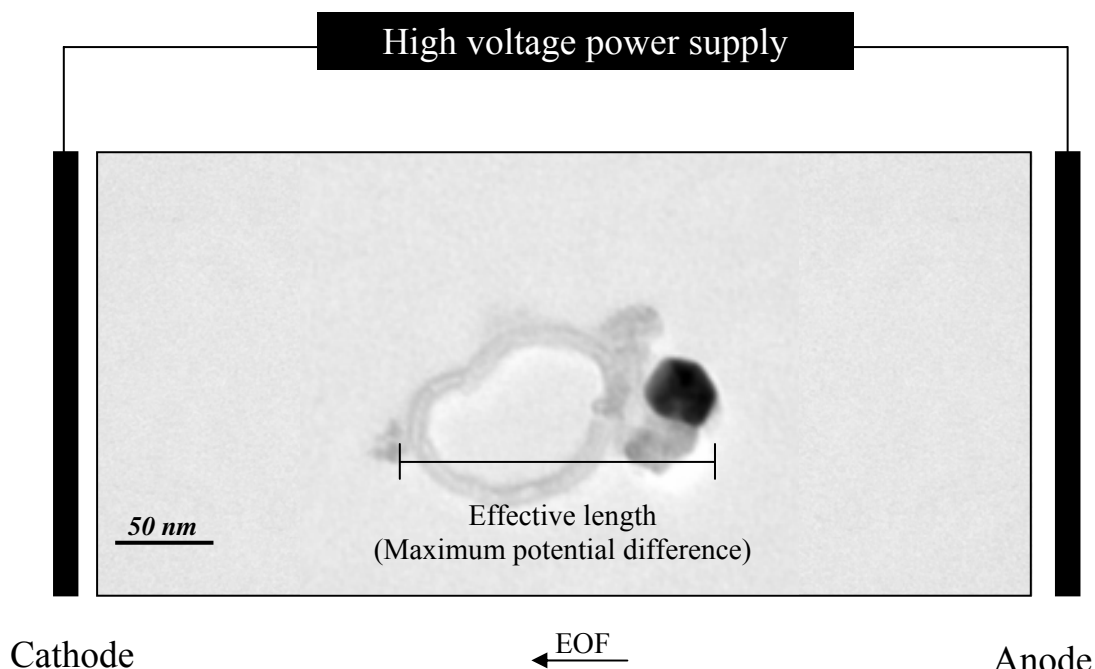


Figure 60 High-magnification TEM image of an irregular curved CNT (obtained after the CE experiment (30 kV, 2 min)), its supposed alignment in the field and its supposed effective length.

The maximum potential drop across an object is defined with respect to the effective length. This effective length is usually less than the actual length when the object is curved. Thus for Equation (14), $V_d = E \times L$, L is the effective length and not the real length of the object anymore. An example of difference in actual length and effective length is as shown in Figure 60.

The relationship between the efficiency of the gold deposition and the length of CNTs is also observed more directly in some of our CE experiments (see Figure 61). The length of nanotube 1 is roughly twice of that of nanotube 2. Supposing that both tubes were well aligned in the field, the relationship expressed in Equation (14), $V_d = E \times L$, shows that a higher potential drop will occur on tube 1 which is consistent with the growth of a much bigger gold particle on this tube compared to tube 2.

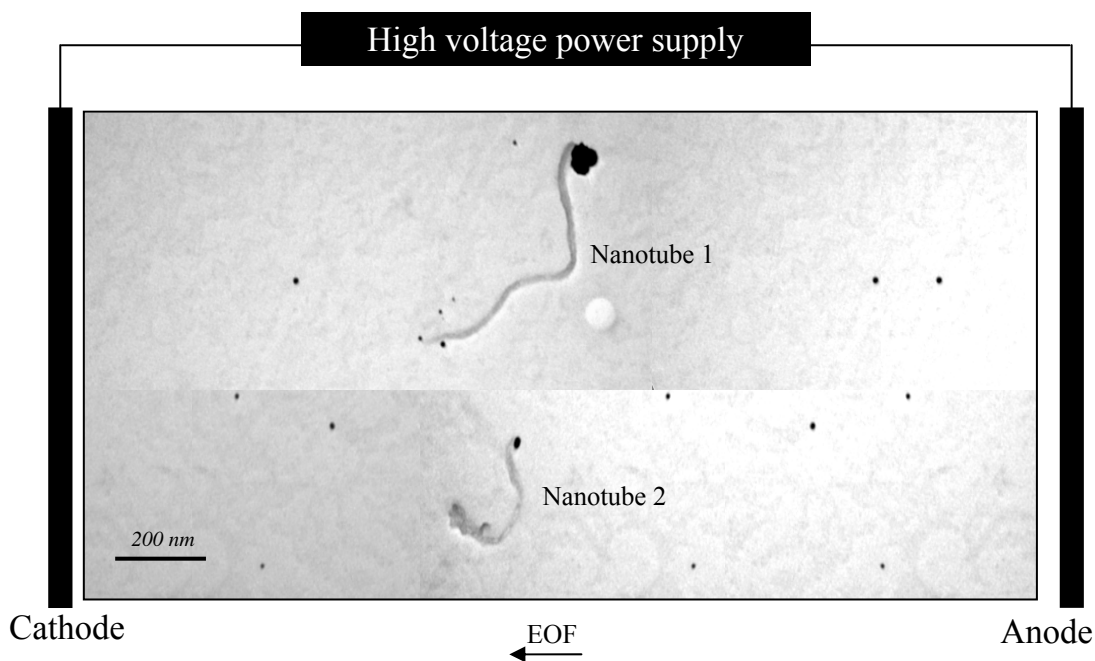


Figure 61 High-magnification TEM image of irregular curved CNTs (obtained after the CE experiment (30 kV, 2 min)), illustrating the different size of the deposited gold particles as a function of the nanotube length.

3.5. Conclusion

Two complementary methods for gold deposition on carbon nanotubes, the electroless and the bipolar electrochemical deposition, were developed and extensively studied here. These methods were shown to generate hybrid gold/carbon nanoobjects with a rich structural diversity. These hybrid objects are expected to open up many applications in the field of analytical chemistry. In the case of the chemical modification procedure metal is generated by dismutation and the carbon nanostructures act as the nucleation site and consequently get covered with a metal layer. Bipolar electrochemistry, which makes it possible to modify an object suspended in the electrolyte, placed between two electrodes, provides naturally a dissymmetric metal deposition on the object without needing a direct contact with an electrode. The bipolar electrochemical technique was studied and developed here to deposit gold layers on carbon nanotubes suspended in the solution. Adapting capillary electrophoresis for this purpose avoids the problem of bubble formation perturbing the orientation of the nanotubes because the bubbles are formed outside of the capillary where the deposition takes place. Capillary electrophoresis allows to deposit gold locally on one end of carbon nanotubes through bipolar electrochemistry. Therefore this technique is very promising not only to deposit metal onto carbon nanostructures but it might also be adapted to deposit other materials (metal oxides, conducting polymers...) onto nanoobjects made out of conducting or at least semiconducting materials.

CHAPTER VI. CONCLUDING REMARKS

Using our experimental setup and optimized synthetic system and conditions, complete and straight carbon nanotubes can be formed with high purity and homogeneous diameter and wall structure in the pores of anodic aluminum oxide. Because of the obtained tube characteristics: straight, metal-catalyst free and uniform in diameter with an empty inner space, this technique is expected to be a very useful technique to produce CNTs for many material applications.

Apart from homogeneity in diameter, high purity and straightness, high dispersibility and high-solubility in the solvent are other requisites. This point was addressed by means of a theoretical approach using the ONIOM2 technique. The calculations revealed that Diels-Alder functionalizations of CNTs is viable and can be improved by the enhancement of their electron deficiency character or by using a reactive diene.

In order to utilize commercial, cheap CNTs, which are normally produced by catalytic the chemical vapor deposition technique, a combination of polyoxometalate and the sonication technique can be used. After the conditions are optimized, this technique can be used to purify, disperse and water-solubilize as-synthesized CNTs, which are impure, aggregate and water-insoluble. A similar procedure can also be employed to shorten CNTs. Because of it has ability to purify, water-solubilize, disperse and shorten CNTs in a single experimental approach, this combined technique is considered to be an important step forward.

Additionally, the functionalization of CNTs is expected to lead to the development of many applications in the field of analytical chemistry and is considered here in the term of metal decoration. Two complementary methods for gold deposition on carbon nanotubes, the electroless and the bipolar electrochemical deposition, were developed and extensively studied. In the case of the chemical modification (electroless deposition), metal is generated by dismutation and the carbon nanostructures act as the nucleation site. Consequently, they become covered with a metal layer. In the case of the

bipolar electrochemical deposition, it brings about the possibility to create a potential gradient along the object. This leads to the electrodeposition of metal without the object being in direct contact with an electrode and, thus, produces naturally a dissymmetric metal deposit. In this study, capillary electrophoresis was adapted to deposit gold locally on one end of carbon nanotubes through bipolar chemistry. This technique is very promising not only to deposit metal onto carbon nanostructures but it might also be adapted to deposit other conducting or semiconducting materials (metal oxides, conducting polymers ...).

LITERATURE CITED

- Abatemarco, T., J. Stickel, J. Belfort, B. P. Frank, P. M. Ajayan and G. Belfort. 1999. Fractionation of Multiwalled Carbon Nanotubes by Cascade Membrane Microfiltration. **J. Phys. Chem. B** 103(18):3534-3538.
- Ajayan, P. M. 1999. Nanotubes from Carbon. **Chem. Rev.** 99(7):1787-1800.
- Alekseev, N. I., S. V. Polovtsev and N. A. Charykov. 2006. On the mechanism of carbon nanotube formation in electrochemical processes. **Technical Physics** 51(3): 349-355.
- Alvarez, M. M., J. T. Khoury, T. G. Schaaff, M. N. Shafigullin, I. Vezmar and R. L. Whetten. 1997. Optical Absorption Spectra of Nanocrystal Gold Molecules. **J. Phys. Chem. B** 101(19):3706-3712.
- Amelinckx, S., X. B. Zhang, D. Bernaerts, X. F. Zhang, V. Ivanov and J. B. Nagy. 1994. A Formation Mechanism for Catalytically Grown Helix-Shaped Graphite Nanotubes. **Science** 265(5172):635-639.
- Axel, D. B. 1992a. Density-functional thermochemistry. I. The effect of the exchange-only gradient correction. **The Journal of Chemical Physics** 96(3):2155-2160.
- Axel, D. B. 1992b. Density-functional thermochemistry. II. The effect of the Perdew--Wang generalized-gradient correlation correction. **The Journal of Chemical Physics** 97(12):9173-9177.
- Axel, D. B. 1993. Density-functional thermochemistry. III. The role of exact exchange. **The Journal of Chemical Physics** 98(7):5648-5652.

- Ayala, P., J. F. L. Freire, L. Gu, D. J. Smith, I. G. Solorzano, D. W. Macedo, J. B. V. Sande, H. Terrones, J. Rodriguez-Manzo and M. Terrones. 2006. Decorating carbon nanotubes with nanostructured nickel particles via chemical methods. **Chemical Physics Letters** 431(1-3):104-109.
- Babaa, M. R., E. McRae, S. Delpoux, J. Ghanbaja, F. Valsaque and F. Beguin. 2004. Surface characterisation of template-synthesised multi-walled carbon nanotubes. **Chemical Physics Letters** 396(1-3):49-53.
- Bahr, J. L., J. Yang, D. V. Kosynkin, M. J. Bronikowski, R. E. Smalley and J. M. Tour. 2001. Functionalization of Carbon Nanotubes by Electrochemical Reduction of Aryl Diazonium Salts: A Bucky Paper Electrode. **J. Am. Chem. Soc.** 123(27):6536-6542.
- Bailar, J. C., H. J. Emeléus, R. Nyholm, A. F. Trotman-Dickenson. 1973. **Comprehensive Inorganic Chemistry**. Vol. 5. Pergamon Press, New York.
- Bakowies, D. and W. Thiel 1996a. Semiempirical treatment of electrostatic potentials and partial charges in combined quantum mechanical and molecular mechanical approaches. **Journal of Computational Chemistry** 17(1):87-108.
- Bakowies, D. and W. Thiel. 1996b. Hybrid Models for Combined Quantum Mechanical and Molecular Mechanical Approaches. **J. Phys. Chem.** 100(25):10580-10594.
- Bandow, S., A. M. Rao, K. A. Williams, A. Thess, R. E. Smalley and P. C. Eklund. 1997. Purification of Single-Wall Carbon Nanotubes by Microfiltration. **J. Phys. Chem. B** 101(44):8839-8842.
- Banerjee, S. and S. S. Wong. 2002a. Rational Sidewall Functionalization and Purification of Single-Walled Carbon Nanotubes by Solution-Phase Ozonolysis. **J. Phys. Chem. B** 106(47):12144-12151.

- Banerjee, S. and S. S. Wong. 2002b. Synthesis and Characterization of Carbon Nanotube-Nanocrystal Heterostructures. **Nano Lett.** 2(3):195-200.
- Banerjee, S. and S. S. Wong. 2003. In Situ Quantum Dot Growth on Multiwalled Carbon Nanotubes. **J. Am. Chem. Soc.** 125(34):10342-10350.
- Barton, T. J., L. M. Bull, W. G. Klemperer, D. A. Loy, B. McEnaney, M. Misono, P. A. Monson, G. Pez, G. W. Scherer, J. C. Vartuli and O. M. Yaghi. 1999. Tailored Porous Materials. **Chem. Mater.** 11(10):2633-2656.
- Baughman, R. H., C. Cui, A. A. Zakhidov, Z. Iqbal, A. Mazzoldi, D. De Rossi, A. G. Rinzler, O. Jaschinski, S. Roth, M. Kertesz, J. N. Barisci, G. M. Spinks and G. G. Wallace. 1999. Carbon nanotube actuators. **Science** 284(5418):1340-1344.
- Bethune, D. S., C. H. Klang, M. S. de Vries, G. Gorman, R. Savoy, J. Vazquez and R. Beyers. 1993. Cobalt-catalysed growth of carbon nanotubes with single-atomic-layer walls. **Nature** 363(6430):605-607.
- Bianco, A. and M. Prato. 2003. Can Carbon Nanotubes be Considered Useful Tools for Biological Applications? **Advanced Materials** 15(20):1765-1768.
- Boul, P. J., J. Liu, E. T. Mickelson, C. B. Huffman, L. M. Ericson, I. W. Chiang, K. A. Smith, D. T. Colbert, R. H. Hauge, J. L. Margrave and R. E. Smalley. 1999. Reversible sidewall functionalization of buckytubes. **Chemical Physics Letters** 310(3-4):367.
- Bradley, J. -C., J. Crawford, M. McGee, and S. G. Stephens. 1998. A Contactless Method for the Directed Formation of Submicrometer Copper Wires. **J. Electrochem. Soc.** 145(3):L45-L47.
- Bradley, J. -C., S. Babu and P. Ndungu. 2005. Contactless Tip-Selective Electrodeposition of Palladium onto Carbon Nanotubes and Nanofibers. Fullerenes, **Nanotubes and Carbon Nanostructures** 13(3):227-237.

- Brumlik, C. J. and C. R. Martin. 1991. Template synthesis of metal microtubules. **J. Am. Chem. Soc.** 113(8):3174-3175.
- Brumlik, C. J., V. P. Menon and C. R. Martin. 1994. Template synthesis of metal microtubule ensembles utilizing chemical, electrochemical, and vacuum deposition techniques. **Journal of Materials Research** 9(5):1174-1183.
- Carrillo, A., J. A. Swartz, J. M. Gamba, R. S. Kane, N. Chakrapani, B. Wei and P. M. Ajayan. 2003. Noncovalent Functionalization of Graphite and Carbon Nanotubes with Polymer Multilayers and Gold Nanoparticles. **Nano Lett.** 3(10):1437-1440.
- Cassell, A. M., J. A. Raymakers, J. Kong and H. Dai. 1999. Large Scale CVD Synthesis of Single-Walled Carbon Nanotubes. **J. Phys. Chem. B** 103(31):6484-6492.
- Che, G., B. B. Lakshmi, E. R. Fisher and C. R. Martin. 1998a. Carbon nanotubule membranes for electrochemical energy storage and production. **Nature** 393(6683):346-349.
- Che, G., B. B. Lakshmi, C. R. Martin, E. R. Fisher and R. S. Ruoff. 1998b. Chemical Vapor Deposition Based Synthesis of Carbon Nanotubes and Nanofibers Using a Template Method. **Chem. Mater.** 10(1):260-267.
- Chen, J., M. A. Hamon, H. Hu, Y. Chen, A. M. Rao, P. C. Eklund and R. C. Haddon. 1998. Solution Properties of Single-Walled Carbon Nanotubes. **Science** 282(5386):95-98.
- Chen, J., M. J. Dyer and M. -F. Yu. 2001a. Cyclodextrin-Mediated Soft Cutting of Single-Walled Carbon Nanotubes. **J. Am. Chem. Soc.** 123(25):6201-6202.

- Chen, J., A. M. Rao, S. Lyuksyutov, M. E. Itkis, M. A. Hamon, H. Hu, R. W. Cohn, P. C. Eklund, D. T. Colbert, R. E. Smalley and R. C. Haddon. 2001b. Dissolution of Full-Length Single-Walled Carbon Nanotubes. **J. Phys. Chem. B** 105(13):2525-2528.
- Chen, J., H. Liu, W.A. Weimer, M. D. Halls, D. H. Waldeck and G. C. Walker. 2002. Noncovalent Engineering of Carbon Nanotube Surfaces by Rigid, Functional Conjugated Polymers. **J. Am. Chem. Soc.** 124(31):9034-9035.
- Chen, R. J., Y. Zhang, D. Wang and H. Dai. 2001c. Noncovalent Sidewall Functionalization of Single-Walled Carbon Nanotubes for Protein Immobilization. **J. Am. Chem. Soc.** 123(16):3838-3839.
- Chen, W., J. Zhao, J. Y. Lee and Z. Liu. 2005. Microwave heated polyol synthesis of carbon nanotubes supported Pt nanoparticles for methanol electrooxidation. **Materials Chemistry and Physics** 91(1):124-129.
- Chen, X., J. Xia, J. Peng, W. Li and S. Xie. 2000. Carbon-nanotube metal-matrix composites prepared by electroless plating. **Composites Science and Technology** 60(2):301-306.
- Chiang, I. W., B. E. Brinson, R. E. Smalley, J. L. Margrave and R. H. Hauge. 2001. Purification and Characterization of Single-Wall Carbon Nanotubes. **J. Phys. Chem. B** 105(6):1157-1161.
- Chichak, K. S., A. Star, M. V. P. Altoé, J. F. Stoddart. 2005. Single-Walled Carbon Nanotubes under the Influence of Dynamic Coordination and Supramolecular Chemistry. **Small** 1(4):452-461.
- Colomer, J. F., P. Piedigrosso, A. Fonseca and J. B. Nagy. 1999. Different purification methods of carbon nanotubes produced by catalytic synthesis. **Synthetic Metals** 103(1-3):2482.

- Cui, J. B., M. Burghard and K. Kern. 2003. Reversible Sidewall Osmylation of Individual Carbon Nanotubes. **Nano Lett.** 3(5):613-615.
- Czerw, R., Z. Guo, P. M. Ajayan, Y. P. Sun and D. L. Carroll. 2001. Organization of Polymers onto Carbon Nanotubes: A Route to Nanoscale Assembly. **Nano Lett.** 1(8):423-427.
- Dai, H., A. G. Rinzler, P. Nikolaev, A. Thess, D. T. Colbert and R. E. Smalley. 1996a. Single-wall nanotubes produced by metal-catalyzed disproportionation of carbon monoxide. **Chemical Physics Letters** 260(3-4):471-475.
- Dai, H., J. H. Hafner, A. G. Rinzler, D. T. Colbert and R. E. Smalley. 1996b. Nanotubes as nanoprobe in scanning probe microscopy. **Nature** 384(6605):147-150.
- Daniel, M. -C. and D. Astruc. 2004. Gold Nanoparticles: Assembly, Supramolecular Chemistry, Quantum-Size-Related Properties, and Applications toward Biology, Catalysis, and Nanotechnology. **Chem. Rev.** 104(1):293-346.
- Dapprich, S., I. Komaromi, K. S. Byun, K. Morokuma and M. J. Frisch. 1999. A new ONIOM implementation in Gaussian98. Part I. The calculation of energies, gradients, vibrational frequencies and electric field derivatives. **Journal of Molecular Structure: THEOCHEM** 461/462:1-21.
- de Heer, W.A., A. Châtelain and D. Ugarte. 1995. A Carbon Nanotube Field-Emission Electron Source. **Science** 270(5239):1179-1180.
- Derycke, V., R. Martel, M. Radosavljevic, F. Ross and P. Avouris. 2002. Catalyst-Free Growth of Ordered Single-Walled Carbon Nanotube Networks. **Nano Lett.** 2(10):1043-1046.

- Dewar, M. J. S. and W. Thiel. 1977. Ground states of molecules. 39. MNDO results for molecules containing hydrogen, carbon, nitrogen, and oxygen. **J. Am. Chem. Soc.** 99(15):4907-4917.
- Diao, P., Z. Liu, B. Wu, X. Nan, J. Zhang, Z. Wei. 2002. Chemically Assembled Single-Wall Carbon Nanotubes and their Electrochemistry. **ChemPhysChem** 3(10):898-991.
- Dirix, Y., C. Bastiaansen, W. Cased and P. Smith. 1999. Oriented pearl-necklace arrays of metallic nanoparticles in polymers: A new route toward polarization-dependent color filters. **Advanced Materials** 11(3):223-227.
- Doorn, S. K., R. E. Fields, H. Hu, M. A. Hamon, R. C. Haddon, J. P. Selegue and V. Majidi. 2002. High Resolution Capillary Electrophoresis of Carbon Nanotubes. **J. Am. Chem. Soc.** 124(12):3169-3174.
- Doorn, S. K., M. S. Strano, M. J. O'Connell, E. H. Haroz, K. L. Rialon, R. H. Hauge and R. E. Smalley. 2003. Capillary Electrophoresis Separations of Bundled and Individual Carbon Nanotubes. **J. Phys. Chem. B** 107(25):6063-6069.
- Dorset, D. L. and J. R. Fryer. 2001. Quantitative Electron Crystallographic Determinations of Higher Fullerenes in the Hexagonal Close Packed Polymorph. **J. Phys. Chem. B** 105(12):2356-2359.
- Duesberg, G. S., J. Muster, V. Krstic, M. Burghard, S. Roth. 1998. Chromatographic size separation of single-wall carbon nanotubes **Applied Physics A: Materials Science & Processing** 67(1):117-119.
- Duesberg, G. S., W. Blau, H. J. Byrne, J. Muster, M. Burghard and S. Roth. 1999. Chromatography of carbon nanotubes. **Synthetic Metals** 103(1-3):2484-2485.

- Dwyer, C., M. Guthold, M. Falvo, S. Washburn, R. Superfine and D. Erie. 2002. DNA-functionalized single-walled carbon nanotubes. **Nanotechnology** 13:601-604.
- Dyke, C. A. and J. M. Tour. 2003a. Solvent-Free Functionalization of Carbon Nanotubes. **J. Am. Chem. Soc.** 125(5):1156-1157.
- Dyke, C. A. and J. M. Tour. 2003b. Unbundled and Highly Functionalized Carbon Nanotubes from Aqueous Reactions. **Nano Lett.** 3(9):1215-1218.
- Dyke, C. A. and J. M. Tour. 2004. Overcoming the Insolubility of Carbon Nanotubes through High Degrees of Sidewall Functionalization. **Chemistry - A European Journal** 10(4):812-817.
- Ebbesen, T. W. and P. M. Ajayan. 1992. Large-scale synthesis of carbon nanotubes. **Nature** 358(6383):220-222.
- Ebbesen, T. W. and P. M. Ajayan, H. Hiura and K. Tanigaki. 1994. Purification of nanotubes. **Nature** 367(6463):519.
- Eklund, P. C., J. M. Holden and R. A. Jishi. 1995. Vibrational modes of carbon nanotubes; Spectroscopy and theory. **Carbon** 33(7):959-972.
- Ellis, A. V., K. Vijayamohan, R. Goswami, N. Chakrapani, P. M. Ajayan, G. Ramanath and L. S. Ramanathan. 2003. Hydrophobic anchoring of monolayer-protected gold nanoclusters to carbon nanotubes. **Nano Lett.** 3(3):279-282.
- Eswaramoorthi, I. and L. -P. Hwang. 2007. Anodic titanium oxide: A new template for the synthesis of larger diameter multi-walled carbon nanotubes. **Diamond and Related Materials** 16(8):1571-1578.

- Fan, S., M. G. Chapline, N. R. Franklin, T. W. Tombler, A. M. Cassell and H. Dai. 1999. Self-Oriented Regular Arrays of Carbon Nanotubes and Their Field Emission Properties **Science** 283(5401):512-514.
- Fasi, A., I. Palinko, J. W. Seo, Z. Konya, K. Hernadi and I. Kiricsi. 2003. Sonication assisted gold deposition on multiwall carbon nanotubes. **Chemical Physics Letters** 372(5-6):848-852.
- Fei, B., H. Lu, Z. Hu and J. H. Xin. 2006. Solubilization, purification and functionalization of carbon nanotubes using polyoxometalate. **Nanotechnology** 17(6):1589.
- Field, M. J., P. A. Bash and M. Karplus. 1990. A combined quantum mechanical and molecular mechanical potential for molecular dynamics simulations. **Journal of Computational Chemistry** 11(6):700-733.
- Fleischmann, M., J. Ghoroghchian and S. Pons. 1985. Electrochemical behavior of dispersions of spherical ultramicroelectrodes. 1. Theoretical considerations. **J. Phys. Chem.** 89(25):5530-5536.
- Fleming, I. 1976. **Frontier Orbitals and Organic Chemical Reactions**. Wiley, New York.
- Fonseca, A., K. Hernadi, J. B. Nagy, D. Bernaerts and A. A. Lucas. 1996. Optimization of catalytic production and purification of buckytubes. **Journal of Molecular Catalysis A: Chemical** 107(1):159-168.
- Fu, Q., C. Lu and J. Liu. 2002. Selective Coating of Single Wall Carbon Nanotubes with Thin SiO₂ Layer. **Nano Lett.** 2(4):329-332.
- Fukui, K. 1971. Recognition of stereochemical paths by orbital interaction. **Acc. Chem. Res.** 4(2):57-64.

- Fukui, K. 1981. The path of chemical reactions - the IRC approach. **Acc. Chem. Res.** 14(12):363-368.
- Gao, J. 1995. Methods and Applications of Combined Quantum Mechanical and Molecular Mechanical Potentials. **Reviews in computational chemistry** 7119-185.
- Garrigue, P., M. H. Delville, C. Labrugere, E. Cloutet, P. J. Kulesza, J. P. Morand and A. Kuhn. 2004. Top-Down Approach for the Preparation of Colloidal Carbon Nanoparticles. **Chem. Mater.** 16(16):2984-2986.
- Ge, M. and K. Sattler. 1994. Observation of fullerene cones. **Chemical Physics Letters** 220(3-5):192-196.
- Georgakilas, V., K. Kordatos, M. Prato, D.M. Guldi, M. Holzinger and A. Hirsch. 2002a. Organic Functionalization of Carbon Nanotubes. **J. Am. Chem. Soc.** 124(5):760-761.
- Georgakilas, V., D. Voulgaris, E. Vazquez, M. Prato, D. M. Guldi, A. Kukovecz and H. Kuzmany. 2002b. Purification of HiPCO Carbon Nanotubes via Organic Functionalization. **J. Am. Chem. Soc.** 124(48):14318-14319.
- Gu, Z., H. Peng, R. H. Hauge, R.E. Smalley and J. L. Margrave. 2002. Cutting Single-Wall Carbon Nanotubes through Fluorination. **Nano Lett.** 2(9):1009-1013.
- Guo, D. J. and H. L. Li. 2005. Highly dispersed Ag nanoparticles on functional MWNT surfaces for methanol oxidation in alkaline solution. **Carbon** 43(6):1259-1264.
- Guo, T., P. Nikolaev, A. Thess, D. T. Colbert and R. E. Smalley. 1995. Catalytic growth of single-walled nanotubes by laser vaporization. **Chemical Physics Letters** 243(1-2):49-54.

- Hammond, G. S. 1955. A Correlation of Reaction Rates. **J. Am. Chem. Soc.** 77(2):334-338.
- Han, L., W. Wu, F. L. Kirk, J. Luo, M. M. Maye, N. N. Kariuki, Y. Lin, C. Wang and C. J. Zhong. 2004. A Direct Route toward Assembly of Nanoparticle-Carbon Nanotube Composite Materials. **Langmuir** 20(14):6019-6025.
- Haruta, M. and M. Daté. 2001. Advances in the catalysis of Au nanoparticles. **Applied Catalysis A: General** 222(1-2):427-437.
- Hernadi, K., A. Fonseca, J. B. Nagy, D. Bernaerts, J. Riga and A. Lucas. 1996. Catalytic synthesis and purification of carbon nanotubes. **Synthetic Metals** 77(1-3):31-34.
- Hernadi, K., A. Siska, L. Thien-Nga, L. Forro and I. Kiricsi. 2001. Reactivity of different kinds of carbon during oxidative purification of catalytically prepared carbon nanotubes. **Solid State Ionics** 141-142:203-209.
- Hill, C. L. and R. B. Brown. 1986. Sustained epoxidation of olefins by oxygen donors catalyzed by transition metal-substituted polyoxometalates, oxidatively resistant inorganic analogs of metalloporphyrins. **J. Am. Chem. Soc.** 108(3):536-538.
- Himmelhaus, M. and H. Takei. 2000. Cap-shaped gold nanoparticles for an optical biosensor. **Sensors and Actuators, B: Chemical** 63(1):24-30.
- Hinds, B. J., N. Chopra, T. Rantell, R. Andrews, V. Gavalas and L. G. Bachas. 2004. Aligned Multiwalled Carbon Nanotube Membranes. **Science** 303(5654):62-65.
- Holzinger, M., A. H., P. Bernier, G. S. Duesberg, M. Burghard. 2000. A new purification method for single-wall carbon nanotubes (SWNTs). **Applied Physics A: Materials Science & Processing** 7(5):599-602.

- Holzinger, M., O. Vostrowsky, A. Hirsch, F. Hennrich, M. Kappes, R. Weiss and F. Jellen. 2001. Sidewall Functionalization of Carbon Nanotubes. **Angewandte Chemie International Edition** 40(21):4002-4005.
- Hornyak, G. L., A. C. Dillon, P. A. Parilla, J. J. Schneider, N. Czap, K. M. Jones, F. S. Fasoon, A. Mason and M. J. Heben. 1999. Template synthesis of carbon nanotubes. **Nanostructured Materials** 12(1-4):83-88.
- Houk, K. N., Y. Li and J. D. Evanseck. 1992a. Transition Structures of Hydrocarbon Pericyclic Reactions. **Angewandte Chemie International Edition in English** 31(6):682-708.
- Houk, K. N., Y. Li and J. D. Evanseck. 1992b. Übergangsstrukturen in pericyclischen Reaktionen von Kohlenwasserstoffen. **Angewandte Chemie** 104(6):711-739.
- Houk, K. N., J. Gonzalez and Y. Li. 1995. Pericyclic Reaction Transition States: Passions and Punctilios, 1935-1995. **Acc. Chem. Res.** 28(2):81-90.
- Hu, C., Z. Chen, A. Shen, X. Shen, J. Li and S. Hu. 2006a. Water-soluble single-walled carbon nanotubes via noncovalent functionalization by a rigid, planar and conjugated diazo dye. **Carbon** 44(3):428-434.
- Hu, H., B. Zhao, M.A. Hamon, K. Kamaras, M.E. Itkis and R.C. Haddon. 2003. Sidewall Functionalization of Single-Walled Carbon Nanotubes by Addition of Dichlorocarbene. **J. Am. Chem. Soc.** 125(48):14893-14900.
- Hu, X., T. Wang, X. Qu and S. Dong. 2006b. In Situ Synthesis and Characterization of Multiwalled Carbon Nanotube/Au Nanoparticle Composite Materials. **J. Phys. Chem. B** 110(2):853-857.
- Huczko, A. 2000. Template-based synthesis of nanomaterials. **Applied Physics A: Materials Science & Processing** 70(4):365-376.

- Huczko, A. 2002. Template-based synthesis of nanomaterials. **Applied Physics A: Materials Science & Processing** 70(4):365-376.
- Hudson, J. L., M. J. Casavant and J. M. Tour. 2004. Water-Soluble, Exfoliated, Nonroping Single-Wall Carbon Nanotubes. **J. Am. Chem. Soc.** 126(36):11158-11159.
- Hugonnot, E., M. -H. Delville and J. -P. Delville. 2005. Dissymmetrization of micro-particle surface by laser-induced photochemical deposition. **Applied Surface Science** 248(1-4):470-474.
- Hulteen J. C. and C. R. Martin. 1997. A general template-based method for the preparation of nanomaterials. **J. Mater. Chem.** 7:1075 – 1087.
- Iijima, S. 1991. Helical microtubules of graphitic carbon. **Nature** 354(6348):56-58.
- Iijima, S. 1993. Growth of carbon nanotubes. **Materials Science and Engineering B** 19(1-2):172-180.
- Iijima, S. and T. Ichihashi. 1993. Single-shell carbon nanotubes of 1-nm diameter. **Nature** 363(6430):603-605.
- Iijima, S., M. Yudasaka, R. Yamada, S. Bandow, K. Suenaga, F. Kokai and K. Takahashi. 1999. Nano-aggregates of single-walled graphitic carbon nanohorns. **Chemical Physics Letters** 309(3-4):165-170.
- Inasawa, S., M. Sugiyama and Y. Yamaguchi. 2005. Laser-Induced Shape Transformation of Gold Nanoparticles below the Melting Point: The Effect of Surface Melting. **J. Phys. Chem. B** 109(8):3104-3111.
- Ito, Y., A. L. Bleloch and L. M. Brown. 1998. Nanofabrication of solidstate fresnel lenses for electron optics. **Nature** 394(6688):49-52.

- Itoh, S., S. Ihara and J. -I. Kitakami. 1993. Toroidal form of carbon C₃₆₀. **Phys. Rev. B** 47(3):1703-1704.
- Jeong, S. -H., O. J. Lee, K. H. Lee, S. H. Oh and C. G. Park. 2002. Preparation of Aligned Carbon Nanotubes with Prescribed Dimensions: Template Synthesis and Sonication Cutting Approach. **Chem. Mater.** 14(4):1859-1862.
- Jeong, S. -H., H. -Y. Hwang, S. -K. Hwang and K. -H. Lee. 2004. Carbon nanotubes based on anodic aluminum oxide nano-template. **Carbon** 42(10):2073-2080.
- Tan, X. J., W. L. Zhu, M. Cui, X. M. Luo, J. D. Gu, I. Silman, J. L. Sussman, H. L. Jiang, R. Y. Ji and K. X. Chen. 2001. Noncovalent interaction or chemical bonding between alkaline earth cations and benzene? A quantum chemistry study using MP2 and density-functional theory methods. **Chemical Physics Letters** 349(1-2):113-122.
- Jiang, K., A. Eitan, L. S. Schadler, P. M. Ajayan, R. W. Siegel, N. Grobert, M. Mayne, M. Reyes-Reyes, H. Terrones and M. Terrones. 2003a. Selective attachment of gold nanoparticles to nitrogen-doped carbon nanotubes. **Nano Letters** 3(3):275-277.
- Jiang, L. and L. Gao. 2003. Modified carbon nanotubes: an effective way to selective attachment of gold nanoparticles. **Carbon** 41(15):2923-2929.
- Jiang, L., L. Gao and J. Sun. 2003b. Production of aqueous colloidal dispersions of carbon nanotubes. **Journal of Colloid and Interface Science** 260(1):89-94.
- Jitianu, A., T. Cacciaguerra, M.-H. Berger, R. Benoit, F. Beguin and S. Bonnamy. 2004. New carbon multiwall nanotubes - TiO₂ nanocomposites obtained by the sol-gel method. **Journal of Non-Crystalline Solids Physics of Non-Crystalline Solids** 10 345-346:596-600.

- Journet, C., W. K. Maser, P. Bernier, A. Loiseau, M. L. de la Chapelle, S. Lefrant, P. Deniard, R. Lee and J. E. Fischer. 1997. Large-scale production of single-walled carbon nanotubes by the electric-arc technique. **Nature** 388(6644):756-758.
- Kajiura, H., S. Tsutsui, H. Huang and Y. Murakami. 2002. High-quality single-walled carbon nanotubes from arc-produced soot. **Chemical Physics Letters** 364(5-6):586-592.
- Kang, Z., E. Wang, B. Mao, Z. Su, C. Tian and L. Xu. 2006. Controlled cutting carbon nanotube with polyoxometalates assisted renewable method. **Materials Letters** 60(17-18):2266.
- Kang, Z., Y. Wang, E. Wang, S. Lian, L. Gao, W. You, C. Hu and L. Xu. 2004. Polyoxometalates nanoparticles: synthesis, characterization and carbon nanotube modification. **Solid State Communications** 129(9):559-564.
- Kastner, J., T. Pichler, H. Kuzmany, S. Curran, W. Blau, D. N. Weldon, M. Delamesiere, S. Draper and H. Zandbergen. 1994. Resonance Raman and infrared spectroscopy of carbon nanotubes. **Chemical Physics Letters** 221(1-2):53-58.
- Keogh, S. M., T. G. Hedderman, E. Gregan, G. Farrell, G. Chambers and H. J. Byrne. 2004. Spectroscopic Analysis of Single-Walled Carbon Nanotubes and Semiconjugated Polymer Composites. **J. Phys. Chem. B** 108(20):6233-6241.
- Khabashesku, V. N., W. E. Billups and J. L. Margrave. 2002. Fluorination of Single-Wall Carbon Nanotubes and Subsequent Derivatization Reactions. **Acc. Chem. Res.** 35(12):1087-1095.
- Kim, B. and W. M. Sigmund. 2004. Functionalized Multiwall Carbon Nanotube/Gold Nanoparticle Composites. **Langmuir** 20(19):8239-8242.

- Kong, J., A. M. Cassell and H. Dai. 1998. Chemical vapor deposition of methane for single-walled carbon nanotubes. **Chemical Physics Letters** 292(4-6):567-574.
- Kong, J., M. G. Chapline and H. Dai. 2001. Functionalized carbon nanotubes for molecular hydrogen sensors. **Advanced Materials** 13(18):1384-1386.
- Kroto, H. W., J. R. Heath, S. C. O'Brien, R. F. Curl and R. E. Smalley. 1985. C₆₀: Buckminsterfullerene. **Nature** 318(6042):162-163.
- Kulesza, P. J., M. Skunik, B. Baranowska, K. Miecznikowski, M. Chojak, K. Karnicka, E. Frackowiak, F. Beguin, A. Kuhn, M. -H. Delville, B. Starobrzynska and A. Ernst. 2006. Fabrication of network films of conducting polymer-linked polyoxometallate-stabilized carbon nanostructures. **Electrochimica Acta** 51:2373-2379
- Kyotani, T., L. -f. Tsai and A. Tomita. 1996. Preparation of Ultrafine Carbon Tubes in Nanochannels of an Anodic Aluminum Oxide Film. **Chem. Mater.** 8(8):2109-2113.
- Lakshmi, B. B., P. K. Dorhout and C. R. Martin. 1997. Sol-Gel Template Synthesis of Semiconductor Nanostructures. **Chem. Mater.** 9(3):857-862.
- Laplaze, D., P. Bernier, W. K. Maser, G. Flamant, T. Guillard and A. Loiseau. 1998. Carbon nanotubes: The solar approach. **Carbon** 36(5):685-688
- Lee, C., W. Yang and R. G. Parr. 1988. Development of the Colle-Salvetti correlation-energy formula into a functional of the electron density. **Physical Review B** 37(2):785.
- Lee, J. S., G. H. Gu, H. Kim, K. S. Jeong, J. Bae and J. S. Suh. 2001. Growth of Carbon Nanotubes on Anodic Aluminum Oxide Templates: Fabrication of a Tube-in-Tube and Linearly Joined Tube. **Chem. Mater.** 13(7):2387-2391.

- Lee, K. Y., M. Kim, J. Hahn, J. S. Suh, I. Lee, K. Kim and S. W. Han. 2006. Assembly of Metal Nanoparticle-Carbon Nanotube Composite Materials at the Liquid/Liquid Interface. **Langmuir** 22(4):1817-1821.
- Lehn, J. –M. 1995. **Supramolecular Chemistry - Concepts and Perspectives**. VCH, Weinheim.
- Li, F., H. M. Cheng, Y. T. Xing, P. H. Tan and G. Su. 2000. Purification of single-walled carbon nanotubes synthesized by the catalytic decomposition of hydrocarbons. **Carbon** 38(14):2041-2045.
- Li, G., Y. Ding, J. Wang, X. Wang and J. Suo. 2007b. New progress of Keggin and Wells-Dawson type polyoxometalates catalyze acid and oxidative reactions. **Journal of Molecular Catalysis A: Chemical** 262(1-2):67-76.
- Li, J., M. Moskovits and T. L. Haslett. 1998. Nanoscale Electroless Metal Deposition in Aligned Carbon Nanotubes. **Chem. Mater.** 10(7):1963-1967.
- Li, J., C. Papadopoulos, J. M. Xu and M. Moskovits. 1999. Highly-ordered carbon nanotube arrays for electronics applications. **Applied Physics Letters** 75(3):367-369.
- Li, R., Z. Shang, G. Wang, Y. Pan, Z. Cai and X. Zhao. 2002. Study on dichlorocarbene cycloaddition isomers of armchair single-walled carbon nanotubes. **Journal of Molecular Structure: THEOCHEM** 583(1-3):241-247.
- Li, W. Z., S. S. Xie, L. X. Qian, B. H. Chang, B. S. Zou, W. Y. Zhou, R. A. Zhao and G. Wang. 1996. Large-Scale Synthesis of Aligned Carbon Nanotubes. **Science** 274(5293):1701-1703.

- Li, Z., V. R., S. Ravaine, P. Garrigue, A. Kuhn. 2007b. Raspberry-like Gold Microspheres: Preparation and Electrochemical Characterization. **Advanced Functional Materials** 17(4):618-622.
- Liang, W. and C. R. Martin. 1990. Template-synthesized polyacetylene fibrils show enhanced supermolecular order. **J. Am. Chem. Soc.** 112(26):9666-9668.
- Lim, S. H., J. Wei, J. Lin, Q. Li and J. Kua You. 2005. A glucose biosensor based on electrodeposition of palladium nanoparticles and glucose oxidase onto Nafion-solubilized carbon nanotube electrode. **Biosensors and Bioelectronics** 20(11):2341-2346.
- Lin, T., W. D. Zhang, J. Huang and C. He. 2005. A DFT Study of the Amination of Fullerenes and Carbon Nanotubes: Reactivity and Curvature. **J. Phys. Chem. B** 109(28):13755-13760.
- Lin, Y., B. Zhou, K. A. Shiral Fernando, P. Liu, L. F. Allard and Y. P. Sun. 2003. Polymeric Carbon Nanocomposites from Carbon Nanotubes Functionalized with Matrix Polymer. **Macromolecules** 36(19):7199-7204.
- Linhardt, R. J. and T. Toida. 2002. CAPILLARY ELECTROPHORESIS: Ultra-High Resolution Separation Comes of Age. **Science** 298(5597):1441-1442.
- Liu, G. and Y. Lin. 2006. Amperometric glucose biosensor based on self-assembling glucose oxidase on carbon nanotubes. **Electrochemistry Communications** 8(2):251-256.
- Liu, J., A. G. Rinzler, H. Dai, J. H. Hafner, R. Kelley Bradley, P.J. Boul, A. Lu, T. Iverson, K. Shelimov, C. B. Huffman, F. Rodriguez-Macias, D. T. Colbert, R.E. Smalley, Y.-S. Shon and T.R. Lee. 1998. Fullerene pipes. **Science** 280(5367):1253-1256.

- Liu, L., T. Wang, J. Li, Z. -X. Guo, L. Dai, D. Zhang and D. Zhu. 2003. Self-assembly of gold nanoparticles to carbon nanotubes using a thiol-terminated pyrene as interlinker. **Chemical Physics Letters** 367(5-6):747-752.
- Liu, Y., M. Wang, F. Zhao, Z. Guo, H. Chen and S. Dong. 2005. Direct electron transfer and electrocatalysis of microperoxidase immobilized on nanohybrid film. **Journal of Electroanalytical Chemistry** 581(1):1-10.
- Liu, Y., J. Tang, X. Chen, W. Chen, G. K. H. Pang and J. H. Xin. 2006. A wet-chemical route for the decoration of CNTs with silver nanoparticles. **Carbon** 44(2):381-383.
- Long, L., X. Lu, F. Tian and Q. Zhang. 2003. Hydroboration of C(100) Surface, Fullerene, and the Sidewalls of Single-Wall Carbon Nanotubes with Borane. **J. Org. Chem.** 68(11):4495-4498.
- Lopez, X., C. Bo and J. M. Poblet. 2002. Electronic Properties of Polyoxometalates: Electron and Proton Affinity of Mixed-Addenda Keggin and Wells-Dawson Anions. **J. Am. Chem. Soc.** 124(42):12574-12582.
- Lordi, V., N. Yao and J. Wei. 2001. Method for Supporting Platinum on Single-Walled Carbon Nanotubes for a Selective Hydrogenation Catalyst. **Chem. Mater.** 13(3):733-737.
- Lu, J. 2007. Effect of surface modifications on the decoration of multi-walled carbon nanotubes with ruthenium nanoparticles. **Carbon** 45(8):1599-1605.
- Lu, X., F. Tian, Y. Feng, X. Xu, N. Wang and Q. Zhang. 2002a. Sidewall Oxidation and Complexation of Carbon Nanotubes by Base-Catalyzed Cycloaddition of Transition Metal Oxide: A Theoretical Prediction. **Nano Lett.** 2(11):1325-1327.

- Lu, X., F. Tian, N. Wang and Q. Zhang. 2002b. Organic Functionalization of the Sidewalls of Carbon Nanotubes by Diels-Alder Reactions: A Theoretical Prediction. **Org. Lett.** 4(24):4313-4315.
- Lu, X., L. Zhang, X. Xu, N. Wang and Q. Zhang. 2002c. Can the Sidewalls of Single-Wall Carbon Nanotubes Be Ozonized? **J. Phys. Chem. B** 106(9):2136-2139.
- Lu, X., F. Tian, X. Xu, N. Wang and Q. Zhang. 2003a. A Theoretical Exploration of the 1,3-Dipolar Cycloadditions onto the Sidewalls of (*n,n*) Armchair Single-Wall Carbon Nanotubes. **J. Am. Chem. Soc.** 125(34):10459-10464.
- Lu, X., Q. Yuan and Q. Zhang. 2003b. The [2+1] Cycloadditions of Dichlorocarbene, Silylene, Germylene, and Oxycarbonylnitrene onto the Sidewall of Armchair (5,5) Single-Wall Carbon Nanotube. **J. Phys. Chem. B** 107(33):8388-8391.
- Lu, X., Q. Yuan and Q. Zhang. 2003c. Sidewall Epoxidation of Single-Walled Carbon Nanotubes: A Theoretical Prediction. **Org. Lett.** 5(19):3527-3530.
- Lustig, S. R., E. D. Boyes, R. H. French, T. D. Gierke, M. A. Harmer, P. B. Hietpas, A. Jagota, R. S. McLean, G. P. Mitchell, G. B. Onoa and K. D. Sams. 2003. Lithographically Cut Single-Walled Carbon Nanotubes: Controlling Length Distribution and Introducing End-Group Functionality. **Nano Lett.** 3(8):1007-1012.
- Ma, X., N. Lun and S. Wen. 2005. Formation of gold nanoparticles supported on carbon nanotubes by using an electroless plating method. **Diamond and Related Materials** 14(1):68-73.
- Ma, X., X. Li, N. Lun and S. Wen. 2006. Synthesis of gold nano-catalysts supported on carbon nanotubes by using electroless plating technique. **Materials Chemistry and Physics** 97(2-3):351-356.

- Mackey, A. L. and H. Terrones. 1991. Diamond from graphite. **Nature** 352(6338):762.
- Mamalis, A. G., L. O. G. Vogtlander and A. Markopoulos. 2004. Nanotechnology and nanostructured materials: trends in carbon nanotubes. **Precision Engineering** 28(1):16-30.
- Marinakos, S. M., L. C. Brousseau, A. Jones and D. L. Feldheim. 1998. Template Synthesis of One-Dimensional Au, Au-Poly(pyrrole), and Poly(pyrrole) Nanoparticle Arrays. **Chem. Mater.** 10(5):1214-1219.
- Martin, C. R. 1996. Membrane-Based Synthesis of Nanomaterials. **Chem. Mater.** 8(8):1739-1746.
- Maseras F. and K. Morokuma 1995. IMOMM: A new integrated *ab initio* + molecular mechanics geometry optimization scheme of equilibrium structures and transition states. **Journal of Computational Chemistry** 16(9):1170-1179.
- Matarredona, O., H. Rhoads, Z. Li, J. H. Harwell, L. Balzano and D. E. Resasco. 2003. Dispersion of Single-Walled Carbon Nanotubes in Aqueous Solutions of the Anionic Surfactant NaDDBS. **J. Phys. Chem. B** 107(48):13357-13367.
- Mathiowitz, E., J. S. Jacob, Y. S. Jong, G. P. Carino, C. A. Santos, K. Vijayaraghavan, S. Montgomery, M. Bassett, C. Morrell, D. E. Chickering and P. Chaturvedi. 1997. Biologically erodable microspheres as potential oral drug delivery systems. **Nature** 386(6623):410-414.
- Maurin, G., I. Stepanek, P. Bernier, J. -F. Colomer, J. B. Nagy and F. Henn. 2001. Segmented and opened multi-walled carbon nanotubes. **Carbon** 39(8):1273-1278.

- Mickelson, E. T., C. B. Huffman, A. G. Rinzler, R. E. Smalley, R. H. Hauge and J. L. Margrave. 1998. Fluorination of single-wall carbon nanotubes. **Chemical Physics Letters** 296(1-2):188-194.
- Mickelson, E. T., I. W. Chiang, J. L. Zimmerman, P. J. Boul, J. Lozano, J. Liu, R. E. Smalley, R. H. Hauge and J. L. Margrave. 1999. Solvation of Fluorinated Single-Wall Carbon Nanotubes in Alcohol Solvents. **J. Phys. Chem. B** 103(21):4318-4322.
- Mizuno, N. and M. Misono. 1998. Heterogeneous Catalysis. **Chem. Rev.** 98(1):199-218.
- Moghaddam, M. J., S. Taylor, M. Gao, S. Huang, L. Dai and M. J. McCall. 2004. Highly Efficient Binding of DNA on the Sidewalls and Tips of Carbon Nanotubes Using Photochemistry. **Nano Lett.** 4(1):89-93.
- Monthieux, M., B. W. Smith, B. Bouteaux, A. Claye, J. E. Fischer and D. E. Luzzi. 2001. Sensitivity of single-wall carbon nanotubes to chemical processing: an electron microscopy investigation. **Carbon** 39(8):1251-1272.
- Niyogi, S., M. A. Hamon, H. Hu, B. Zhao, P. Bhowmik, R. Sen, M. E. Itkis and R. C. Haddon. 2002. Chemistry of Single-Walled Carbon Nanotubes. **Acc. Chem. Res.** 35(12):1105-1113.
- Numata, M., M. Asai, K. Kaneko, A. H. Bae, T. Hasegawa, K. Sakurai and S. Shinkai. 2005. Inclusion of Cut and As-Grown Single-Walled Carbon Nanotubes in the Helical Superstructure of Schizophyllan and Curdlan. **J. Am. Chem. Soc.** 127(16):5875-5884.
- Oberlin A. and M. Endo. 1976. Filamentous growth of carbon through benzene decomposition. **J. Cryst. Growth** 32(3): 335-349.

- O'Connell, M. J., S. M. Bachilo, C. B. Huffman, V. C. Moore, M. S. Strano, E. H. Haroz, K. L. Rialon, P. J. Boul, W. H. Noon, C. Kittrell, J. Ma, R. H. Hauge, R. B. Weisman and R. E. Smalley. 2002. Band Gap Fluorescence from Individual Single-Walled Carbon Nanotubes. **Science** 297(5581):593-596.
- Oh, S. -D., B. -K. So, S. -H. Choi, A. Gopalan, K. -P. Lee, K. Ro Yoon and I. S. Choi. 2005. Dispersing of Ag, Pd, and Pt-Ru alloy nanoparticles on single-walled carbon nanotubes by [γ]-irradiation. **Materials Letters** 59(10):1121-1124.
- Okotrub, A. V., L. G. Bulusheva and D. Tomanek. 1998. X-ray spectroscopic and quantum-chemical study of carbon tubes produced in arc-discharge. **Chemical Physics Letters** 289(3-4):341-349.
- Ouahab, L. 1997. Organic/Inorganic Supramolecular Assemblies and Synergy between Physical Properties. **Chem. Mater.** 9(9):1909-1926.
- Paloniemi, H., T. Aaritalo, T. Laiho, H. Liuke, N. Kocharova, K. Haapakka, F. Terzi, R. Seeber and J. Lukkari. 2005. Water-Soluble Full-Length Single-Wall Carbon Nanotube Polyelectrolytes: Preparation and Characterization. **J. Phys. Chem. B** 109(18):8634-8642.
- Pan, D., J. Chen, W. Tao, L. Nie and S. Yao. 2006. Polyoxometalate-Modified Carbon Nanotubes: New Catalyst Support for Methanol Electro-oxidation. **Langmuir** 22(13):5872-5876.
- Papadopoulos, C., A. Rakitin, J. Li, A. S. Vedenev and J. M. Xu. 2000. Electronic Transport in Y-Junction Carbon Nanotubes. **Physical Review Letters** 85(16):3476-3480.
- Pradhan, B. K., T. Toba, T. Kyotani and A. Tomita. 1998. Inclusion of Crystalline Iron Oxide Nanoparticles in Uniform Carbon Nanotubes Prepared by a Template Carbonization Method. **Chem. Mater.** 10(9):2510-2515.

- Parthangal, P. M., R. E Cavicchi and M. R. Zachariah. 2007 A generic process of growing aligned carbon nanotube arrays on metals and metal alloys. **Nanotechnology** 18:185605-185610.
- Parthasarathy, R. V., K. L. N. Phani, C. R. Martin. 1995. Template synthesis of graphitic nanotubules. **Advanced Materials** 7(11):896-897.
- Pope, M. T. and A. Müller. 1991. Polyoxometalate Chemistry: An Old Field with New Dimensions in Several Disciplines. **Angewandte Chemie International Edition in English** 30(1):34-48.
- Pradhan, B. K., T. Toba, T. Kyotani and A. Tomita. 1998. Inclusion of Crystalline Iron Oxide Nanoparticles in Uniform Carbon Nanotubes Prepared by a Template Carbonization Method. **Chem. Mater.** 10(9):2510-2515.
- Qin, Y., J. Shi, W. Wu, X. Li, Z.-X. Guo and D. Zhu. 2003. Concise Route to Functionalized Carbon Nanotubes. **J. Phys. Chem. B** 107(47):12899-12901.
- Rahman, G. M. A., D. M. Guldi, E. Zambon, L. Pasquato, N. Tagmatarchis, M. Prato. 2005. Dispersable Carbon Nanotube/Gold Nanohybrids: Evidence for Strong Electronic Interactions. **Small** 1(5):527-530.
- Ramanathan, T., F. T. Fisher, R. S. Ruoff and L. C. Brinson. 2005. Amino-Functionalized Carbon Nanotubes for Binding to Polymers and Biological Systems. **Chem. Mater.** 17(6):1290-1295.
- Ravindran, S., S. Chaudhary, B. Colburn, M. Ozkan and C. S. Ozkan. 2003. Covalent Coupling of Quantum Dots to Multiwalled Carbon Nanotubes for Electronic Device Applications. **Nano Lett.** 3(4):447-453.
- Ren, Z. F., Z. P. Huang, J. W. Xu, J. H. Wang, P. Bush, M. P. Siegal and P. N. Provencio. 1998. Synthesis of Large Arrays of Well-Aligned Carbon Nanotubes on Glass. **Science** 282(5391):1105-1107.

- Riggs, J. E., D. B. Walker, D. L. Carroll and Y. P. Sun. 2000. Optical Limiting Properties of Suspended and Solubilized Carbon Nanotubes. **J. Phys. Chem. B** 104(30):7071-7076.
- Rinzler, A. G., J. Liu, H. Dai, P. Nikolaev, C. B. Huffman, F. J. Rodríguez-Macías, P. J. Boul, A. H. Lu, D. Heymann, D. T. Colbert, R. S. Lee, J. E. Fischer, A. M. Rao, P. C. Eklund, R. E. Smalley. 1998. Large-scale purification of single-wall carbon nanotubes: process, product, and characterization. **Applied Physics A: Materials Science & Processing** 67(1):29-37.
- Rohlfing, D. F. and A. Kuhn. 2006. Preparation and characterization of polyoxometalate-modified carbon nanosheets. **Carbon** 44(10):1942-1948.
- Rowley, D. and H. Steiner. 1951. Kinetics of diene reactions at high temperatures. **Discuss. Faraday Soc.** 10:198 - 213.
- Rueckes, T., E. Joselevich, G. Y. Tseng, C. -L. Cheung, C. M. Lieber and K. Kim. 2000. Carbon nanotube-based nonvolatile random access memory for molecular computing. **Science** 289(5476):94-97.
- Sainsbury, T., J. Stolarczyk and D. Fitzmaurice. 2005. An Experimental and Theoretical Study of the Self-Assembly of Gold Nanoparticles at the Surface of Functionalized Multiwalled Carbon Nanotubes. **J. Phys. Chem. B** 109(34):16310-16325.
- Saito, R., M. Fujita, G. Dresselhaus and M. S. Dresselhaus. 1992. Electronic structure of chiral graphene tubules. **Applied Physics Letters** 60(18):2204-2206.
- Salernitano, E., L. Giorgi, T. Dikonimos Makris, R. Giorgi, N. Lisi, V. Contini and M. Falconieri. 2007. Purification of MWCNTs grown on a nanosized unsupported Fe-based powder catalyst. **Diamond and Related Materials** 16(8):1565-1570.

- Sander, M. S. and L. -S. Tan 2003. Nanoparticle Arrays on Surfaces Fabricated Using Anodic Alumina Films as Templates. **Advanced Functional Materials** 13(5):393-397.
- Satishkumar, B. C., C. N. R. Rao, E. M. Vogl and A. Govindaraj. 1996. The decoration of carbon nanotubes by metal nanoparticles. **Journal of Physics D: Applied Physics** 29(12):3173-3176.
- Schneider, J. J., N. I. Maksimova, J. Engstler, R. Joshi, R. Schierholz and R. Feile. 2006. Catalyst free growth of a carbon nanotube-alumina composite structure. **Inorganica Chimica Acta** In Press, Corrected Proof
- Shelimov, K. B., R. O. Esenaliev, A. G. Rinzler, C. B. Huffman and R. E. Smalley. 1998. Purification of single-wall carbon nanotubes by ultrasonically assisted filtration. **Chemical Physics Letters** 282(5-6):429-434.
- Shi, J., Y. Qin, W. Wu, X. Li, Z. -X. Guo and D. Zhu. 2004. In situ synthesis of CdS nanoparticles on multi-walled carbon nanotubes. **Carbon** 42(2):455-458.
- Shi, Z., Y. Lian, F. Liao, X. Zhou, Z. Gu, Y. Zhang and S. Iijima. 1999. Purification of single-wall carbon nanotubes. **Solid State Communications** 112(1):35-37.
- Shim, M., N.W. Shi Kam, R. J. Chen, Y. Li and H. Dai. 2002. Functionalization of Carbon Nanotubes for Biocompatibility and Biomolecular Recognition. **Nano Lett.** 2(4):285-288.
- Showkat, A. M., K.- P. Lee, A. I. Gopalan, S. -H. Choi and Y. C. Nho. 2007. Dispersion of gold nanoparticles into thiol-functionalized carbon nanotubes by [gamma]-radiation. **Diamond and Related Materials** 16(8):1688-1692.

- Singh, U. C. and P. A. Kollman 1986. A combined *ab initio* quantum mechanical and molecular mechanical method for carrying out simulations on complex molecular systems: Applications to the $\text{CH}_3\text{Cl} + \text{Cl}^-$ exchange reaction and gas phase protonation of polyethers. **Journal of Computational Chemistry** 7(6):718-730.
- Slanina, Z., S. Leszek, T. Piotr, L. Hong-Ming and A. Ludwik. 2003. Quantum-Chemical Model Evaluations of Thermodynamics and Kinetics of Oxygen Atom Additions to Narrow Nanotubes **Journal of Nanoscience and Nanotechnology** 2(1-2):193-198.
- Song, W. C., M. R. Ayers and A. J. Hunt. 1995. Carbon nanostructures in silica aerogel composites. **Journal of Materials Research** 10(2):251.
- Star, A. and J. F. Stoddart. 2002. Dispersion and Solubilization of Single-Walled Carbon Nanotubes with a Hyperbranched Polymer. **Macromolecules** 35(19):7516-7520.
- Star, A., D. W. Steuerman, J. R. Heath, and J. F. Stoddart. 2002. Starched Carbon Nanotubes. **Angewandte Chemie International Edition** 41(14):2508-2512.
- Star, A., Y. Liu, K. Grant, L. Ridvan, J. F. Stoddart, D. W. Steuerman, M. R. Diehl, A. Boukai and J. R. Heath. 2003. Noncovalent Side-Wall Functionalization of Single-Walled Carbon Nanotubes. **Macromolecules** 36(3):553-560.
- Stepanek, I., G. Maurin, P. Bernier, J. Gavillet, A. Loiseau, R. Edwards and O. Jaschinski. 2000. Nano-mechanical cutting and opening of single wall carbon nanotubes. **Chemical Physics Letters** 331(2-4):125-131.
- Stephane, H., S. Stefan and M. Keiji. 1996. The IMOMO method: Integration of different levels of molecular orbital approximations for geometry optimization of large systems: Test for n-butane conformation and $\text{S}_{\text{N}}2$ reaction: $\text{RCl} + \text{Cl}^-$. **The Journal of Chemical Physics** 105(5):1959-1967.

- Steuerman, D. W., A. Star, R. Narizzano, H. Choi, R. S. Ries, C. Nicolini, J. F. Stoddart and J. R. Heath. 2002. Interactions between Conjugated Polymers and Single-Walled Carbon Nanotubes. **J. Phys. Chem. B** 106(12):3124-3130.
- Suh, J. S. and J. S. Lee. 1999. Highly ordered two-dimensional carbon nanotube arrays. **Applied Physics Letters** 75(14):2047-2049.
- Sun, H. D., Z. K. Tang, J. Chen and G. Li. 1999. Polarized Raman spectra of single-wall carbon nanotubes mono-dispersed in channels of AlPO_4^{-5} single crystals. **Solid State Communications** 109(6):365-369.
- Sun, Z., Z. Liu, B. Han, S. Miao, Z. Miao and G. An. 2006. Decoration carbon nanotubes with Pd and Ru nanocrystals via an inorganic reaction route in supercritical carbon dioxide-methanol solution. **Journal of Colloid and Interface Science** 304(2):323.
- Svensson, M., S. Humbel, R. D. J. Froese, T. Matsubara, S. Sieber and K. Morokuma. 1996. ONIOM: A Multilayered Integrated MO + MM Method for Geometry Optimizations and Single Point Energy Predictions. A Test for Diels-Alder Reactions and $\text{Pt}(\text{P}(t\text{-Bu})_3)_2 + \text{H}_2$ Oxidative Addition. **J. Phys. Chem.** 100(50):19357-19363.
- Tang, H., J. Chen, S. Yao, L. Nie, G. Deng and Y. Kuang. 2004. Amperometric glucose biosensor based on adsorption of glucose oxidase at platinum nanoparticle-modified carbon nanotube electrode. **Analytical Biochemistry** 331(1):89-97.
- Terrill, R. H., T. A. Postlethwaite, C. -h. Chen, C. -D. Poon, A. Terzis, A. Chen, J. E. Hutchison, M. R. Clark, G. Wignall, J. D. Londono, R. Superfine, M. Falvo, C. S. Johnson Jr., E. T. Samulski and R. W. Murray. 1995. Monolayers in Three Dimensions: NMR, SAXS, Thermal, and Electron Hopping Studies of Alkanethiol Stabilized Gold Clusters. **J. Am. Chem. Soc.** 117(50):12537-12548.

- Terrones, H., M. Terrones, E. Hernández, N. Grobert, J. -C. Charlier and P. M. Ajayan. 2000. New Metallic Allotropes of Planar and Tubular Carbon. **Phys. Rev. Lett.** 84(8):1716-1719.
- Terrones, M., N. Grobert, J. Olivares, J. P. Zhang, H. Terrones, K. Kordatos, W. K. Hsu, J. P. Hare, P. D. Townsend, K. Prassides, A. K. Cheetham, H. W. Kroto and D. R. M. Walton. 1997. Controlled production of aligned-nanotube bundles. **Nature** 388(6637):52-55.
- Thess, A., R. Lee, P. Nikolaev, H. Dai, P. Petit, J. Robert, C. Xu, Y. H. Lee, S. G. Kim, A. G. Rinzler, D. T. Colbert, G. E. Scuseria, D. Tománek, J. E. Fischer, R. E. Smalley. 1997. Crystalline Ropes of Metallic Carbon Nanotubes. **Science** 273(5274):483 – 487.
- Tohji, K., T. Goto, H. Takahashi, Y. Shinoda, N. Shimizu, B. Jeyadevan, I. Matsuoka, Y. Saito, A. Kasuya, T. Ohsuna, K. Hiraga and Y. Nishina. 1996. Purifying single-walled nanotubes. **Nature** 383(6602):679.
- Torres-Garcia, G. and J. Mattay. 1996. Exohedral functionalization of [60]fullerene by [4+2] cycloadditions. Diels-Alder reactions of [60]fullerene with electron rich 2,3-dioxysubstituted-1,3-butadienes. **Tetrahedron** 52(15):5421-5426.
- Uchiyama, M., T. Tomioka and A. Amano. 1964. Thermal Decomposition of Cyclohexene. **J. Phys. Chem.** 68(7):1878-1881.
- Vander Wal R. L., T. M. Tichich and V. E. Curtis. 2000. Diffusion flame synthesis of single-walled carbon nanotubes. **Chem. Phys. Lett.** 323(3-4):217-233.
- Wang, J., M. Li, Z. Shi, N. Li and Z. Gu. 2002. Direct Electrochemistry of Cytochrome *c* at a Glassy Carbon Electrode Modified with Single-Wall Carbon Nanotubes. **Anal. Chem.** 74(9):1993-1997.

- Wong, Y. M., S. Wei, W. P. Kang, J. L. Davidson, W. Hofmeister, J. H. Huang and Y. Cui. 2004. Carbon nanotubes field emission devices grown by thermal CVD with palladium as catalysts. **Diamond and Related Materials** 13(11-12):2105-2112.
- Wu, K. and S. Hu. 2004. Deposition of a thin film of carbon nanotubes onto a glassy carbon electrode by electropolymerization. **Carbon** 42(15):3237-3242.
- Wu, Y. and S. Hu. 2005. The fabrication of a colloidal gold-carbon nanotubes composite film on a gold electrode and its application for the determination of cytochrome c. **Colloids and Surfaces B: Biointerfaces** 41(4):299-304.
- Xing, Y. 2004. Synthesis and Electrochemical Characterization of Uniformly-Dispersed High Loading Pt Nanoparticles on Sonochemically-Treated Carbon Nanotubes. **J. Phys. Chem. B** 108(50):19255-19259.
- Yamamoto, K., S. Akita and Y. Nakayama 1998. Orientation and purification of carbon nanotubes using AC electrophoresis. **J. Phys. D: Appl. Phys.** 31:L34-L36.
- Yang, M., Y. Yang, Y. Liu, G. Shen and R. Yu. 2006a. Platinum nanoparticles-doped sol-gel/carbon nanotubes composite electrochemical sensors and biosensors. **Biosensors and Bioelectronics** 21(7):1125-1131.
- Yang, M., Y. Yang, H. Yang, G. Shen and R. Yu. 2006b. Layer-by-layer self-assembled multilayer films of carbon nanotubes and platinum nanoparticles with polyelectrolyte for the fabrication of biosensors. **Biomaterials** 27(2):246-255.
- Yu, R., L. Chen, Q. Liu, J. Lin, K. L. Tan, S. C. Ng, H. S. O. Chan, G. Q. Xu and T.S.A. Hor. 1998. Platinum Deposition on Carbon Nanotubes via Chemical Modification. **Chem. Mater.** 10(3):718-722.

- Yudasaka, M., M. Z., C. Jabs, S. Iijima. 2000. Effect of an organic polymer in purification and cutting of single-wall carbon nanotubes. **Applied Physics A: Materials Science & Processing** 71(4):449-451.
- Yuzvinsky, T. D., A. M. Fennimore, W. Mickelson, C. Esquivias and A. Zettl. 2005. Precision cutting of nanotubes with a low-energy electron beam. **Applied Physics Letters** 86(5):053109-053111.
- Zanella, R., E. V. Basiuk, P. Santiago, V. A. Basiuk, E. Mireles, I. Puente-Lee and J. M. Saniger. 2005. Deposition of Gold Nanoparticles onto Thiol-Functionalized Multiwalled Carbon Nanotubes. **J. Phys. Chem. B** 109(34):16290-16295.
- Zhang, J., J. K. Lee, Y. Wu and R. W. Murray. 2003. Photoluminescence and Electronic Interaction of Anthracene Derivatives Adsorbed on Sidewalls of Single-Walled Carbon Nanotubes. **Nano Lett.** 3(3):403-407.
- Zhang, M., M. Yudasaka, A. Koshio, C. Jabs, T. Ichihashi and S. Iijima. 2002. Structure of single-wall carbon nanotubes purified and cut using polymer. **Applied Physics A: Materials Science & Processing** 74(1):7-10.
- Zhang, M., L. Su and L. Mao. 2006. Surfactant functionalization of carbon nanotubes (CNTs) for layer-by-layer assembling of CNT multi-layer films and fabrication of gold nanoparticle/CNT nanohybrid. **Carbon** 44(2):276-283.
- Zheng, M., A. Jagota, E. D. Semke, B. A. Diner, R. S. McLean, S. R. Lustig, R. E. Richardson and N.G. Tassi. 2003. DNA-assisted dispersion and separation of carbon nanotubes. **Nature Materials** 2(5):338-342.
- Zhou, O., H. Shimoda, B. Gao, S. Oh, L. Fleming and G. Yue. 2002. Materials Science of Carbon Nanotubes: Fabrication, Integration, and Properties of Macroscopic Structures of Carbon Nanotubes. **Acc. Chem. Res.** 35(12):1045-1053.

Zhu, N., Z. Chang, P. He and Y. Fang. 2005. Electrochemical DNA biosensors based on platinum nanoparticles combined carbon nanotubes. **Analytica Chimica Acta** 545(1):21-26.

Ziegler, K. J., Z. Gu, H. Peng, E. L. Flor, R.H. Hauge and R.E. Smalley. 2005a. Controlled Oxidative Cutting of Single-Walled Carbon Nanotubes. **J. Am. Chem. Soc.** 127(5):1541-1547.

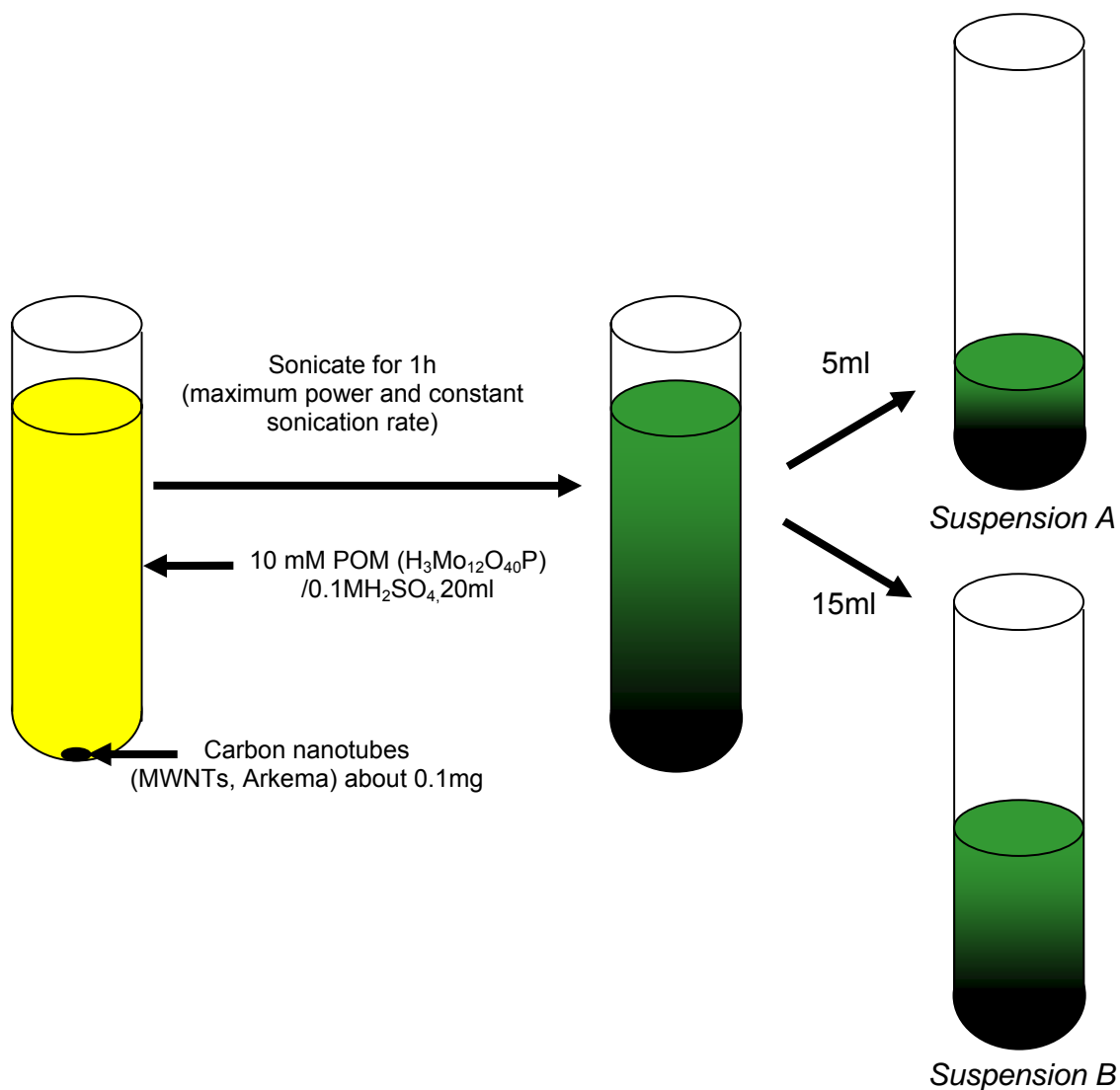
Ziegler, K. J., Z. Gu, J. Shaver, Z. Chen, E. L. Flor, D. J. Schmidt, C. Chan, R. H. Hauge and R. E. Smalley. 2005b. Cutting single-walled carbon nanotubes. **Nanotechnology** 16:S539-S544.

Zorbas, V., A. Ortiz-Acevedo, A. B. Dalton, M. M. Yoshida, G. R. Dieckmann, R. K. Draper, R. H. Baughman, M. Jose-Yacaman and I. H. Musselman. 2004. Preparation and Characterization of Individual Peptide-Wrapped Single-Walled Carbon Nanotubes. **J. Am. Chem. Soc.** 126(23):7222-7227.

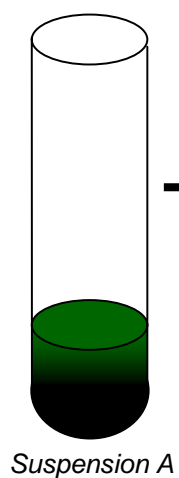
APPENDIX

Appendix A

Details of the experimental method for the purification, shortening and dispersion of carbon nanotubes



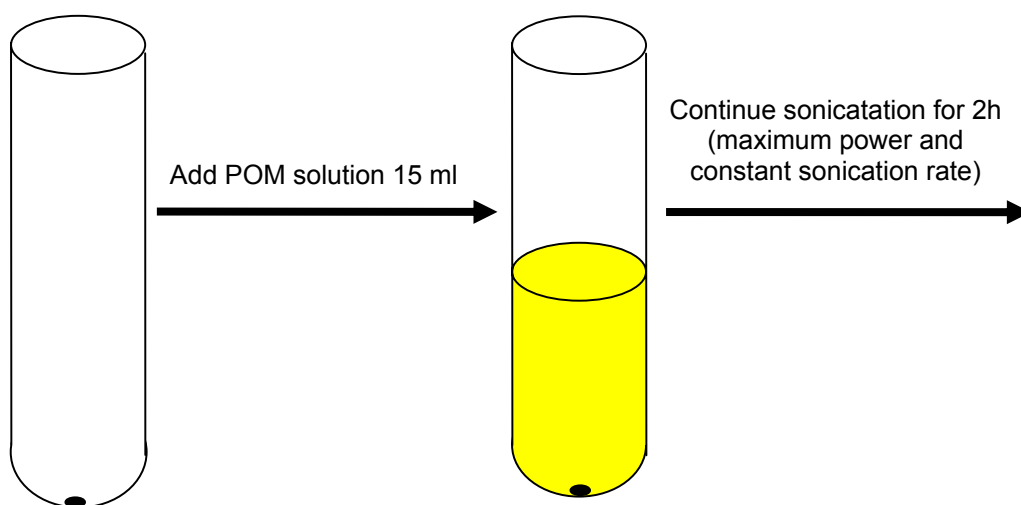
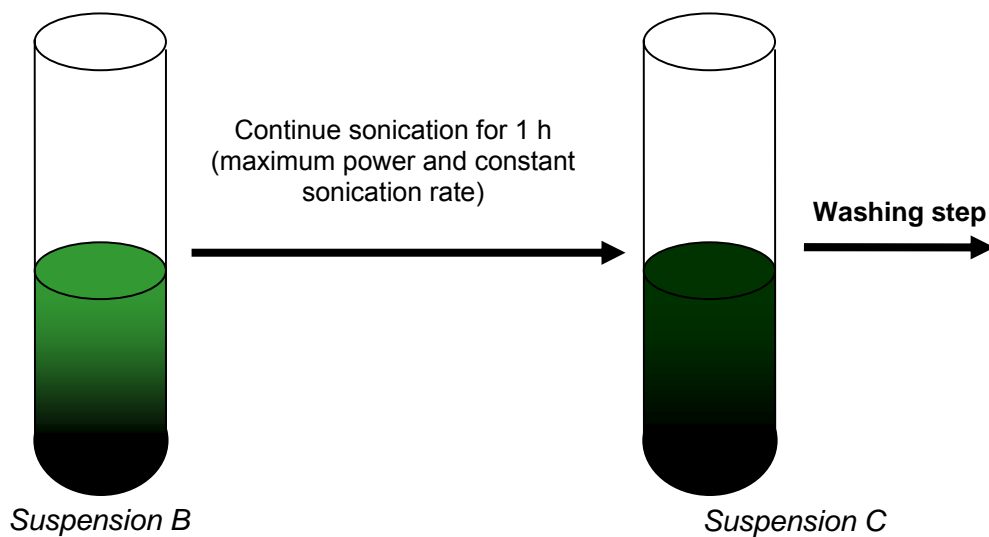
Suspension A

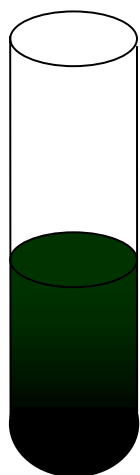


1. "Washing step"

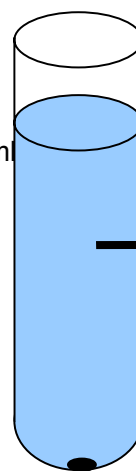
2. Add "ultrapure water" about 5 ml and sonicate by ultrasonic bath for 2min (the purpose of this step is to redisperse the obtained CNTs in water)
3. Characterize by TEM, HRTEM

Note: ultrapure water is the distilled water which is filtered by 0.2 μ m cellulose acetate filter, WHATMAN

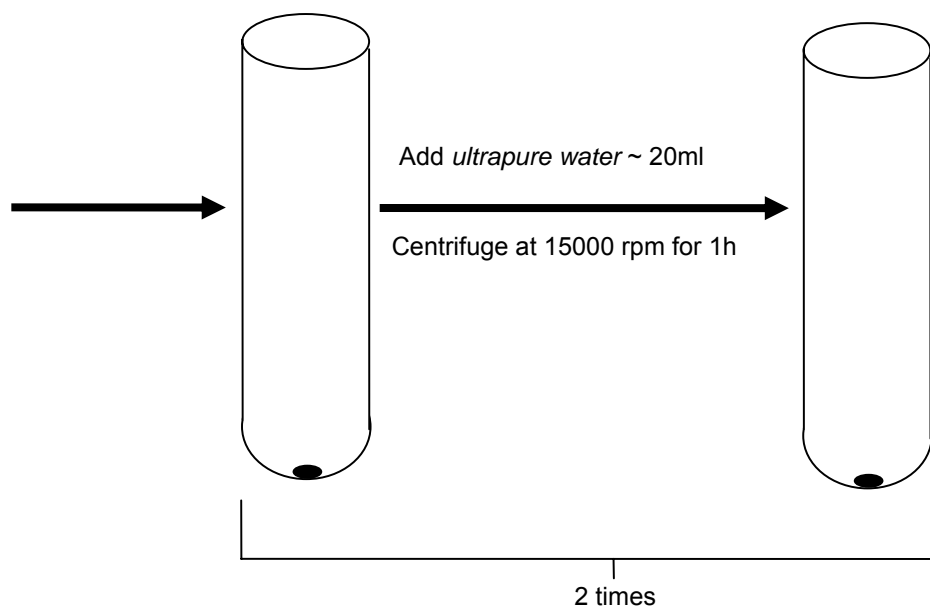
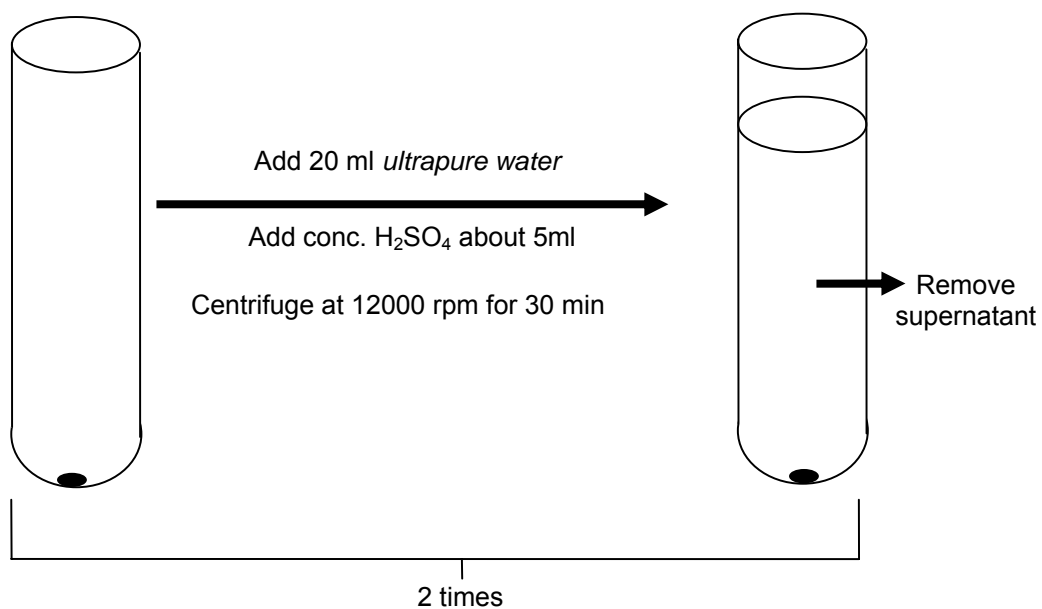
Suspension B

Suspension B (continued)**1. Washing step**

2. Add ultrapure water about 5 ml and sonicate by ultrasonic bath for 2 min (Purpose: Redisperse the prepared CNTs in water)
4. Characterize by TEM, Zetasizer, and HRTEM

*Suspension D***Washing step (suspension A, C and D)**Add conc. H₂SO₄ about 5mlCentrifuge at 15000 rpm
for 30 minRemove
supernatant*Suspension A, C and D*

Washing step (suspension A, C and D) (continued)



Appendix B

Details of the experimental method for the bipolar electrochemical gold deposition on a carbon fiber

Appendix Table B1 Detailed experimental method for the bipolar electrochemical gold deposition on a carbon fiber by using 10 mM HAuCl₄ solution as a starting reagent.

Step	Details
1	Cut a carbon fiber with scissor to millimeter length.
2	Suspend the shortened carbon fiber in 10 mM HAuCl ₄ (about 5 ml).
3	Vertical immersion of the capillary into the suspension (containing the fibers and HAuCl ₄ solution) will drag the liquid inside the capillary. Fill the capillary with the suspension until the capillary is full.
4	Position the fiber in the middle of the capillary by mild tilting.
5	Make a small hole at the bottom of each plastic vial.
6	Put the end of the capillary to each vial and locate the vials almost at the end of the capillary.
7	Clog connections between the capillary and the vials with the resin.
8	Cut the gold coated slide into two small pieces (dimension about 0.7×5cm).
9	Connect an electric cable to each gold slide.
10	Clean the electrodes by submerging in ethanol solvent and then sonicate for 30s in ultrasonic bath
11	Let the electrodes dry in air.
12	Use forceps to place each gold electrode vertically in each vial next to the capillary end.
13	Fix the electrodes at the walls of the vials by the resin at top of the vials.
14	Place the connected vials and capillary (<i>VIALS/CAPPILLARY</i>) on stage of the microscope.
15	Connect the electrodes to DC power supply without applying electricity.
16	Fill both vials slowly with 10 mM HAuCl ₄ until the capillary is completely submerged in the solution.

Appendix Table B1 (Continued)

Step	Details
17	Adjust position of the <i>VIALS/CAPPILLARY</i> , magnification, light mode and focus of the microscope until the image of the carbon fiber in capillary is clear. (Carbon fiber should be horizontally aligned and in the middle of the image.)
18	Change observation mode of the microscopy to camera visualization.
19	Vary the voltage (from DC power supply) from 0 V gradually. Wait for 3min after every change of 5V. Stop voltage increasing when gold deposition on the negatively polarized end of the carbon fiber is observed. Calculate the lowest voltage needed to induce sufficient potential difference which can drive the redox couple on carbon structures (see Appendix C).
20	Take images of gold deposition of carbon fiber every minute until the deposited gold has significantly grown.
21	Stop applying voltage and take the fiber out by forceps (clamp on the opposite side of the gold deposited side) from capillary. Wash the fiber gently by water. Dry fiber in air and characterize by SEM.

Appendix C

Estimation of the lowest voltage needed to drive gold deposition in 10 mM HAuCl_4 solution onto tubular carbon structures that are straight and parallel to the field lines

We will use the relation of the potential difference, field intensity, and length of the substrate shown in equation (4) (Page xx), $V_d = E \times L$, where V_d is the potential difference between the tips of the substrate, L is the length of the substrate and E is the applied electric field. The lowest voltage needed to induce a sufficient potential difference to drive the redox reactions involving AuCl_4^- and H_2O , in the electrolyte (HAuCl_4 solution), on any carbon structures that is straight and oriented parallel to the field lines can be roughly estimated by a test experiment with a HAuCl_4 solution and a carbon fiber. In case of a carbon fiber with 1.3 mm length approximately ($L = 1.3\text{mm}$) (the used electrolyte was 10 mM HAuCl_4), the lowest voltage needed to the drive gold deposition reaction was 70V. The distance between the two gold electrodes was about 10 cm. Consequently the electric field is calculated as 70V/10cm ($E = 7\text{V/cm}$). From this we can calculate the minimum potential difference between the tips of carbon nanostructures (V_d) as 0.9V ($\frac{7\text{V}}{\text{cm}} \times 1.3\text{mm} = \frac{7\text{V}}{\text{cm}} \times 1.3 \times 10^{-1}\text{cm}$). The lowest voltage (x) to generate gold on any carbon structures with y nm length ($L = y$) placed between separated electrodes with distance of z cm can be roughly estimated by the following calculation:

$$\begin{aligned}
 V_d &= E \times L \\
 0.9\text{V} &= \frac{x\text{V}}{z\text{cm}} \times y\text{nm} \\
 x &= \frac{0.9 \times z\text{cm}}{y\text{nm}} \\
 &= \frac{0.9z}{y} \times 10^{-2} \times 10^9 \\
 &= \frac{9z}{y} \times 10^6
 \end{aligned}$$

CIRRICULUM VITAE

NAME : Ms. Chompunuch Warakulwit

BIRTH DATE : March 20, 1982

BIRTH PLACE : Bangkok, Thailand

EDUCATION	: <u>YEAR</u>	<u>INSTITUTE</u>	<u>DEGREE/DIPLOMA</u>
	2002	Silpakorn University	B.Sc. (Chemistry)
	2004	Kasetsart University	M.S. (Chemistry)

SCHOLARSHIP :

2002-2003 Higher Education Development Project Scholarship
Postgraduate Education and Research Program in Physical
Chemistry

2005-2007 The Commission on Higher Education scholarship

2006 Research Scholarship, Graduate School, Kasetsart University

PUBLICATION :

C. Warakulwit, S. Bamrungsap, P. Luksirikul, P. Khongpracha and J. Limtrakul,
*Diels-Alder Cycloadditions of Single-Wall Carbon Nanotubes and Fullerenes with
Electron-Rich Dienes*. Study in Surface Science and Catalysis (2005), 156, 823-828.

CONFERENCES (ORAL AND POSTER PRESENTATIONS) :

P. Khongpracha, C. Warakulwit, S. Bamrungsap, P. Luksirikul and J. Limtrakul,
*Interaction of the different types of dienes with single wall carbon nanotube
(SWNT) and C₆₀: A QM/MM study (Poster Session)*. 229th ACS National Meeting,
San Diego, CA, United States, March 13-17, 2005

C. Warakulwit, S. Bamrungsap and J. Limtrakul, *Diels-Alder cycloaddition reactivity
of C₆₀ and single-wall carbon nanotubes with the benzo-fused five membered ring
diene (Oral presentation)*. 31st Congress in Science and Technology of Thailand,
Suranaree University, Nakorn Ratchasima, Thailand. October 18-20, 2005

C. Warakulwit, S. Bamrungsap, P. Pantu and J. Limtrakul, *Cycloaddition reactivity of C₆₀, single-wall carbon nanotubes and their metal cation embedded clusters with the 2H-benzocyclopentadiene (Poster Session)*. 231st ACS National Meeting, Atlanta, GA, United States, March 26-30, 2006

C. Warakulwit, M. -H. Delville, J. Limtrakul and A. Kuhn, *Décoration métallique de nanostructures de carbone (Poster presentation)*. Comité Scientifique des Journées d'Electrochimie 2007, Lyon, France, 2-6 July 2007

C. Warakulwit, *Metal decoration of carbon nanostructures (Oral presentation)*. The First Thailand National Nanotechnology Conference on Nanomaterials, Pharmaceuticals, Devices and Applications, Chiang-Mai, Thailand, August 14-16 2007

C. Warakulwit, M. -H. Delville, J. Limtrakul and A. Kuhn, *Metal decoration of carbon nanostructures (Poster Session)*, 58th Annual ISE Meeting in Banff, Canada, September 9-14, 2007

RÉSUMÉ DE LA THÈSE

DANS CE TRAVAIL NOUS AVONS EXPLORÉ DES NOUVELLES VOIES POUR SYNTHÉTISER ET FONCTIONNALISER DES NANOTUBES DE CARBONE. DES TUBES DE DIAMÈTRE ET DE LONGUEUR BIEN DÉFINIE ON ÉTÉ OBTENU EN UTILISANT UNE APPROCHE « TEMPLATE » POUR LA SYNTHÈSE. PAR LA SUITE DES NANOTUBES ONT ÉTÉ SOLUBILISÉS EN UTILISANT UNE APPROCHE À LA FOIS SIMPLE ET ORIGINALE. ENFIN NOUS AVONS PU METTRE AU POINT UNE TECHNIQUE PERMETTANT DE FONCTIONNALISER SÉLECTIVEMENT UNE EXTRÉMITÉ DE CES NANOTUBES AVEC UNE COUCHE MÉTALLIQUE EN UTILISANT LE CONCEPT D'ÉLECTROCHIMIE BIPOLAIRE. LE TRAVAIL A ÉTÉ COMPLÉTÉ PAR UNE ÉTUDE THÉORIQUE DE LA RÉACTIVITÉ DE CES OBJETS.